

CHAPTER 3

TRANSFERS TO LUNAR LIBRATION ORBITS

3.1 EXECUTIVE SUMMARY

This chapter focuses on the performance of low-energy transfers to lunar libration orbits and other three-body orbits in the Earth–Moon system. This chapter presents surveys of direct transfers as well as low-energy transfers to libration orbits, and provides details about how to construct a desirable transfer, be it a short-duration direct transfer or a longer-duration low-energy transfer. The work presented here uses lunar halo orbits as destinations, but any unstable three-body orbit may certainly be used in place of those example destinations.

For illustration, Figs. 3-1 and 3-2 show some example direct and low-energy transfers to lunar halo orbits, respectively. One can see that these transfers are ballistic in nature: they require a standard trans-lunar injection maneuver, a few trajectory correction maneuvers, and a halo orbit insertion maneuver. One may also add Earth phasing orbits and/or lunar flybys to the trajectories, which change their performance characteristics.

Many thousands of direct and low-energy trajectories are surveyed in this chapter. Table 3-1 provides a quick guide for several types of transfers that are presented here, comparing their launch energy costs, the breadth of their launch period, that is, the

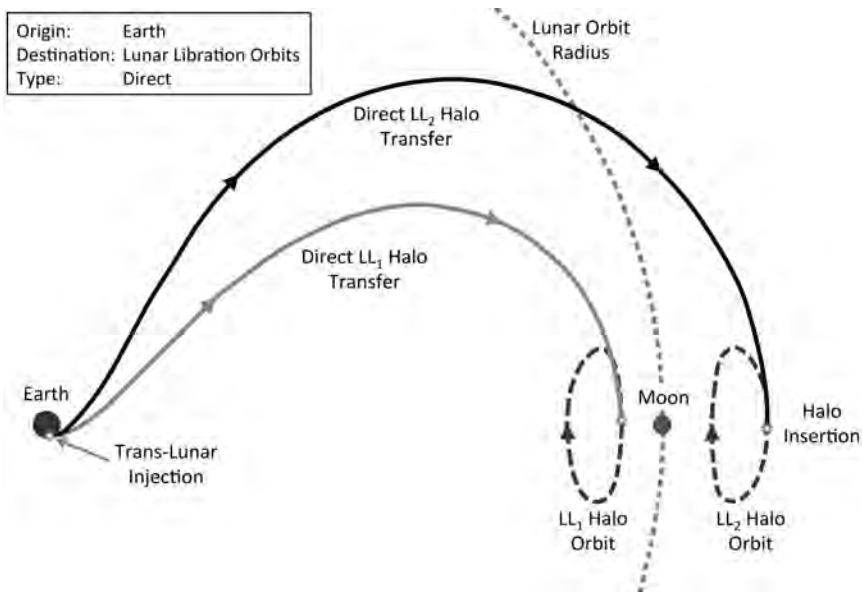


Figure 3-1 The profile for a simple direct transfer from the Earth to a lunar libration orbit about either the Earth–Moon L₁ or L₂ point.

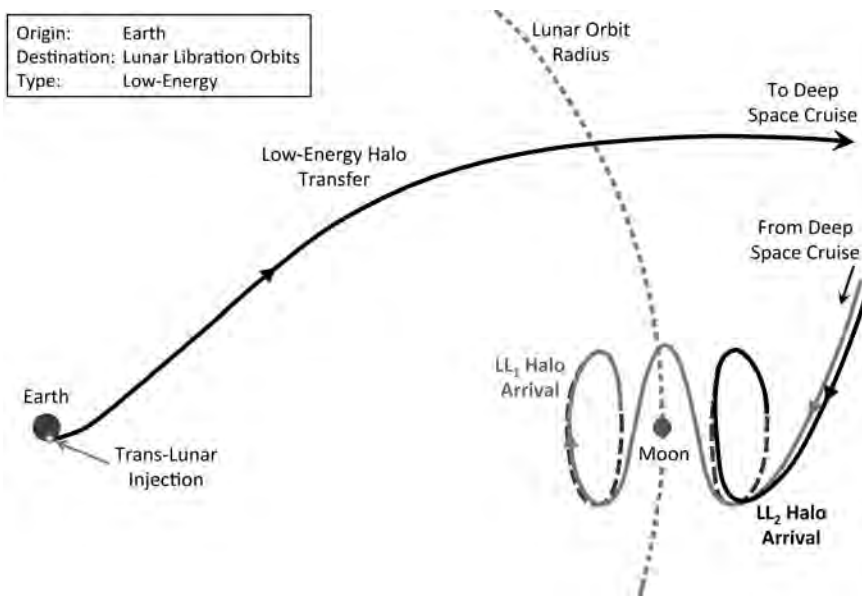


Figure 3-2 The profile for a simple, low-energy transfer from the Earth to a lunar libration orbit about either the Earth–Moon L₁ or L₂ point.

Table 3-1 A summary of several parameters that are typical for different mission scenarios to libration orbits about either the Earth–Moon L_1 or L_2 points. EPOs = Earth phasing orbits, BLT = low-energy ballistic lunar transfer.

Mission Element	Direct Transfer	Direct w/EPOs	Simple BLT	BLT w/Outbound Lunar Flyby	BLT w/EPOs
Launch C_3 (km^2/s^2)	-2.2 to -1.5	< -1.5	-0.7 to -0.4	-2.1 to -0.7	< -1.5
Launch Period	Short	Extended	Extended	Short	Extended
Transfer Duration (days)	3–6	13+	70–120+	70–120+	80–130+
Outbound Lunar Flyby	No	No	No	Yes	Yes
Libration Orbit Insertion ΔV (m/s)	~500	~500	~0	~0	~0

number of consecutive days they may be launched, their transfer duration, and the relative magnitude of the orbit insertion change in velocity (ΔV) upon arriving at the lunar libration orbit. These are representative and may be used for high-level mission design judgements, though the details will likely vary from mission to mission.

Direct transfers to lunar libration orbits are presented in Section 3.3. That section surveys thousands of transfers to libration orbits about both the Earth–Moon L_1 and L_2 points and presents methods to construct them. The trajectories minimize the halo orbit insertion ΔV cost while keeping the total transfer duration low, between 5 days and 2 months. The trajectories include no maneuvers other than the trans-lunar injection maneuver and the halo orbit insertion maneuver. Hence, there are no high-risk maneuvers, such as powered lunar flybys, though such maneuvers may indeed reduce the total transfer ΔV cost [172].

The surveys show that one may depart the Earth from any parking orbit, certainly including low-altitude parking orbits with an inclination of 28.5 degrees (deg). The transfers involve trans-lunar injections with launch injection energy (C_3) requirements as low as $-2.6 \text{ km}^2/\text{s}^2$ and as high as $-2.0 \text{ km}^2/\text{s}^2$ for transfers to LL_1 or as high as $-1.0 \text{ km}^2/\text{s}^2$ for transfers to LL_2 . The halo orbit insertion maneuver may be as low as 430 meters per second (m/s) or as high as 950 m/s, depending on the mission’s requirements, though most are in the range of 500–600 m/s. The quickest transfers arrive at their libration orbit destinations within 5 or 6 days. Some missions can reduce the total transfer ΔV by ~ 50 m/s by implementing a longer, 30-day transfer. In some cases it is beneficial to extend the duration to 40 or 50 days. Finally, direct lunar transfers exist in families, such that very similar transfers exist to neighboring libration orbits. That is, if a

mission's requirements change slightly and a new libration orbit is required, one can usually build a very similar transfer to that orbit as to the original orbit.

Low-energy transfers to lunar libration orbits are presented in Section 3.4. Much like the analyses of direct transfers, Section 3.4 surveys thousands of transfers to libration orbits about both the Earth–Moon L_1 and L_2 points and presents methods to construct them. The trajectories are always entirely ballistic, except for the trans-lunar injection maneuver. None of the transfers studied requires an orbit insertion maneuver; every trajectory asymptotically arrives at the target orbit and inserts automatically. Trajectories are studied with a wide variety of geometry characteristics, but all require less ΔV than direct transfers.

Much like the analyses of direct transfers, the surveys in Section 3.4 show that one may depart the Earth from any given low Earth parking orbit, or any higher orbit as needed. The transfers involve trans-lunar injections with C_3 requirements as low as $-0.75 \text{ km}^2/\text{s}^2$ and as high as $-0.35 \text{ km}^2/\text{s}^2$. This C_3 requirement may be reduced to about $-2.1 \text{ km}^2/\text{s}^2$ if a lunar flyby is implemented at an altitude of about 2000 km. The quickest transfers identified require about 83 days between the trans-lunar injection and the point when the trajectory has arrived within 100 km of the lunar libration orbit. Many transfer options exist that require 90–140 days between the injection point and the orbit arrival point. Since the transfers asymptotically approach the target libration orbit, they are essentially at the target orbit as many as 10 days prior to the “arrival” time. Finally, much like direct transfers to lunar libration orbits, low-energy transfers exist in families, such that very similar transfers exist to neighboring libration orbits. Very similar transfers also exist to the same orbit when the arrival time or arrival location is adjusted.

This chapter summarizes nearly ballistic transfers between the Earth and lunar libration orbits. Techniques to use these transfers in practical spacecraft mission design (for example, building launch periods, and budgeting station keeping ΔV) are studied in Chapter 6.

3.2 INTRODUCTION

This chapter describes methods to construct both direct and low-energy transfers between the Earth and libration orbits near the Moon. The focus of this book is on the analysis and construction of low-energy transfers, but it is helpful to have a good understanding of the costs and benefits of direct transfers as well. In addition, this chapter provides some transfers that one may take after arriving at a lunar libration orbit; transfers are presented from those libration orbits to other libration orbits, to low lunar orbits, and to the lunar surface.

Direct transfers include any sort of high-energy conventional trajectories using chemical propulsion systems. Low-energy transfers use the same propulsion systems but travel well beyond the orbit of the Moon, taking advantage of the Sun's gravity to reduce the ΔV cost of the transfer. Direct transfers to lunar libration orbits (and other

three-body orbits) typically require 3–6 days, though there are benefits to increasing the transfer duration as long as 1 or 2 months. Low-energy transfers typically require 3–4 months of transfer time or more in some circumstances.

Figure 3-1 illustrates two example direct transfers between the Earth and libration orbits about the Earth–Moon L_1 and L_2 points. Figure 3-2 illustrates two low-energy transfers to the same two libration orbits, viewed in the same reference frame. One can see that the trajectories traverse beyond the orbit of the Moon and return after 2–3 months to arrive at the Moon in such a way that they insert into the target orbits without requiring any insertion maneuver. The lack of a large orbit insertion maneuver is the primary reason why these transfers save so much fuel (the direct transfers require an orbit insertion maneuver near 500 m/s).

Figure 3-3 illustrates two different low-energy transfers viewed in the Sun–Earth rotating frame to show that spacecraft may fly either toward the Sun or away from it during their transfers.

This chapter describes techniques to build direct and low-energy transfers to lunar libration orbits and surveys the performance of both types of transfers. Section 3.3 describes the techniques and provides performance data for direct transfers to lunar libration orbits. Section 3.4 does the same for low-energy transfers to the same orbits. Section 3.5 provides information about orbit transfers from the libration orbits to other libration orbits, to low lunar orbits, and to the lunar surface. Finally, Section 3.5 discusses transfers that a spacecraft could take to depart its lunar libration orbit and travel to another three-body orbit, a low lunar orbit, the lunar surface, or back to the Earth.

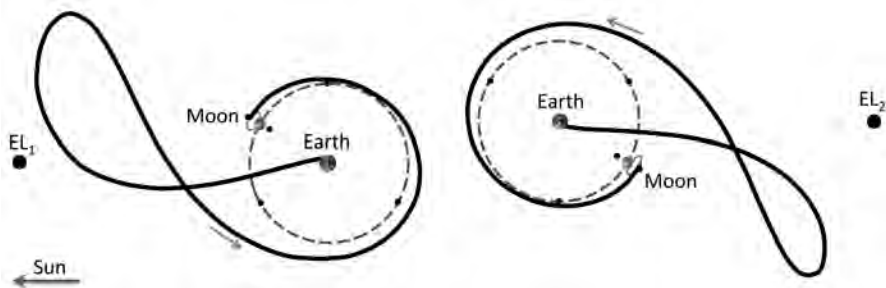


Figure 3-3 Two example low-energy transfers between the Earth and an LL_2 libration orbit. The transfers are viewed from above in the Sun–Earth rotating coordinate frame [44] (Copyright © 2009 by American Astronautical Society Publications Office, all rights reserved, reprinted with permission of the AAS.).

3.3 DIRECT TRANSFERS BETWEEN EARTH AND LUNAR LIBRATION ORBITS

As of 2012 no missions have flown a direct transfer from the Earth to a lunar libration orbit. Many researchers have considered the problem, dating back to 1970 when Edelbaum studied the case of transferring a spacecraft from the Earth to the L_1 point itself via a direct transfer [173]. Certainly NASA has considered the problem as it considers destinations for future missions [126]. The work presented here is based upon the work of Parker and Born [174, 175], who performed a robust survey of direct transfers to lunar halo orbits about both L_1 and L_2 . Several other authors have also studied this problem, including Rausch [176], Gordon [177], and Alessi et al. [178].

The trajectories generated here are constructed by intersecting a low Earth orbit (LEO) parking orbit with a trajectory within the stable invariant manifold of the target libration orbit. Hence, the trajectories include two maneuvers: a maneuver to depart the Earth and a maneuver to inject onto the target orbit's stable manifold. Once on the stable manifold, the spacecraft asymptotically arrives at the target orbit.

3.3.1 Methodology

Direct transfers are constructed here by targeting states within the stable manifold of a desirable halo orbit or other libration orbit. This strategy has been implemented before for transfers to many types of Sun–Earth libration orbits, yielding trajectories for missions such as *Genesis* [72], *Wilkinson Microwave Anisotropy Probe (WMAP)* [70], and *Solar and Heliospheric Observatory (SOHO)* [66]. The technique has been highly successful for missions in the Sun–Earth system because the stable manifolds of many Sun–Earth halo orbits intersect the Earth. Unfortunately, as one can begin to see in Fig. 3-4, the stable manifolds of libration orbits near the Earth–Moon L_1 and L_2 points do not intersect the Earth within as much as two months of time. Consequently, at least two maneuvers must be performed to directly transfer onto the lunar halo orbit's stable manifold from an initial LEO parking orbit, rather than the single maneuver required to inject onto the stable manifold of a Sun–Earth halo orbit.

In theory, a direct transfer to a lunar halo orbit could involve many burns, each performed in some arbitrary direction. We have chosen to survey the simplest type of direct lunar halo orbit transfers, namely, transfers with only two burns that are each performed in a direction tangential to the spacecraft's velocity vector. These transfers are not guaranteed to have the lowest ΔV cost of any type of direct lunar halo transfer, but they should provide a good estimate for the ΔV requirement of such transfers. Even with this simplification, this design problem yields a very rich design space and is a useful foundation for future studies.

Figure 3-5 shows two perspectives of a scenario that illustrates the strategy used here to transfer a spacecraft from a 185-km LEO parking orbit to a lunar L_1 halo orbit. The scenario requires a large maneuver at the LEO injection point (ΔV_{LEO} ; also known as the trans-lunar injection maneuver) and a second large maneuver at the manifold injection point (ΔV_{MI}). The two ballistic mission segments are referred to

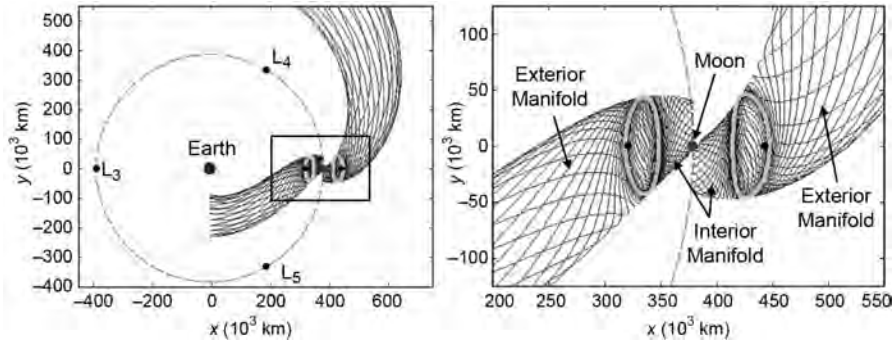


Figure 3-4 Plots of the stable manifolds of example L_1 and L_2 halo orbits, viewed from above in the Earth–Moon synodic reference frame. A spacecraft that travels along any one of these trajectories will asymptotically arrive onto the corresponding halo orbit [174] (Copyright © 2008 by American Astronautical Society Publications Office, all rights reserved, reprinted with permission of the AAS).

as the *bridge* segment and the *manifold* segment. Once the spacecraft arrives onto the manifold segment, after performing the ΔV_{MI} maneuver, it asymptotically transfers onto the lunar halo orbit.

It is assumed that each transfer constructed here begins in a 185-km circular prograde Earth parking orbit. In this way, the performance of each transfer may be directly compared. In reality, the same sorts of transfers that are constructed here may begin from a LEO parking orbit at any altitude and with any eccentricity, or even from the surface of the Earth, provided that the vehicle is at the correct position at the correct time to perform the ΔV_{LEO} maneuver successfully.

The following strategy has been followed to construct direct transfers to lunar halo orbits:

Step 1. Construct the desired halo orbit.

Step 2. Construct the *manifold* segment:

1. Choose a τ -value, that is, a point along the halo orbit as illustrated in Fig. 2-10 (page 50); choose a direction, that is, either “interior” or “exterior” as shown in Fig. 3-4; and choose a manifold propagation duration, Δt_m .
2. The manifold segment is constructed by propagating the specific trajectory in the halo orbit’s stable manifold that corresponds to the given τ -value. The trajectory departs the halo orbit either in the interior or exterior direction, as indicated. It is propagated in the Earth–Moon three-body system backward in time for the given duration.

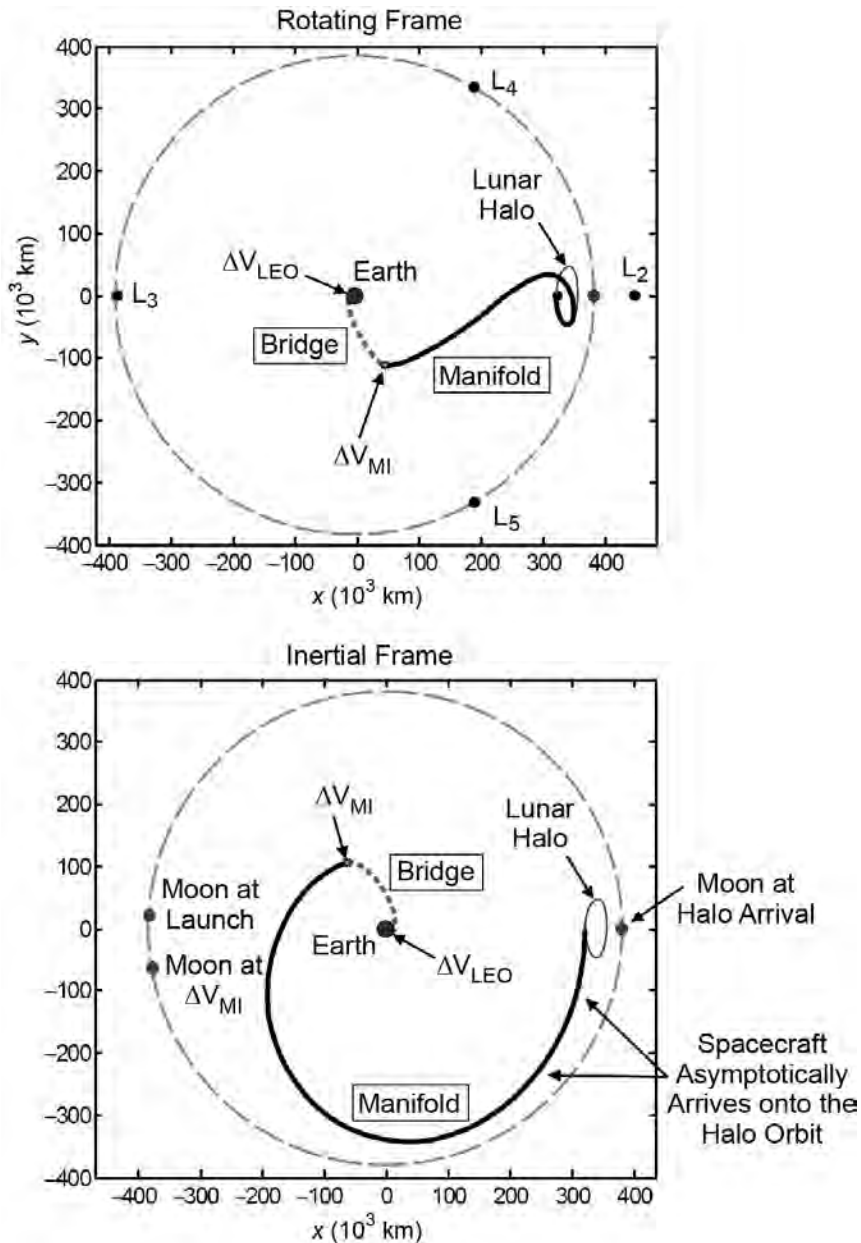


Figure 3-5 Two perspectives of an example scenario that may be used to transfer a spacecraft from a 185-km LEO parking orbit to a lunar L_1 halo orbit. The transfer is shown in the Earth–Moon rotating frame (top) and the corresponding inertial frame of reference (bottom). The halo orbit is shown in the inertial frame only for reference.

Step 3. Define X_{MI} to be the final state of the manifold segment. This is the state that a spacecraft would need to obtain in order to inject onto the manifold segment.

Step 4. Construct ΔV_{MI} and the *bridge* segment:

1. Define ΔV_{MI} to be the tangential ΔV that may be applied to X_{MI} in order to construct the bridge segment.
2. When propagated further backward in time, the bridge segment will encounter the prograde 185-km LEO orbit at the bridge's first perigee point. The bridge segment is propagated in the Earth–Moon three-body system.

Step 5. Construct ΔV_{LEO} , the tangential ΔV that may be applied to transfer the spacecraft from its LEO orbit onto the bridge segment.

This procedure is used here to produce a direct, two-burn transfer to a lunar halo orbit given an arbitrary lunar halo orbit and any given value for those parameters specified in Step 2 above. A significant benefit of this procedure is that it requires no knowledge of what a transfer should look like, except that the bridge segment is only propagated backward in time to its first perigee passage.

This process generates three-dimensional transfers in the idealized Earth–Moon circular restricted three-body problem (CRTBP). The inclination of the Earth departure is a free variable; it is computed and reported, but not targeted in any way. Furthermore, since no date is specified, the inclination is presented relative to the orbital plane of the Moon. The performance of actual transfers to real halo orbits will vary based on the date and orientations of each body and its orbit in the Solar System. Nevertheless, this exploration sheds light on what sorts of transfers exist and their approximate performance.

Several scenarios have been explored to identify optimal transfers, given the confines of this survey. The first suspicion is that the optimal transfer may be constructed by building a bridge segment that connects the LEO departure with the manifold segment's perigee point. Since energy-change maneuvers are more efficient when a spacecraft is traveling faster [97], the perigee of the manifold segment seems like a good location to perform the ΔV_{MI} maneuver. The best transfer for a specific halo orbit would then be the one that requires the least total ΔV over all τ -values. This *perigee-point* scenario is presented first. It turns out that this strategy does not produce the most efficient transfers—the next strategy generates better transfers—but the *perigee-point* scheme will still be presented because it illuminates the problem very well.

3.3.2 The Perigee-Point Scenario

Figure 3-6 shows two perspectives of several example trajectories that may be used to transfer a spacecraft onto a single lunar L_1 halo orbit using the perigee-point scheme. Each transfer implements a different τ -value about the same halo orbit. For

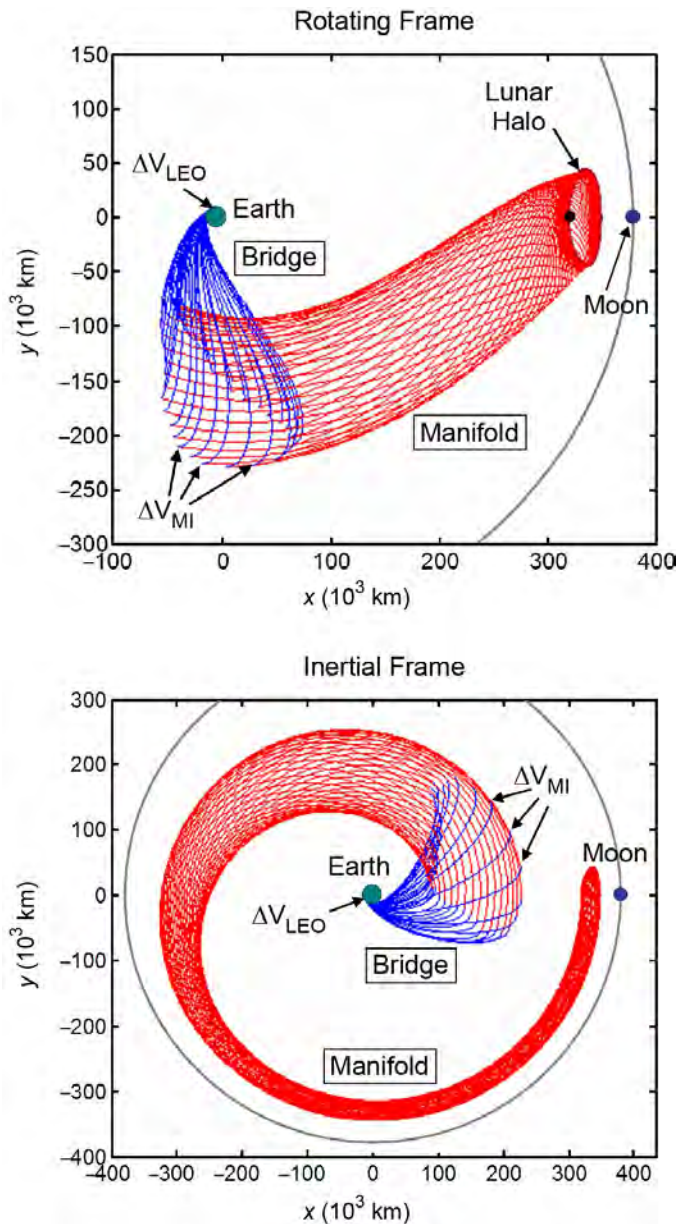


Figure 3-6 Example trajectories that implement the *perigee-point* scheme to directly transfer from LEO to a lunar L_1 halo orbit. The transfers are shown in the Earth–Moon rotating frame (top) and the corresponding inertial frame of reference (bottom). (See insert for color representation of this figure.)

reference, the halo orbit is a northern L_1 halo orbit with an x_0 -value of approximately 319,052 kilometers (km). The manifold segment in each case has been propagated to its perigee point, and the corresponding bridge segment has been constructed to transfer from a 185-km prograde LEO orbit to that perigee point. The trajectories are shown in both the Earth–Moon rotating frame and the corresponding inertial frame of reference.

Several of the trajectories shown in the left plot of Fig. 3-6 appear to have non-tangential ΔV_{MI} maneuvers; this is only a visual effect caused by the rotating frame of reference. As the spacecraft departs the Earth on the bridge segment, it quickly crosses a point where the frame of reference rotates about the Earth faster than the spacecraft. After that point, the spacecraft appears to travel in a retrograde fashion about the Earth, seemingly in conflict with its inertially prograde orbit. If the spacecraft then performs a large enough ΔV_{MI} maneuver, the spacecraft's rotational velocity will once again exceed the rotational velocity of the frame of reference. The spacecraft will appear to have switched directions when it actually just increased its inertial velocity.

Figure 3-7 shows plots of the magnitudes of the two required maneuvers, ΔV_{LEO} and ΔV_{MI} , as well as the total maneuver cost as functions of the parameter τ . One can see that the minimum ΔV cost to transfer from the 185-km LEO orbit to this halo orbit using the perigee-point scheme is approximately 4.14 kilometers per second (km/s). One can also see that this minimum occurs at the point where ΔV_{LEO} is at its maximum. Figure 3-8 shows plots of the minimum- and maximum- ΔV transfers and verifies that the minimum- ΔV transfer involves the largest bridge segment observed in Fig. 3-6. The total transfer duration from the point where the spacecraft performs its ΔV_{LEO} maneuver to the point where it is within 100 km of the given halo orbit ranges between approximately 17.7 days ($\tau \approx 0.30$) and 22.9 days ($\tau \approx 0.83$).

3.3.3 The Open-Point Scenario

Although it may be intuitive to perform ΔV_{MI} at the manifold segment's perigee point because of the energy considerations, it is actually better to perform a larger ΔV_{LEO} and a smaller, although less-efficient, ΔV_{MI} . This is because the maneuver at LEO can take advantage of its close proximity to the Earth to make the total energy change required in the transfer as efficient as possible. That is, it is most efficient to change as much of the spacecraft's energy at LEO as possible, since that is the location where the spacecraft will be traveling the fastest during the lunar transfer. This result is evident by studying the results of the perigee-point scheme.

An alternate scheme is presented here where the second maneuver, ΔV_{MI} , may be placed anywhere along the stable manifold of the halo orbit. The manifold segment may be propagated well beyond its perigee point, although it has an imposed maximum propagation time of 1 or 2 months: 1 month for exterior manifolds since they depart the Moon's vicinity quickly and 2 months for interior manifolds since they linger near the Moon for longer amounts of time. The transfers have an additional degree of freedom compared with the perigee-point scheme, but they are otherwise constructed in exactly the same manner as listed above. This new scheme will be

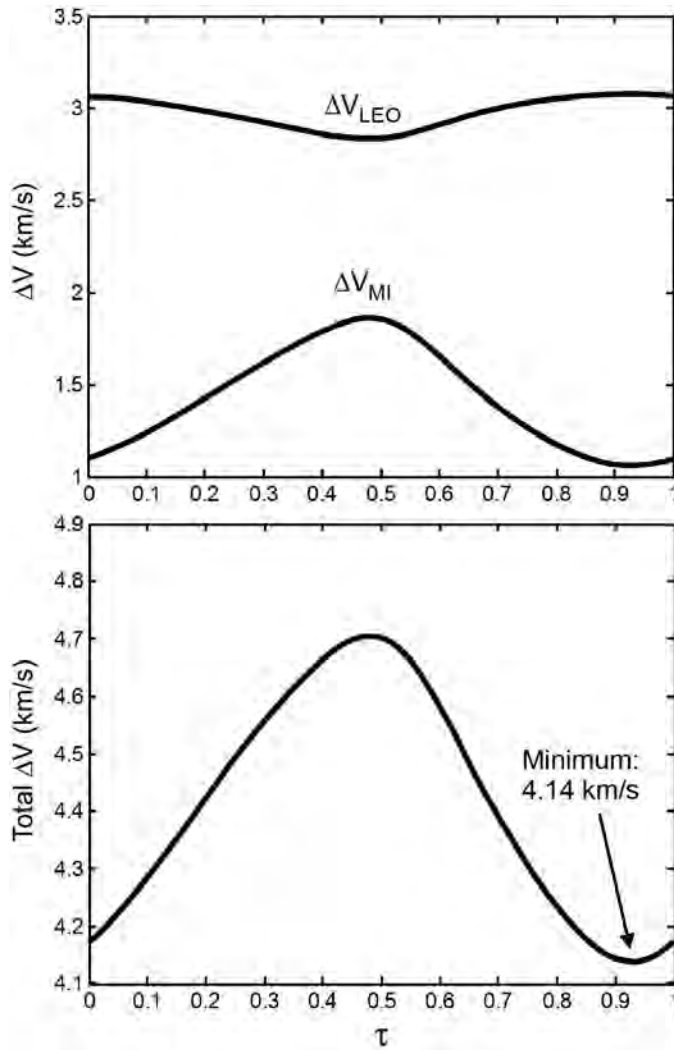


Figure 3-7 Plots of the maneuver requirements to transfer onto a lunar L_1 halo orbit using the perigee-point scheme. Top: the magnitudes of the two maneuvers ΔV_{LEO} and ΔV_{MI} as functions of τ ; bottom: the total ΔV cost as a function of τ .

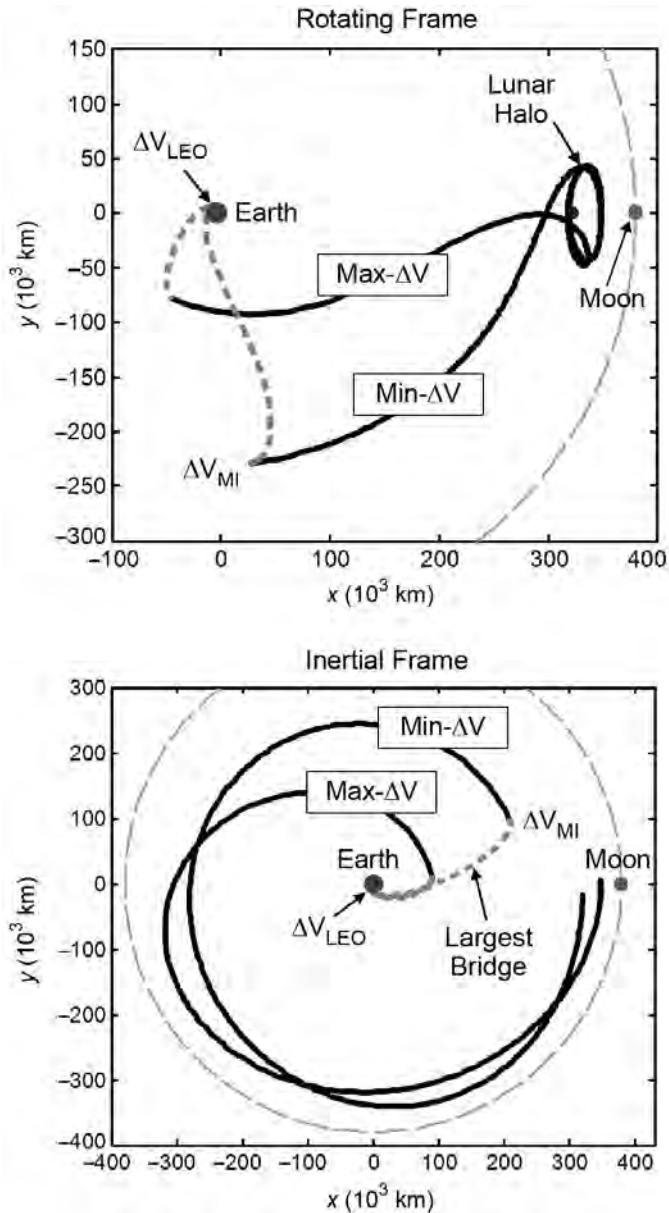


Figure 3-8 The minimum- and maximum- ΔV transfers produced using the perigee-point scheme. One can see that the minimum- ΔV transfer contains the largest bridge segment observed in Fig. 3-6 [174] (Copyright © 2008 by American Astronautical Society Publications Office, all rights reserved, reprinted with permission of the AAS).

referred to as the *open-point* scheme, since the manifold insertion point has had its position constraint opened.

To demonstrate the open-point transfer strategy, Fig. 3-9 shows several transfers that may be constructed from LEO to an arbitrary trajectory along the stable manifold of a particular halo orbit. The halo orbit shown in Fig. 3-9 is the same northern L_1 halo orbit presented in Section 3.3.2, and the manifold shown has a τ -value of 0.3. Figure 3-10 shows the maneuver cost associated with transferring to various points along the manifold, where the location of ΔV_{MI} is specified by the manifold propagation duration, Δt_m . One can see that there are two local minima that correspond to low-energy lunar transfers: one at a Δt_m of approximately 10.0 days and the next at a Δt_m of approximately 22.7 days, neither of which corresponds to a mission that transfers to the manifold segment's perigee point, which has a Δt_m of approximately 16.86 days. In fact, these transfers correspond to missions where the bridge segment connects the spacecraft to a point very near the apogee of the manifold segment. Figure 3-11 shows plots of the extreme cases, namely, the four transfers indicated by the labels (1)–(4) in Fig. 3-10. One can see that the two local minima observed in Fig. 3-10, that is, the trajectories marked with a (2) and a (4), coincide very near to the manifold segment's apogee locations.

Figures 3-9 to 3-11 have demonstrated the open-point scheme applied to a single trajectory (where $\tau = 0.3$) on the stable manifold of a single halo orbit (the lunar L_1 halo orbit with an x_0 -value of approximately 319,052 km). The open-point scheme is easily extended to cover many trajectories along the halo orbit's stable manifold. Figure 3-12 summarizes the required maneuvers and the total maneuver cost associated with the least expensive lunar transfer for each trajectory on the stable manifold of the same halo orbit. One can see that the lowest-energy open-point transfer constructed to this particular halo orbit requires a total ΔV of approximately 3.62 km/s. This low-energy transfer implements the trajectory in the orbit's stable manifold with a τ -value of approximately 0.48. For verification, Fig. 3-12 shows that the trajectory with a τ -value of 0.3 requires a minimum ΔV of approximately 3.67 km/s: the same result as that shown in Fig. 3-10.

Note that in Fig. 3-12 the least-expensive transfers to this halo orbit use the first maneuver, ΔV_{LEO} , to perform the vast majority of the spacecraft's energy change. This is consistent with the notion that the most efficient transfer performs as much ΔV as possible deep within the Earth's gravity well where the spacecraft is traveling fastest.

3.3.4 Surveying Direct Lunar Halo Orbit Transfers

The previous section illustrates the open-point scheme applied to a single halo orbit about the Earth–Moon L_1 point using the halo orbit's exterior stable manifold. The process results in a low-energy, two-maneuver, direct lunar transfer to that halo orbit, following the exterior stable manifold. This section surveys low-energy direct lunar transfers to a large number of orbits within the families of halo orbits about both the Earth–Moon L_1 and L_2 points, taking advantage of both the exterior and interior

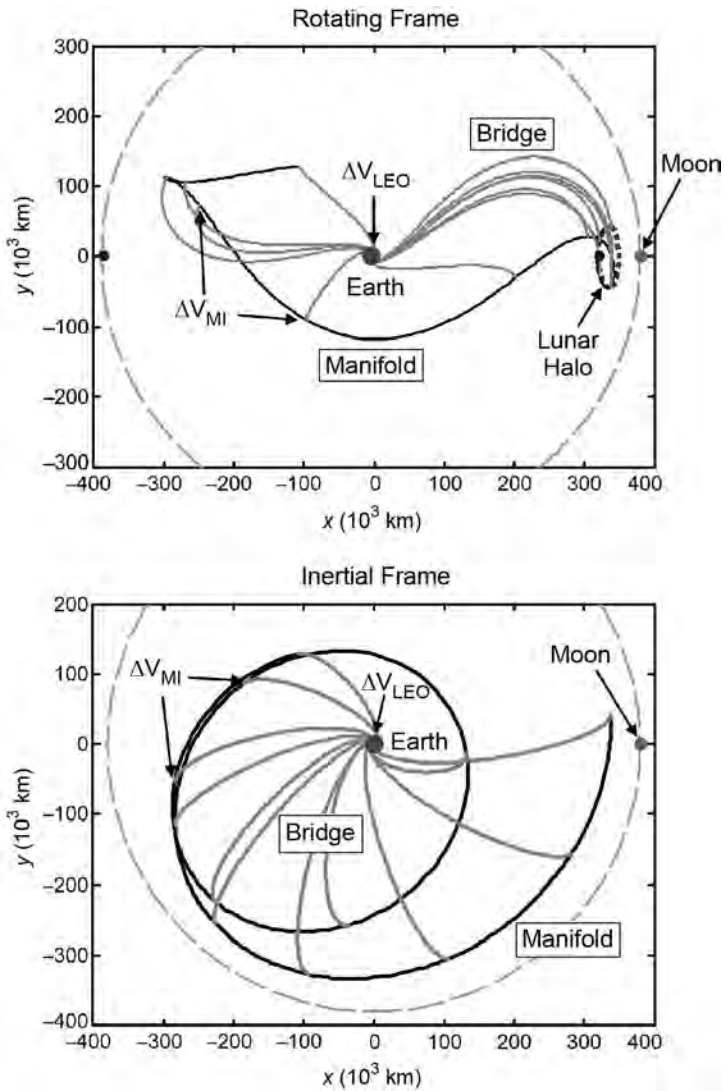


Figure 3-9 Example trajectories that implement the open-point scheme to directly transfer from LEO to a specific manifold of a particular lunar L_1 halo orbit.

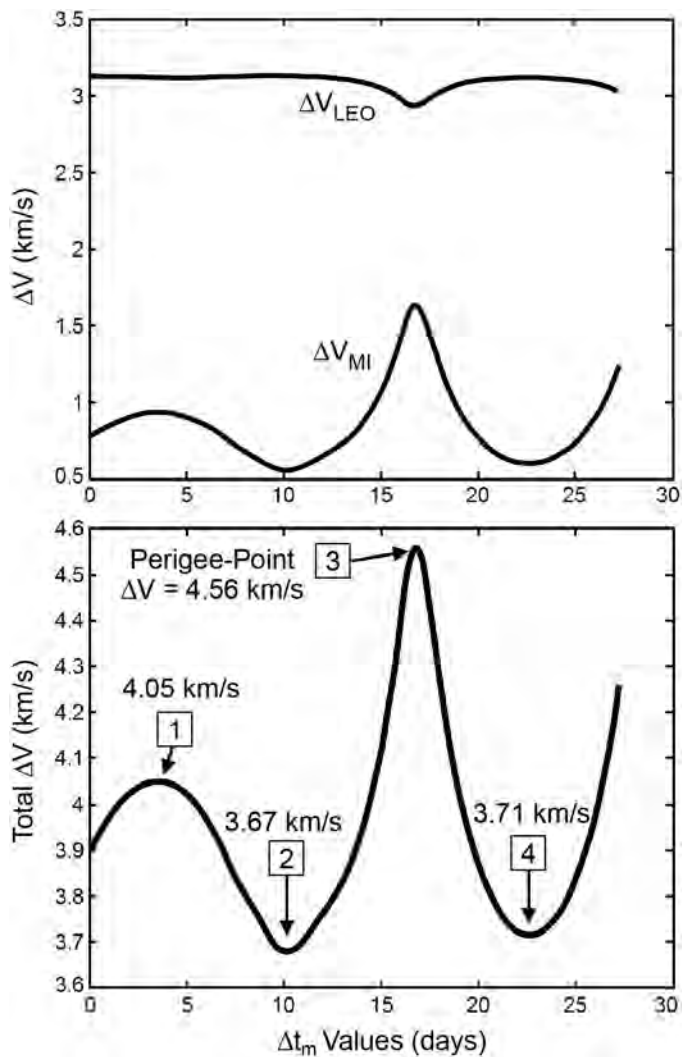


Figure 3-10 Plots of the maneuver requirements to transfer onto a specific manifold of a specific lunar L_1 halo orbit using the open-point scheme. Top: the magnitudes of the two maneuvers ΔV_{LEO} and ΔV_{MI} as functions of Δt_m ; bottom: the total ΔV cost as a function of Δt_m .

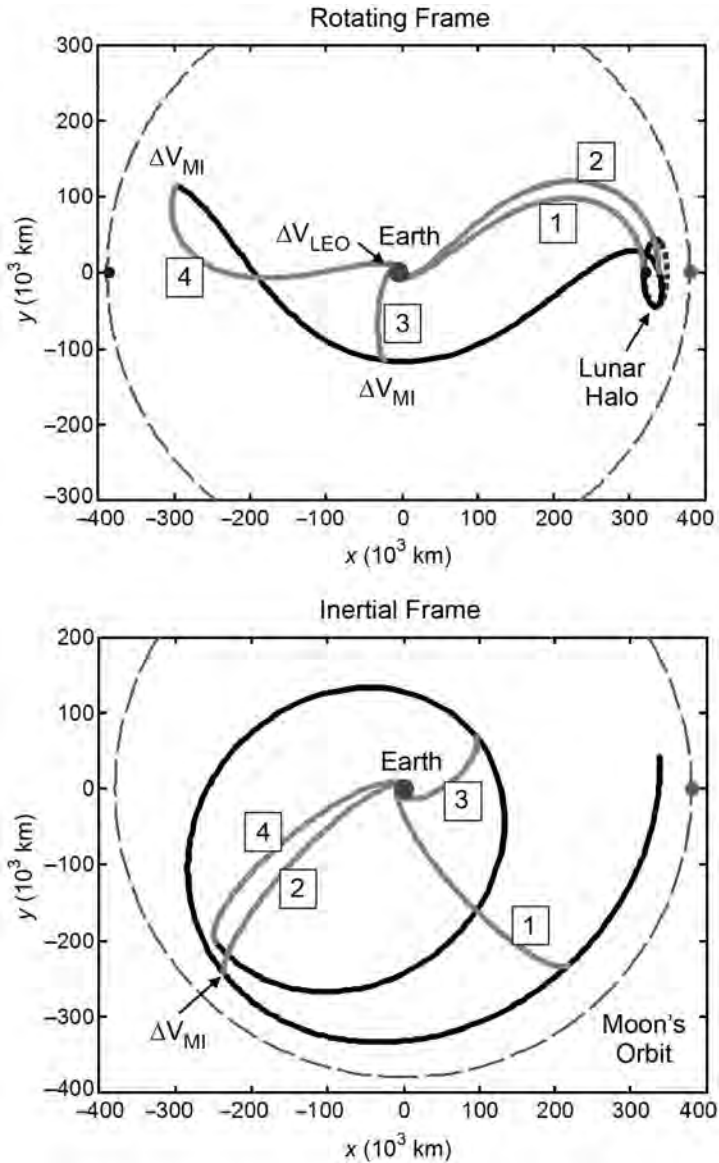


Figure 3-11 The four transfers with locally extreme ΔV requirements as indicated by the labels (1)–(4) in Fig. 3-10. The transfers are shown in the Earth–Moon rotating frame (top) and the corresponding inertial frame of reference (bottom) [174] (Copyright © 2008 by American Astronautical Society Publications Office, all rights reserved, reprinted with permission of the AAS).

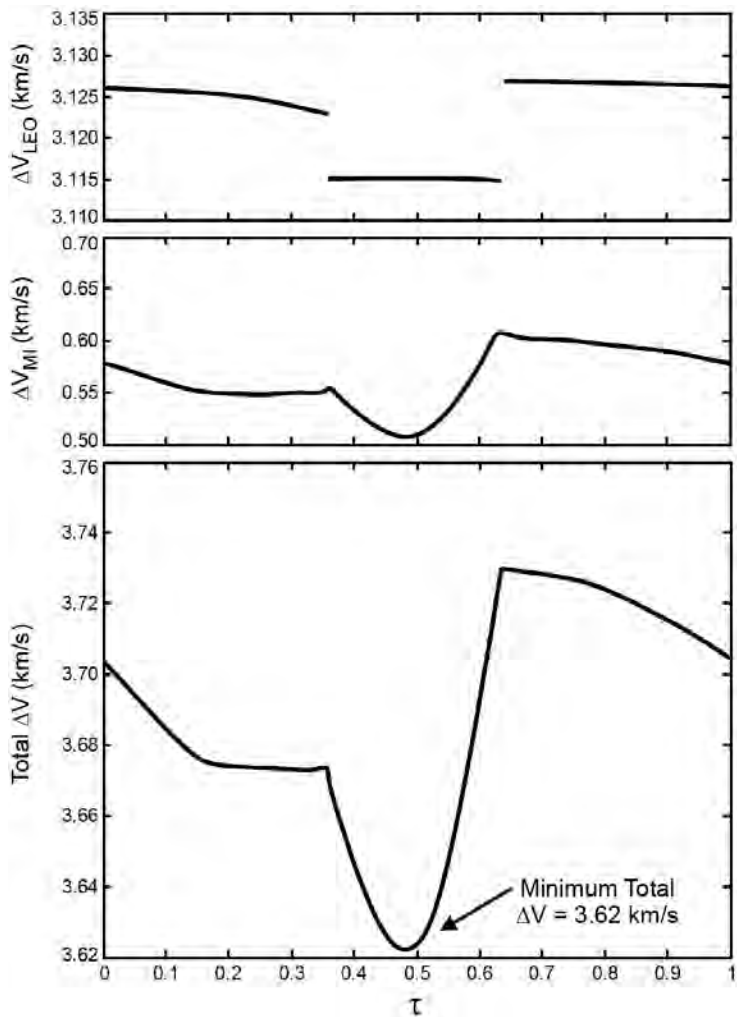


Figure 3-12 Plots of the magnitudes of the two required maneuvers ΔV_{LEO} and ΔV_{MI} (top) and the total ΔV cost (bottom) associated with the least-expensive lunar transfer for each trajectory on the stable manifold of a single lunar L_1 halo orbit.

stable manifolds. These results should be representative of other three-body orbits as well, such as Lissajous and vertical Lyapunov orbits.

The following sections summarize the results of four surveys performed here:

Section	Halo Family	Interior/Exterior Stable Manifold	Page Number
Section 3.3.4.1	L_1	Exterior	136
Section 3.3.4.2	L_1	Interior	140
Section 3.3.4.3	L_2	Exterior	142
Section 3.3.4.4	L_2	Interior	146

In each of these four cases, it would be ideal to perform an exhaustive search for the very best transfer to each halo orbit implementing the given stable manifold. However, it is very time-consuming to construct a transfer to each point along each trajectory in each halo orbit's stable manifold. The corresponding phase space is three-dimensional, and every combination of parameters takes a significant amount of computation time. To reduce the computation load, while still performing a survey of a large portion of the phase space, several numerical optimization routines have been implemented.

It has been found that a combination of hill-climbing and genetic algorithms performs very well at identifying the least-expensive transfers to a given halo orbit very swiftly [46]. The numerical algorithms use the state $X = [x_0, \tau, \Delta t_m]^T$ to define a direct two-maneuver lunar transfer, given the procedure outlined in Section 3.3.1. The numerical optimization process begins by implementing a genetic algorithm to identify a local ΔV -minimum in the phase space. The implementation of the genetic algorithm will not be discussed here for brevity, but may be found in many sources in literature [179]. After several iterations of the genetic algorithm, the state that corresponds to the least-expensive lunar transfer is refined using a dynamic hill-climbing algorithm, also known as the steepest-descent algorithm [180]. In this way, the local minima of the three-dimensional phase space are quickly explored. In order to survey specific orbits within a family of halo orbits, the parameter x_0 is held constant and the remaining two parameters are varied.

The majority of the locally-optimal transfers found in this work were identified by specifying a value for x_0 and varying the values of τ and Δt_m using ten iterations of a genetic algorithm with a population of twenty states. The least-expensive state resulting from the genetic algorithm was then iterated in the dynamic hill-climbing algorithm until a solution was found whose ΔV cost could not be improved by varying τ by more than 1×10^{-5} or by varying Δt_m by more than 4 seconds.

The numerical optimization routine is not guaranteed to converge on the most efficient transfer, but it easily converges on relatively efficient transfers. The results given in the following sections include the most efficient transfers identified, as well as somewhat less efficient transfers. The results then trace out a Pareto front of optimal solutions [181]. Other nonoptimal points have been added to the results to give an impression of the range of costs of transfers that exist. Each result is discussed in more detail in the following sections.

3.3.4.1 Survey of Exterior Transfers to L_1 Halo Orbits This section presents the results of open-point transfers constructed between 185-km LEO parking orbits and the exterior stable manifold of halo orbits in the family of lunar L_1 halo orbits. Figure 3-13 shows the cost of many such example transfers to halo orbits in the family. One can see that there are several types of efficient transfers. To help identify the trends and differences between each type of transfer, Fig. 3-14 shows plots of several example transfers. Finally, Tables 3-2 through 3-5 provide additional information about sample transfers of several varieties observed in the figures. Table 3-2 summarizes the characteristics of the numbered transfers shown in Fig. 3-14; Table 3-3 provides details about the shortest-duration transfers identified; Tables 3-4 and 3-5 summarize the transfers labeled “efficient” and “complex” in Fig. 3-13, respectively.

Figures 3-13 and 3-14 show many interesting patterns. After studying the transfers presented in these figures, as well as the corresponding data presented in Tables 3-2 through 3-5, the following observations have been made:

- The majority of the least-expensive transfers of this type are very fast transfers, requiring only five days to transfer to a close proximity of each corresponding halo orbit. Table 3-3 provides details about examples of such fast transfers. Their bridge segments take the spacecraft nearly directly to the halo orbit. These transfers compose the majority of the Pareto front observed in the figures.

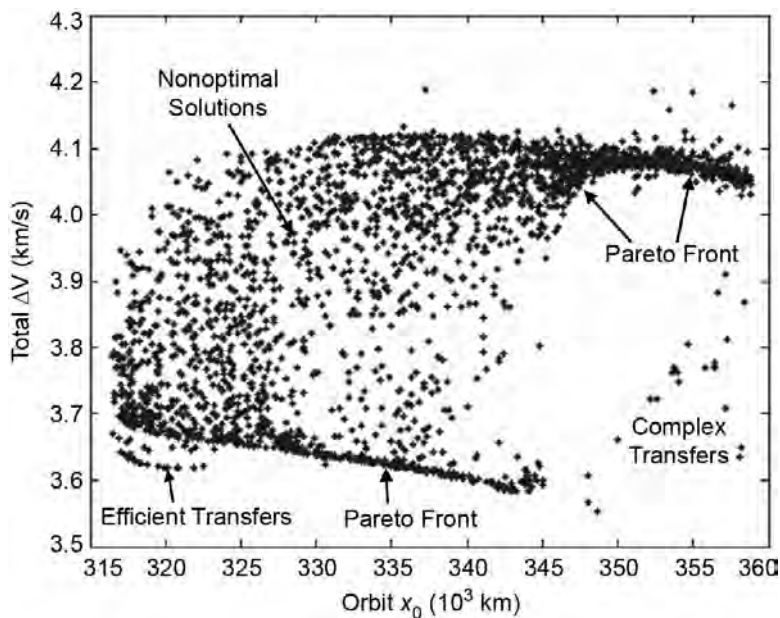


Figure 3-13 The total ΔV cost of many surveyed transfers to the exterior stable manifold of orbits in the family of lunar L_1 halo orbits.

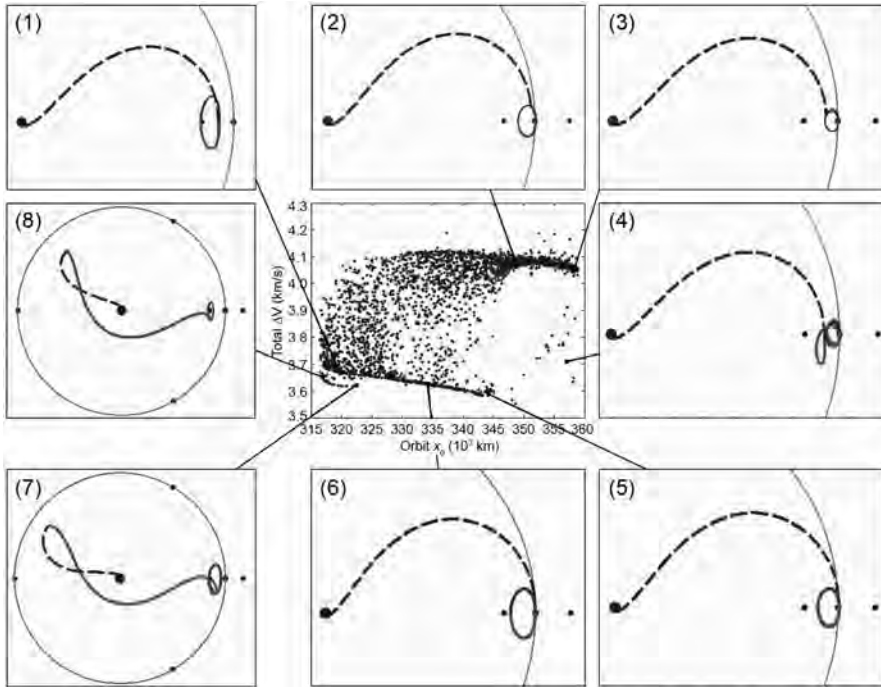


Figure 3-14 Several example transfers between 185-km LEO parking orbits and the exterior stable manifold of lunar L_1 halo orbits. The parameters of the numbered transfers are summarized in Table 3-2.

Table 3-2 Characteristics of the numbered transfers identified in Fig. 3-14 [174] (Copyright © 2008 by American Astronautical Society Publications Office, all rights reserved, reprinted with permission of the AAS).

#	x_0 (km)	ΔV_{LEO} (m/s)	ΔV_{MI} (m/s)	Total ΔV (m/s)	Inc* (deg)	Transfer Δt (days)	Bridge Δt (days)	Manifold Δt (days)	τ
1	320265	3128.0	539.0	3667.0	26.3	13.1	4.5	8.5	0.179
2	348963	3134.1	934.1	4068.2	8.2	8.8	4.7	4.1	0.888
3	357643	3132.9	923.1	4056.0	16.1	7.5	4.6	2.9	0.500
4	357177	3129.0	579.0	3708.0	25.7	30.6	4.6	26.0	0.501
5	342539	3136.2	453.5	3589.7	48.1	22.1	4.9	17.2	0.461
6	334016	3135.9	493.6	3629.5	46.9	28.8	4.9	23.9	0.911
7	322568	3119.2	503.1	3622.2	9.8	31.3	4.0	27.3	0.800
8	317035	3111.3	531.7	3643.0	5.0	23.5	3.4	20.1	0.281

*The inclination of the LEO parking orbit in the CRTBP.

Table 3-3 Characteristics of example fast transfers identified in Figs. 3-13 and 3-14 [174] (Copyright © 2008 by American Astronautical Society Publications Office, all rights reserved, reprinted with permission of the AAS).

x_0 (km)	ΔV_{LEO} (m/s)	ΔV_{MI} (m/s)	Total ΔV (m/s)	Inc (deg)	Transfer Δt (days)	Bridge Δt (days)	Manifold Δt (days)	τ
317406	3123.6	572.1	3695.7	17.0	7.6	4.4	3.1	0.757
318240	3125.3	558.3	3683.6	21.1	9.0	4.4	4.5	0.863
320569	3129.4	540.9	3670.3	30.0	5.4	4.6	0.7	0.543
324912	3133.4	522.2	3655.6	38.3	6.6	4.8	1.8	0.638
328382	3134.8	511.3	3646.2	42.2	6.8	4.8	2.0	0.664
332715	3135.7	497.9	3633.5	45.9	5.7	4.9	0.7	0.562
335440	3135.9	488.6	3624.5	47.7	5.7	4.9	0.8	0.566
339191	3136.1	471.9	3608.0	49.3	6.5	4.8	1.7	0.673
341814	3136.1	457.9	3594.0	49.5	8.2	4.8	3.5	0.878
345948	3135.8	876.0	4011.8	26.0	8.3	4.9	3.4	0.874
347333	3135.2	915.6	4050.8	13.4	7.3	4.8	2.5	0.745
350325	3133.4	940.5	4073.9	8.6	5.9	4.7	1.3	0.500
353906	3132.5	940.7	4073.2	12.7	6.7	4.6	2.1	0.500
357643	3132.9	923.1	4056.0	16.1	7.5	4.6	2.9	0.500

Table 3-4 Characteristics of example transfers from the family labeled “Efficient Transfers” in Fig. 3-13 [174] (Copyright © 2008 by American Astronautical Society Publications Office, all rights reserved, reprinted with permission of the AAS).

x_0 (km)	ΔV_{LEO} (m/s)	ΔV_{MI} (m/s)	Total ΔV (m/s)	Inc (deg)	Transfer Δt (days)	Bridge Δt (days)	Manifold Δt (days)	τ
316507	3108.9	561.7	3670.6	1.4	22.3	3.4	18.9	0.204
317035	3111.3	531.7	3643.0	5.0	23.5	3.4	20.1	0.281
317353	3112.1	524.8	3636.9	5.7	24.0	3.5	20.5	0.312
317721	3112.9	519.0	3631.9	6.3	24.6	3.5	21.1	0.348
318219	3113.8	513.2	3627.0	6.9	25.4	3.6	21.8	0.398
318745	3114.7	508.7	3623.4	7.5	26.2	3.6	22.6	0.453
319497	3115.8	504.6	3620.3	8.1	27.4	3.7	23.7	0.525
320179	3116.7	502.3	3619.0	8.6	28.3	3.7	24.6	0.583
320899	3117.6	501.2	3618.8	9.1	29.2	3.8	25.5	0.645
321932	3118.7	501.1	3619.8	9.6	30.7	3.8	26.8	0.743

- The bridge segments that do connect the spacecraft nearly directly with the halo orbit appear to do so in an organized manner. For halo orbits with x_0 -values below a value of approximately 345,000 km, the bridge segments connect the spacecraft with the far side of the halo orbit. Beyond x_0 -values of 345,000 km,

Table 3-5 Characteristics of example transfers from those labeled “Complex Transfers” in Fig. 3-13 [174] (Copyright © 2008 by American Astronautical Society Publications Office, all rights reserved, reprinted with permission of the AAS).

x_0 (km)	ΔV_{LEO} (m/s)	ΔV_{MI} (m/s)	Total ΔV (m/s)	Inc (deg)	Transfer Δt (days)	Bridge Δt (days)	Manifold Δt (days)	τ
348011	3137.0	430.7	3567.6	31.9	28.4	4.2	24.2	0.476
352619	3135.9	587.1	3723.0	32.7	31.7	4.5	27.3	0.904
354615	3136.4	669.3	3805.7	19.7	29.9	4.3	25.6	0.703
358106	3134.2	501.1	3635.3	24.8	31.2	4.9	26.3	0.499
358150	3131.1	519.1	3650.2	15.7	31.8	4.6	27.2	0.499

that is, for very large z -amplitude halo orbits, the optimal direct transfers tend to connect closer to the near-side of the halo orbit. This pattern may be observed in the plots shown around the perimeter of Fig. 3-14.

- A family of very efficient direct transfers of this kind appears for transfers to halo orbits with x_0 -values between approximately 316,000 km and approximately 323,000 km. The bridge segments of these transfers connect the spacecraft with the first apogee of the manifold segments after the manifold segments traverse to the opposite side of the Earth–Moon system. This family of transfers may be seen on the left side of the figures and corresponds to halo orbits that have small z -amplitudes. Table 3-4 summarizes additional details about these transfers.
- A few transfers have been found that require less total ΔV than the vast majority of locally optimal transfers. These transfers appear toward the lower right portion of the plot shown in Fig. 3-13 and are labeled as complex transfers. These transfers tend to involve several close flybys of the Moon. This study has not fully explored these transfers, since they are much more complicated by nature, but Table 3-5 provides details about several example transfers of this type.
- The transfers shown in Figs. 3-13 and 3-14 implement LEO parking orbits with ecliptic inclinations anywhere between 0 deg and 50 deg. The equatorial inclination, by comparison, depends on the specific launch date and varies from the ecliptic inclination by as much as ± 23.45 deg.
- The duration of time required to transfer within 100 km of the halo orbit may be anywhere between 5–30 days. Transfers may certainly be constructed that require more time; however, these transfers are not considered in this study since they may be more influenced by the Sun’s gravity.
- The least-expensive transfers to lunar L_1 halo orbits following their exterior stable manifolds generally require a total ΔV no smaller than approximately

3.60 km/s, depending on the halo orbit of choice. Halo orbits with x_0 -values greater than approximately 345,000 km tend to require more total ΔV : in the range of $4.05 \text{ km/s} \leq \Delta V \leq 4.08 \text{ km/s}$.

In many practical missions, the launch vehicle provides a set amount of ΔV , given a payload mass, and mission designers must optimize their transfer trajectories around that performance. Hence, many times it is useful to consider the two transfer maneuvers separately as well as the total cost of the transfer. Figure 3-15 shows the magnitudes of the two maneuvers separately, which combine to produce the total ΔV cost of the transfers shown in Figs. 3-13 and 3-14. One can see that nearly all of the transfers require the magnitude of the trans-lunar injection maneuver (ΔV_{LEO}) to be between 3.120 and 3.136 km/s. This suggests that the same launch vehicle can perform the trans-lunar injection maneuver for nearly all of these transfers given the same payload mass. Although it is difficult to see in these plots, the least-expensive transfers require the most-expensive ΔV_{LEO} -magnitudes. The second maneuver, ΔV_{MI} , contributes most of the variations seen in the total cost of the lunar transfer.

3.3.4.2 Survey of Interior Transfers to L_1 Halo Orbits This section presents the survey of transfers constructed between 185-km LEO parking orbits and the interior stable manifold of halo orbits in the family of lunar L_1 halo orbits. Figure 3-16 shows the cost of many such example transfers, where several families of locally optimal transfers have been plotted in a more prominent shade. Other nonoptimal transfers have been scattered about the plot to demonstrate that an entire field of options are available. To help identify the trends and differences between each type of transfer, Fig. 3-17 shows plots of several example transfers and Tables 3-6 through 3-9 summarize the characteristics of many of these transfer types.

The following observations may be made after studying the plots shown in Figs. 3-16 and 3-17 and the data displayed in Tables 3-6 through 3-9:

- The same types of *fast* transfers exist to L_1 halo orbits via their interior stable manifolds as via their exterior stable manifolds, because the manifold segments of those transfers do not extend far beyond the halo orbits. Hence, the cost and performance of such fast transfers closely resemble the cost of the fast transfers explored in Section 3.3.4.1. This is apparent when comparing the data shown in Tables 3-3 and 3-7.
- Many families of longer-duration transfers exist that often require less total ΔV than the faster transfers. Examples of these transfers may be seen in the lower left and lower right regions of Figs. 3-16 and 3-17, as well as in Tables 3-8 and 3-9. In general, each of these transfers involves at least one close lunar encounter, and many are constructed by intersecting the transfer's bridge segment with a point very near apogee of the transfer's manifold segment.
- The transfers shown in Figs. 3-16 and 3-17 implement LEO parking orbits with ecliptic inclinations anywhere between 0 deg and 60 deg. Again, the equatorial inclinations of the LEO parking orbits depend on the launch date.

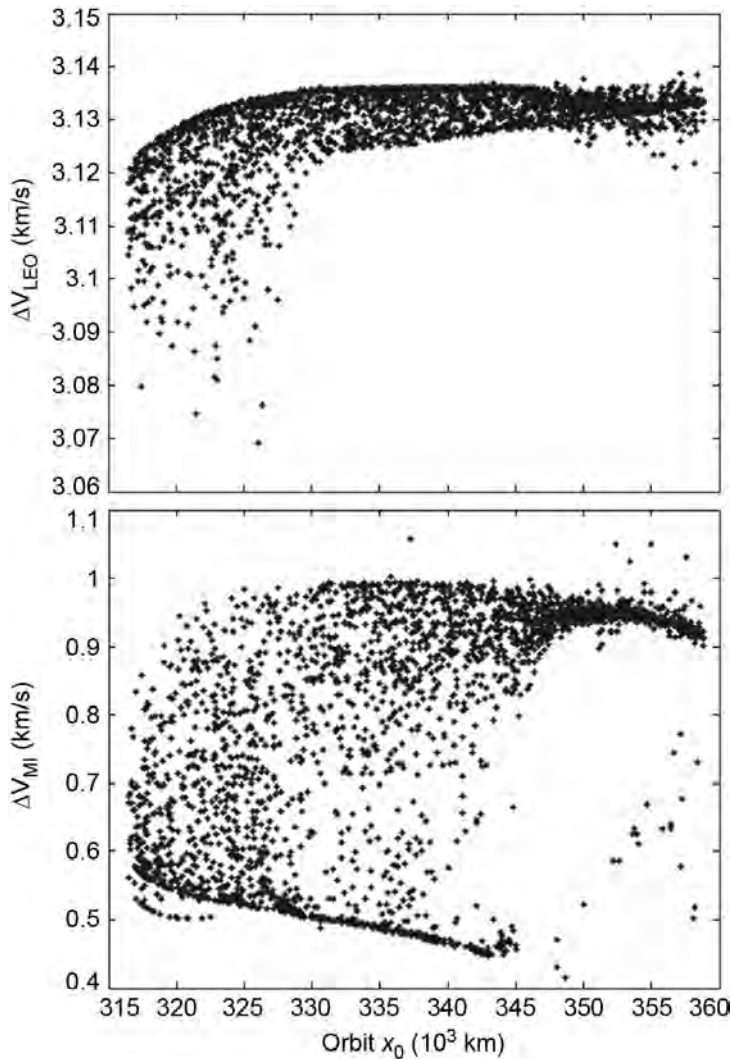


Figure 3-15 The two transfer maneuver magnitudes that combine to produce the total ΔV cost of the transfers shown in Figs. 3-13 and 3-14. Top: The magnitudes of the trans-lunar injection maneuvers (ΔV_{LEO}) in each transfer; bottom: The magnitudes of the manifold-insertion maneuvers (ΔV_{MI}) in each transfer.

- The least-expensive transfers to lunar L_1 halo orbits following their interior stable manifolds generally require a total ΔV no smaller than approximately 3.60 km/s, depending on the halo orbit of choice. The trend is very similar to that presented in Section 3.3.4.1 for short-duration lunar halo transfers.

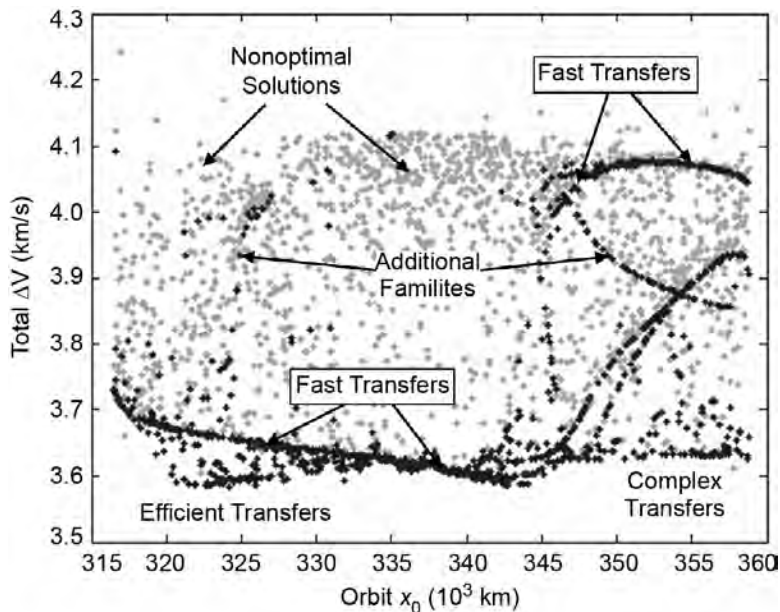


Figure 3-16 The total ΔV cost of many surveyed transfers to the interior stable manifold of orbits in the family of lunar L_1 halo orbits. Dark points correspond to locally optimal trajectories; faint points represent additional nonoptimal solutions.

To continue this analysis, Fig. 3-18 shows the magnitudes of the two deterministic maneuvers separately. One can see that the total ΔV cost of each transfer is divided between the two maneuvers in a very similar way as the exterior transfers shown in Section 3.3.4.1. Many of the transfers require a trans-lunar injection maneuver magnitude (ΔV_{LEO}) between 3.120 and 3.136 km/s. Some of the families of more-efficient transfers require smaller ΔV_{LEO} -magnitudes. Even with these slight reductions, the second maneuver, ΔV_{MI} , still contributes most of the variations seen in the total cost of the lunar transfer.

3.3.4.3 Survey of Exterior Transfers to L_2 Halo Orbits This section presents the survey of transfers constructed between 185-km LEO parking orbits and the exterior stable manifold of halo orbits in the family of lunar L_2 halo orbits. Figure 3-19 shows the cost of many such example transfers to halo orbits in the family, including a Pareto front of optimal transfers. To help identify the trends and differences between each type of transfer, Fig. 3-20 shows plots of several example transfers, and Tables 3-10 through 3-13 summarize the characteristics of many sample transfers of this type.

Figures 3-19 and 3-20 show many interesting patterns. After studying the transfers presented in these figures, and the data summarized in Tables 3-10 through 3-13, the following observations have been made:

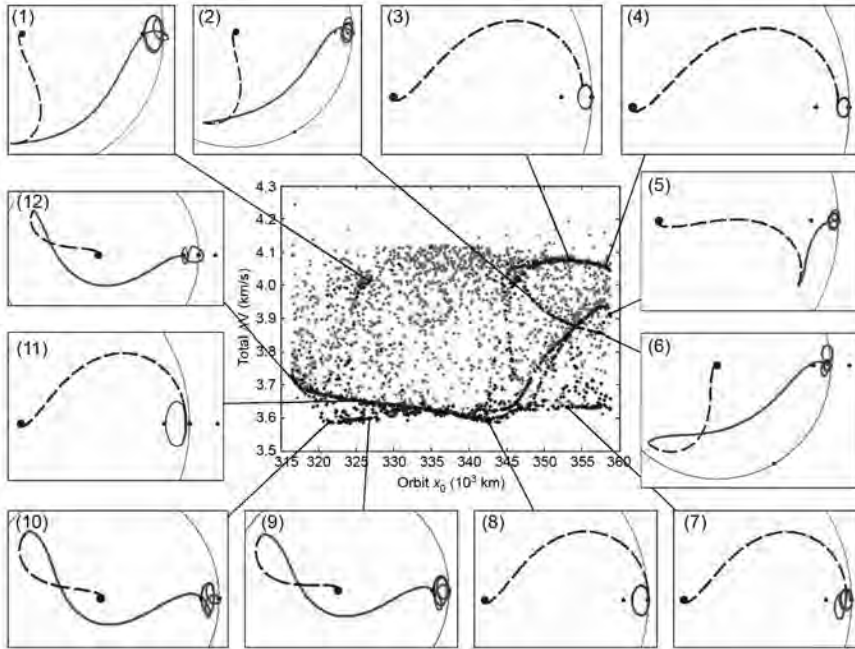


Figure 3-17 Several example transfers between 185-km LEO parking orbits and the interior stable manifold of lunar L_1 halo orbits. The parameters of the numbered transfers are summarized in Table 3-6. Dark points correspond to locally optimal trajectories; faint points represent additional nonoptimal solutions.

- Two dominant types of efficient transfers exist that transfer to the halo orbits' exterior stable manifold. The first one, indicated by the upper prominent curve in Fig. 3-19, includes transfers whose bridge segments connect the spacecraft directly with the far side of the L_2 halo orbit. These are short-duration transfers, characterized by data shown in Table 3-11, and they are similar to the short-duration transfers explored in Sections 3.3.4.1 and 3.3.4.2. The second dominant type of transfer, indicated by the lower prominent curve in Fig. 3-19, includes trajectories whose bridge segments send the spacecraft well beyond the Moon, where they intersect the corresponding manifold segments near the segments' apogee points. The first type of transfer requires only 5–6 days to accomplish, whereas the second type requires as many as 35–50 days before the spacecraft is within 100 km of the lunar halo orbit.
- Additional benefit may be obtained for transfers to L_2 halos with x_0 -values greater than approximately 425,000 km by flying near the Moon en route to the ΔV_{MI} maneuver. The lunar flyby reduces the total required ΔV , albeit at the expense of more sensitive navigation requirements near that lunar flyby.

Table 3-6 Characteristics of the numbered transfers identified in Fig. 3-17 [174] (Copyright © 2008 by American Astronautical Society Publications Office, all rights reserved, reprinted with permission of the AAS).

#	x_0 (km)	ΔV_{LEO} (m/s)	ΔV_{MI} (m/s)	Total ΔV (m/s)	Inc* (deg)	Transfer Δt (days)	Bridge Δt (days)	Manifold Δt (days)	τ
1	326808	3111.3	902.6	4013.9	12.2	48.8	3.5	45.4	0.447
2	348529	3118.2	837.7	3955.9	12.1	58.4	3.9	54.6	0.193
3	353325	3132.6	941.9	4074.5	12.0	8.7	4.6	4.1	0.772
4	358234	3129.9	920.8	4050.8	18.3	24.1	4.5	19.6	0.499
5	358745	3116.7	796.4	3913.1	17.5	39.4	3.9	35.5	0.660
6	357400	3127.1	729.5	3856.6	10.6	57.3	4.3	53.0	0.008
7	353001	3133.0	498.9	3631.9	27.0	37.6	4.7	32.9	0.456
8	341601	3136.2	462.4	3598.6	51.9	25.7	4.9	20.8	0.848
9	326786	3121.0	477.5	3598.5	9.3	48.5	3.9	44.6	0.756
10	321441	3117.8	469.6	3587.4	7.9	39.7	3.8	35.9	0.121
11	325594	3133.8	520.1	3653.9	39.5	6.2	4.8	1.4	0.609
12	317083	3111.4	593.1	3704.5	6.7	31.5	3.5	28.0	0.079

*The inclination of the LEO parking orbit in the CRTBP.

Table 3-7 Characteristics of example fast transfers identified in Figs. 3-16 and 3-17 [174] (Copyright © 2008 by American Astronautical Society Publications Office, all rights reserved, reprinted with permission of the AAS).

x_0 (km)	ΔV_{LEO} (m/s)	ΔV_{MI} (m/s)	Total ΔV (m/s)	Inc (deg)	Transfer Δt (days)	Bridge Δt (days)	Manifold Δt (days)	τ
316536	3121.0	607.9	3728.9	7.0	8.2	4.3	3.9	0.834
318562	3126.3	556.5	3682.9	23.3	7.5	4.5	3.0	0.738
320977	3130.0	538.2	3668.2	31.3	6.5	4.7	1.8	0.635
324263	3133.1	523.2	3656.4	37.5	9.5	4.7	4.7	0.892
328038	3134.8	513.0	3647.8	41.7	4.9	4.8	0.1	0.487
331309	3135.5	500.8	3636.2	44.2	9.2	4.8	4.3	0.905
335684	3135.9	485.5	3621.5	47.6	9.2	4.8	4.4	0.946
339602	3136.1	469.3	3605.4	50.0	7.7	4.8	2.9	0.805
341979	3136.1	456.2	3592.3	49.9	9.5	4.8	4.7	0.025
345722	3135.9	859.6	3995.5	30.4	6.6	4.9	1.7	0.671
347918	3134.8	924.3	4059.2	10.1	7.1	4.8	2.4	0.707
349968	3133.6	939.0	4072.6	8.4	8.5	4.6	3.8	0.828
351974	3132.9	942.7	4075.6	10.4	8.3	4.6	3.7	0.764
354725	3132.5	939.9	4072.5	13.7	5.0	4.7	0.3	0.256
358661	3133.3	910.4	4043.7	16.7	7.8	4.6	3.2	0.500

Table 3-8 Characteristics of example transfers from the region labeled “Efficient Transfers” in Fig. 3-16. The rows of the table are organized in groups, where each group describes example transfers in a different family [174] (Copyright © 2008 by American Astronautical Society Publications Office, all rights reserved, reprinted with permission of the AAS).

x_0 (km)	ΔV_{LEO} (m/s)	ΔV_{MI} (m/s)	Total ΔV (m/s)	Inc (deg)	Transfer Δt (days)	Bridge Δt (days)	Manifold Δt (days)	τ
320688	3117.0	473.3	3590.3	7.9	38.3	3.8	34.6	0.057
321925	3118.2	468.3	3586.6	7.9	40.6	3.8	36.8	0.173
323219	3119.4	470.2	3589.6	8.0	44.6	3.8	40.8	0.456
324345	3120.2	476.2	3596.4	8.3	46.2	3.9	42.4	0.556
326087	3120.9	477.5	3598.4	8.8	47.8	3.9	43.9	0.686
327737	3121.3	480.6	3601.8	9.5	49.6	3.9	45.7	0.859
327189	3127.3	497.7	3625.0	15.3	45.4	4.3	41.1	0.658
328326	3129.4	491.6	3621.0	20.1	46.3	4.5	41.8	0.745
329353	3131.5	486.5	3618.0	25.9	47.1	4.7	42.5	0.830
330278	3133.7	480.9	3614.6	33.9	47.9	4.9	43.1	0.933
322265	3126.8	495.6	3622.4	18.1	31.2	4.4	26.8	0.212
325061	3128.2	498.4	3626.6	20.1	36.2	4.4	31.8	0.599
326012	3129.2	496.2	3625.4	22.5	36.9	4.5	32.5	0.669
328613	3130.8	496.3	3627.1	26.6	39.5	4.6	34.9	0.947
329737	3136.3	486.6	3622.8	52.5	29.0	4.9	24.1	0.861
329778	3136.5	486.8	3623.3	52.9	30.0	5.0	25.0	0.972
330195	3136.2	484.3	3620.6	51.8	33.7	4.8	28.8	0.326
330545	3136.2	487.4	3623.6	51.5	30.4	4.9	25.5	0.018

These transfers may be seen in the lower right portions of the plots shown in Figs. 3-19 and 3-20; Tables 3-12 and 3-13 compare the characteristics of transfers with and without the lunar flyby.

- The transfers shown in Figs. 3-19 and 3-20 implement LEO parking orbits with different ranges of ecliptic inclinations. The transfers indicated by the upper prominent curve in Fig. 3-19 may be launched from LEO parking orbits with ecliptic inclination values anywhere in the range of 0 deg–25 deg. Those transfers indicated by the lower prominent curve have a narrower range of 0 deg–19 deg. Finally, the lowest ΔV transfers shown in the lower right portion of the figures may implement LEO parking orbits with a much more broad range of ecliptic inclinations: anywhere in the range of 20 deg–120 deg and possibly beyond.

Table 3-9 Characteristics of example transfers in the region labeled “Complex Transfers” in Fig. 3-16. The examples summarized here belong to many different families, demonstrating the variety of transfers that exist [174] (Copyright © 2008 by American Astronautical Society Publications Office, all rights reserved, reprinted with permission of the AAS).

x_0 (km)	ΔV_{LEO} (m/s)	ΔV_{MI} (m/s)	Total ΔV (m/s)	Inc (deg)	Transfer Δt (days)	Bridge Δt (days)	Manifold Δt (days)	τ
351166	3134.5	501.3	3635.8	34.8	37.4	4.8	32.6	0.448
351444	3121.5	506.1	3627.5	11.6	49.9	3.9	46.0	0.515
352138	3135.3	528.4	3663.7	40.2	35.2	4.7	30.5	0.260
353639	3120.0	522.0	3642.0	12.7	50.0	3.8	46.3	0.508
355251	3135.1	529.1	3664.2	35.3	35.3	4.7	30.5	0.250
355550	3131.2	504.5	3635.7	19.5	37.5	4.6	32.9	0.405
355848	3121.8	508.6	3630.4	12.1	49.2	4.0	45.3	0.454
358221	3135.3	532.3	3667.6	31.6	35.1	4.7	30.4	0.108
358332	3130.8	501.3	3632.1	15.9	37.9	4.5	33.4	0.317
358677	3122.8	502.7	3625.5	13.0	50.2	4.0	46.2	0.374
358837	3135.6	523.4	3659.0	28.1	36.6	4.7	31.8	0.142

- The total ΔV cost of the least-expensive transfers to lunar L_2 halo orbits following their exterior stable manifolds greatly depend on which halo orbit is being targeted. Halo orbits with x_0 -values less than 385,000 km, that is, very large z -amplitude halo orbits, require no less than approximately 3.95 km/s to reach in this way. The cost steadily decreases for halo orbits with x_0 -values between 385,000 km and 415,000 km. Halo orbits with x_0 -values greater than approximately 415,000 km, that is, very low z -amplitude halo orbits, require no less than approximately 3.77 km/s to reach in this way. Finally, those halo orbits that may be reached using an additional lunar flyby en route have a total ΔV requirement that may be reduced to as low as approximately 3.69 km/s.

Once again, to continue this analysis, Fig. 3-21 shows the magnitudes of the two transfer maneuvers separately. One can see that the total ΔV cost of each transfer is divided between the two maneuvers in a similar way as the transfers shown in Sections 3.3.4.1 and 3.3.4.2. However, in these exterior transfers to the L_2 halo orbits, the first maneuver, ΔV_{LEO} , must perform somewhat larger ΔV s than it did for transfers to L_1 halo orbits: between 3.145 and 3.185 km/s. The second maneuver, ΔV_{MI} , still contributes most of the variations seen in the total cost of the lunar transfer.

3.3.4.4 Survey of Interior Transfers to L_2 Halo Orbits This section presents the survey of transfers constructed between 185-km LEO parking orbits and the interior stable manifold of halo orbits in the family of lunar L_2 halo orbits. Figure 3-22 shows the cost of many such example transfers to halo orbits in the family. Several families of locally optimal transfers have been highlighted in a more prominent

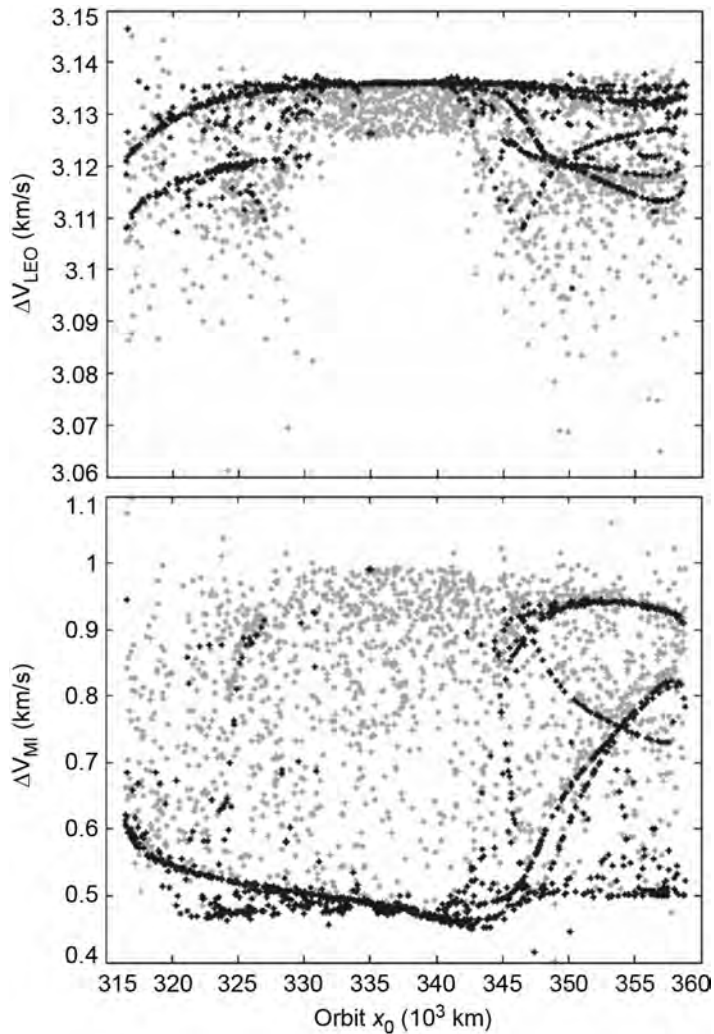


Figure 3-18 The two transfer maneuver magnitudes that combine to produce the total ΔV cost of the transfers shown in Figs. 3-16 and 3-17. Dark points correspond to locally optimal trajectories; faint points represent additional nonoptimal solutions. Top: The magnitudes of the trans-lunar injection maneuvers (ΔV_{LEO}) in each transfer; Bottom: The magnitudes of the manifold-insertion maneuvers (ΔV_{MI}) in each transfer.

shade to be distinguished from the scattered nonoptimal transfers. To help identify the trends and differences between each type of transfer, Fig. 3-23 shows plots of several example transfers and Tables 3-14 through 3-16 summarize the characteristics of many sample transfers of this type.

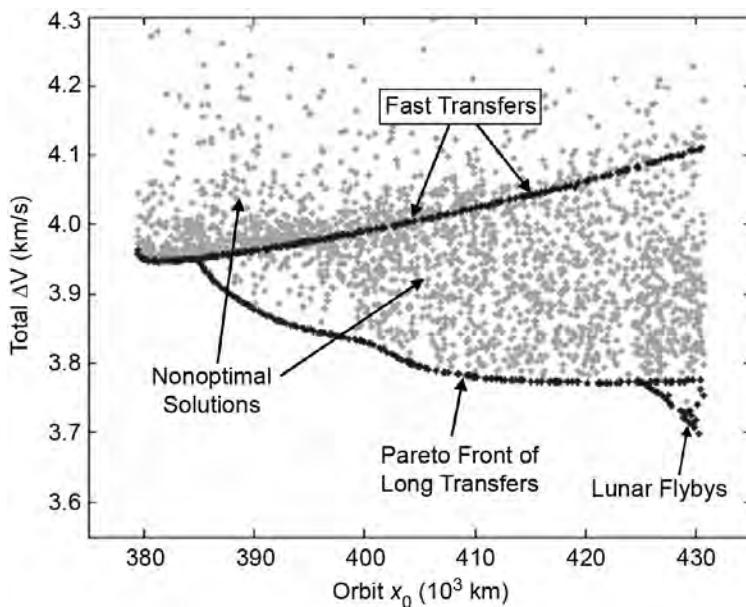


Figure 3-19 The total ΔV cost of many surveyed transfers to the exterior stable manifold of orbits in the family of lunar L_2 halo orbits, including a Pareto front of optimal solutions. Dark points correspond to locally optimal trajectories; faint points represent additional nonoptimal solutions.

The following observations may be made after studying the plots shown in Figs. 3-22 and 3-23 and the data presented in Tables 3-14 through 3-16:

- The most prominent upper curve in Fig. 3-22 is nearly identical to the most prominent curve in Fig. 3-19 from Section 3.3.4.3. This is because the manifold segments of the transfers along both of those curves do not depart far from the corresponding halo orbits. Both of these curves correspond to the shortest-duration transfers to lunar L_2 halo orbits, although they are certainly not the least-expensive in most cases.
- Many transfers exist that may be modeled as a transfer from LEO to an orbit about the Moon's L_1 point, followed by a transfer from L_1 to L_2 . It makes sense, then, that many transfers to L_2 require no more ΔV than transfers to L_1 . These transfers require more transfer time than the shortest-duration transfers previously described.
- The transfers shown in the lower left plots in Fig. 3-23 include manifold segments that extend well beyond the lunar vicinity. The bridge segments in those transfers connect with a point near one of the apogee points of the corresponding manifold segments. Several such families exist; in fact, a

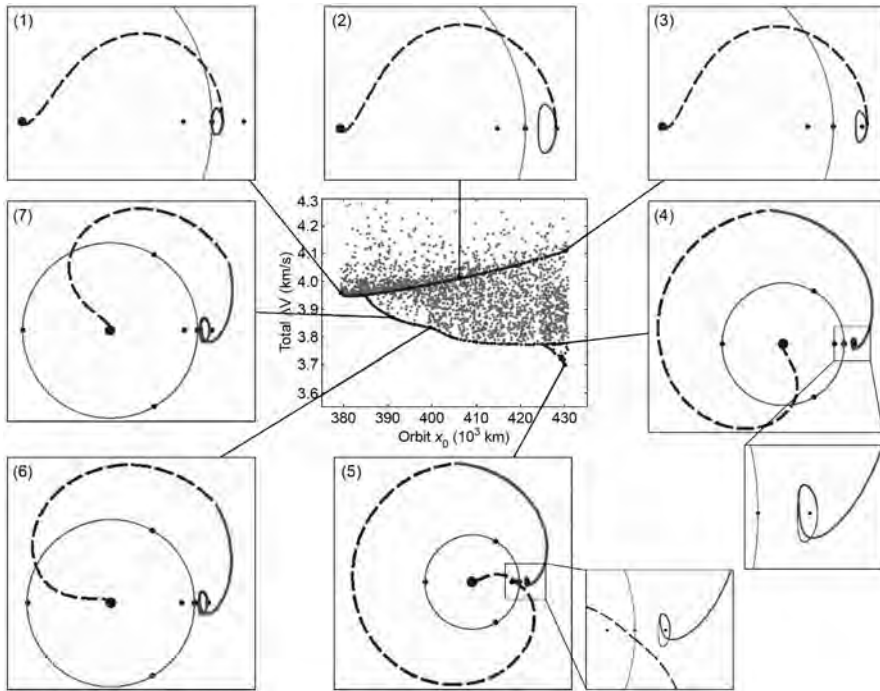


Figure 3-20 Several example transfers between 185-km low Earth orbits and the exterior stable manifold of lunar L_2 halo orbits. Dark points correspond to locally optimal trajectories; faint points represent additional nonoptimal solutions. Parameters of the transfers shown are summarized in Table 3-10.

different family may be produced for transfers that connect with any given apogee of the corresponding manifold segments. Figure 3-23 shows two plots of transfers that connect with the manifold segment's first apogee point opposite of the Moon, as well as one plot of a transfer that connects with the manifold segment's second apogee point. Families of transfers that intersect with later apogee points have not been produced here because they require longer transfer durations. The characteristics of example transfers from several of these families are shown in Table 3-16.

- There exist many types of transfers that make at least one close lunar passage en route to the L_2 halo orbit. It is apparent when studying the figures that the total required ΔV of a transfer is very dependent on the distance between the Moon and the manifold-insertion maneuver. That is, as the proximity of ΔV_{MI} with the Moon is reduced the total required ΔV in the transfer is reduced. This makes sense because more of the energy change in the transfer is performed

Table 3-10 Characteristics of the numbered transfers identified in Fig. 3-20 [174] (Copyright © 2008 by American Astronautical Society Publications Office, all rights reserved, reprinted with permission of the AAS).

#	x_0 (km)	ΔV_{LEO} (m/s)	ΔV_{MI} (m/s)	Total ΔV (m/s)	Inc* (deg)	Transfer Δt (days)	Bridge Δt (days)	Manifold Δt (days)	τ
1	379441	3142.6	820.4	3963.0	22.9	25.6	5.3	20.3	0.046
2	406016	3150.5	860.0	4010.4	13.4	9.4	5.9	3.5	0.740
3	430307	3152.4	957.0	4109.4	1.7	13.3	6.0	7.3	0.970
4	427287	3185.5	588.5	3774.1	3.2	44.2	16.9	27.3	0.465
5	430167	3162.2	536.4	3698.6	85.4	51.5	24.2	27.3	0.593
6	399548	3173.9	659.5	3833.4	9.1	39.2	11.9	27.3	0.004
7	391748	3169.2	696.2	3865.3	9.8	37.4	10.1	27.3	0.203

*The inclination of the LEO parking orbit in the CRTBP.

Table 3-11 Characteristics of example fast transfers observed in Figs. 3-19 and 3-20 [174] (Copyright © 2008 by American Astronautical Society Publications Office, all rights reserved, reprinted with permission of the AAS).

x_0 (km)	ΔV_{LEO} (m/s)	ΔV_{MI} (m/s)	Total ΔV (m/s)	Inc (deg)	Transfer Δt (days)	Bridge Δt (days)	Manifold Δt (days)	τ
382074	3146.3	801.5	3947.7	19.0	6.2	5.6	0.6	0.547
388716	3148.2	811.5	3959.7	17.1	7.5	5.7	1.8	0.636
400469	3149.9	842.4	3992.3	14.8	7.3	5.9	1.5	0.594
407319	3150.6	864.3	4014.8	13.4	6.2	6.0	0.2	0.506
412311	3151.0	881.8	4032.8	12.1	6.2	6.0	0.3	0.506
418589	3151.4	905.9	4057.3	10.0	6.2	6.0	0.3	0.506
423782	3151.8	927.8	4079.6	7.7	6.3	6.0	0.3	0.506
430202	3152.1	957.8	4109.9	2.0	6.3	6.0	0.2	0.506

deeper in a gravity well, where the spacecraft is traveling faster. The transfer shown in the lower right plot of Fig. 3-23 is a good example of this effect: its ΔV_{MI} is performed very close to the Moon; hence, its total ΔV cost is lower.

- Several of the nonoptimal transfers (plotted in a lighter shade in Fig. 3-22) appear to require less total ΔV than other locally optimal transfers. It is likely that those nonoptimal transfers are in a different class of transfer, that is, they require a different combination of lunar flybys en route to the L_2 halo orbit, such that the optimized transfers of that class require a longer transfer time. Only transfers requiring fewer than 60 days are plotted in the figures; the locally optimal transfers that require more than 60 days, and perhaps less total ΔV , are not displayed.

Table 3-12 Characteristics of example long-duration transfers observed in Figs. 3-19 and 3-20 that do not include a lunar flyby [174] (Copyright © 2008 by American Astronautical Society Publications Office, all rights reserved, reprinted with permission of the AAS).

x_0 (km)	ΔV_{LEO} (m/s)	ΔV_{MI} (m/s)	Total ΔV (m/s)	Inc (deg)	Transfer Δt (days)	Bridge Δt (days)	Manifold Δt (days)	τ
384950	3152.7	795.4	3948.1	12.3	33.2	6.4	26.8	0.650
392617	3169.9	689.9	3859.8	9.7	37.6	10.4	27.3	0.172
399992	3173.8	657.8	3831.5	9.1	39.1	11.8	27.3	0.988
407598	3178.5	607.7	3786.1	8.6	41.0	13.7	27.3	0.725
415027	3181.8	593.0	3774.7	7.2	42.4	15.1	27.3	0.600
422804	3184.3	588.5	3772.7	5.0	43.6	16.3	27.3	0.508
430370	3186.4	589.4	3775.8	0.9	44.7	17.4	27.3	0.440

Table 3-13 Characteristics of example long-duration transfers seen in Figs. 3-19 and 3-20 that do include a lunar flyby in their corresponding bridge segments.

x_0 (km)	ΔV_{LEO} (m/s)	ΔV_{MI} (m/s)	Total ΔV (m/s)	Inc (deg)	Transfer Δt (days)	Bridge Δt (days)	Manifold Δt (days)	τ
424719	3183.8	592.0	3775.9	22.1	50.9	23.6	27.3	0.684
426208	3182.5	578.6	3761.1	23.5	50.8	23.6	27.3	0.655
427590	3179.4	562.6	3742.0	30.9	51.0	23.7	27.3	0.631
428819	3174.2	549.2	3723.4	48.4	51.2	23.9	27.3	0.612
430167	3162.2	536.4	3698.6	85.4	51.5	24.2	27.3	0.593

- The transfers shown in Figs. 3-22 and 3-23 implement LEO parking orbits with ecliptic inclinations generally in the range of 0–55 deg.
- The duration of time required to transfer within 100 km of the halo orbit may be anywhere between 5 and 60 days.
- The least-expensive transfers to lunar L_2 halo orbits following their exterior stable manifolds generally require a total ΔV no smaller than approximately 3.60 or 3.65 km/s, depending on the halo orbit of choice.

The final analysis in this section is to study the performance of the two maneuvers separately for each interior lunar L_2 halo transfer. Figure 3-24 shows the magnitudes of the two transfer maneuvers. One can see that the majority of each transfer's ΔV cost is performed in the first maneuver, ΔV_{LEO} , but the variations in the magnitude of ΔV_{LEO} between transfers is very small, ranging between approximately 3.11 and 3.15 km/s. The second maneuver, ΔV_{MI} , although much smaller, has a great deal more variability and therefore determines the total cost of the transfer.

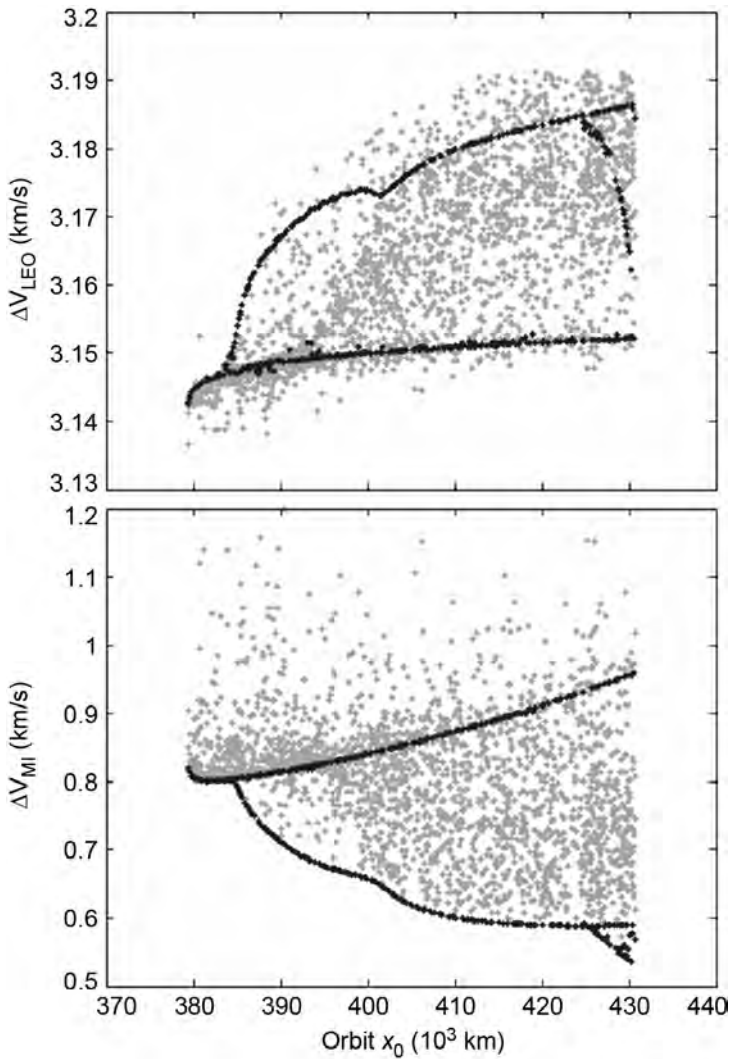


Figure 3-21 The two transfer maneuver magnitudes that combine to produce the total ΔV cost of the transfers shown in Figs. 3-19 and 3-20. Dark points correspond to locally optimal trajectories; faint points represent additional nonoptimal solutions. Top: The magnitudes of the trans-lunar injection maneuvers (ΔV_{LEO}) in each transfer. Bottom: The magnitudes of the manifold-insertion maneuvers (ΔV_{MI}) in each transfer.

3.3.5 Discussion of Results

The previous four sections surveyed four different types of direct lunar halo transfers; this section studies them together to draw several overall conclusions.

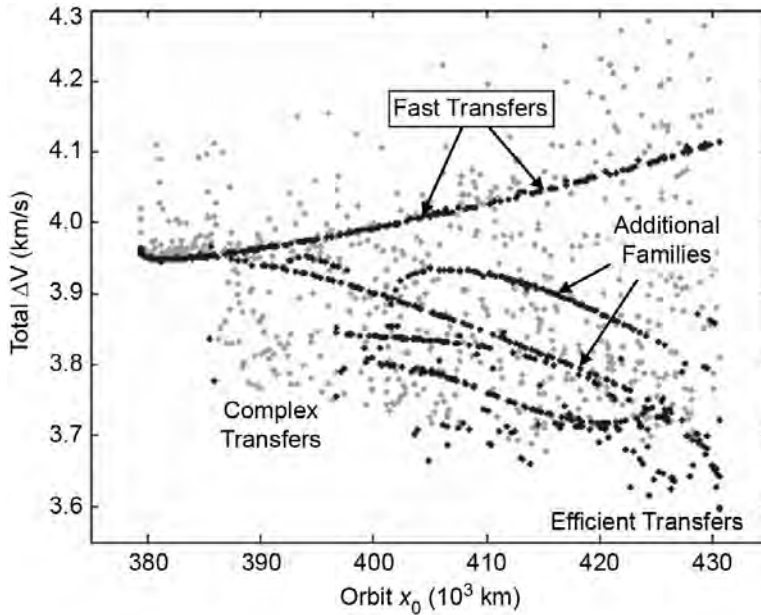


Figure 3-22 The total ΔV cost of many surveyed transfers to the interior stable manifold of orbits in the family of lunar L_2 halo orbits. Dark points correspond to locally optimal trajectories; faint points represent additional nonoptimal solutions.

Each of the results presented above implemented direct lunar transfers found by searching through only one half of the stable manifold of the targeted halo orbits. In reality, it most likely doesn't matter whether a particular trajectory implements an interior or an exterior transfer—just that the spacecraft arrives at the halo orbit in some way. Figure 3-25 shows a summary of the ΔV requirements for both interior and exterior transfers to lunar L_1 halo orbits, plotted in the same axes. Hence, Fig. 3-25 may be used to identify the least-expensive transfers to any lunar L_1 halo orbit no matter which type of manifold is taken. Figure 3-26 shows the same ΔV summary for transfers to lunar L_2 halo orbits.

Theoretically, it is possible to transfer to any given lunar L_2 halo orbit from a lunar L_1 halo orbit with the same Jacobi constant, and vice versa. The dynamical systems methodology presented in this work has been used in previous studies to construct low-energy orbit transfers and orbit chains [162]. To explore this concept further, Fig. 3-27 shows a plot of the Jacobi constant, C , of the lunar halo orbits surveyed in this work as a function of the halo orbits' x_0 -values. One can see that there is a lunar L_1 halo orbit with the same Jacobi constant as each and every lunar L_2 halo orbit in this study. The family of lunar L_2 halo orbits includes orbits with Jacobi constants in the approximate range $3.015 < C < 3.152$; the family of lunar L_1 halo orbits spans that entire range and then extends a bit further in each direction. In theory, it is thus

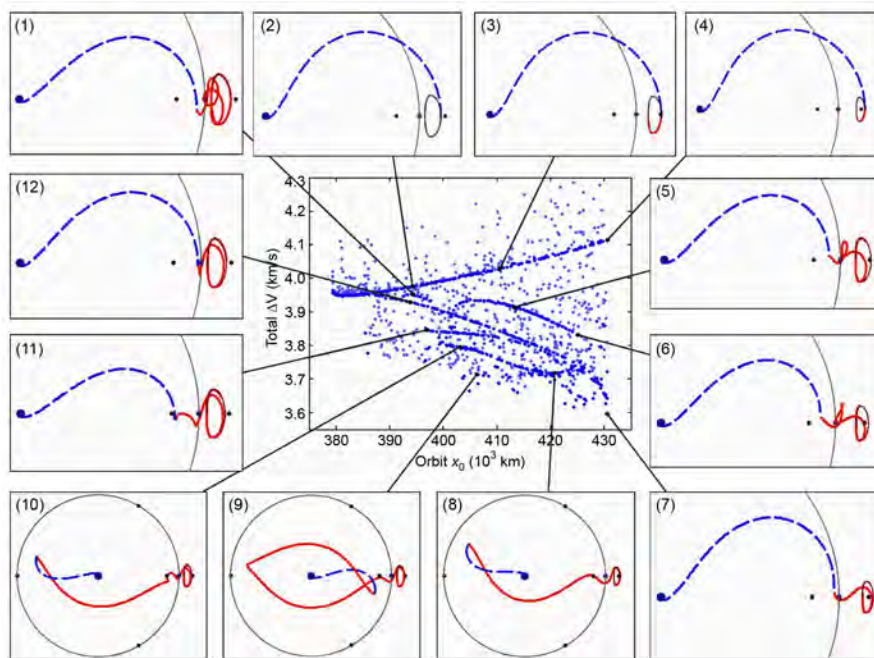


Figure 3-23 Several example transfers between 185-km LEO parking orbits and the interior stable manifold of lunar L_2 halo orbits. Dark points correspond to locally optimal trajectories; faint points represent additional nonoptimal solutions. The parameters of the numbered transfers are summarized in Table 3-14.

possible to transfer to any lunar L_2 halo orbit from the corresponding lunar L_1 halo orbit for very little energy.

Figure 3-28 shows the same results shown in Figs. 3-25 and 3-26, but now plotted as a function of the halo orbits' Jacobi constant values (C -values) rather than their x_0 -values. In this way, one can observe the minimum total ΔV required to reach any halo orbit of a particular Jacobi constant. Then, once in that orbit, one can theoretically transfer to a different desired orbit, provided the desired orbit has the same Jacobi constant. The left part of Fig. 3-28 shows transfers that may be used to reach only lunar L_1 halo orbits, since there are no lunar L_2 halo orbits with Jacobi constant values below 3.015. Figure 3-28 also shows that if a low-energy transfer can be found between halo orbits about L_1 and L_2 of a given Jacobi constant, it is almost always more efficient to transfer directly to the lunar L_1 halo orbit first, and then take the low-energy transfer over to the lunar L_2 halo orbit.

Halo orbits exist in two families: a northern and a southern family as illustrated in Fig. 2-25. Every lunar L_1 halo orbit explored in this work has been a member of the

Table 3-14 Characteristics of the numbered transfers identified in Fig. 3-23 [174] (Copyright © 2008 by American Astronautical Society Publications Office, all rights reserved, reprinted with permission of the AAS).

#	x_0 (km)	ΔV_{LEO} (m/s)	ΔV_{MI} (m/s)	Total ΔV (m/s)	Inc* (deg)	Transfer Δt (days)	Bridge Δt (days)	Manifold Δt (days)	τ
1	394370	3132.7	817.6	3950.3	31.9	38.6	4.7	34.0	0.951
2	394096	3149.0	824.6	3973.6	16.2	6.4	5.8	0.6	0.537
3	411239	3150.8	878.7	4029.4	12.4	12.4	5.9	6.5	0.948
4	429222	3152.0	953.8	4105.8	3.6	9.2	5.9	3.3	0.708
5	415075	3129.0	776.3	3905.3	19.9	25.4	4.5	20.9	0.288
6	425204	3126.7	705.0	3831.7	13.0	23.5	4.5	19.0	0.177
7	430641	3133.4	464.8	3598.2	5.6	18.3	5.2	13.1	0.034
8	420255	3112.2	605.2	3717.4	9.7	31.5	3.6	27.9	0.868
9	406534	3112.8	599.5	3712.3	20.9	49.2	3.8	45.4	0.112
10	403368	3113.6	676.7	3790.3	16.3	43.6	3.6	40.0	0.284
11	396769	3122.9	728.2	3851.1	17.9	31.3	4.1	27.2	0.356
12	393789	3135.7	792.6	3928.3	26.9	25.9	4.9	21.0	0.485

*The inclination of the LEO parking orbit in the CRTBP.

Table 3-15 Characteristics of example fast transfers observed in Figs. 3-22 and 3-23 [174] (Copyright © 2008 by American Astronautical Society Publications Office, all rights reserved, reprinted with permission of the AAS).

x_0 (km)	ΔV_{LEO} (m/s)	ΔV_{MI} (m/s)	Total ΔV (m/s)	Inc (deg)	Transfer Δt (days)	Bridge Δt (days)	Manifold Δt (days)	τ
383881	3147.0	802.9	3949.9	18.4	5.7	5.7	0.1	0.497
392708	3148.8	821.0	3969.8	16.5	5.9	5.8	0.1	0.495
401069	3149.9	844.3	3994.2	14.9	6.0	5.9	0.1	0.494
408865	3150.7	869.6	4020.3	13.1	6.0	5.9	0.1	0.494
416071	3151.2	896.0	4047.3	11.0	6.1	6.0	0.1	0.494
429548	3152.0	954.7	4106.7	3.2	6.1	6.1	0.0	0.493

northern family; every lunar L_2 halo orbit has been a member of the southern family. To access the symmetric family of halo orbits, in either case, the transfer must be reflected about the $z = 0$ plane. The only difference that would be noticeable in such a symmetric transfer would be that the LEO parking orbit's inclination relative to the Moon's orbital plane would have the opposite sign.

Table 3-16 Characteristics of example transfers within a collection of seven different sample families observed in Figs. 3-22 and 3-23. The families are identified by the number of the corresponding example plot shown around the perimeter of Fig. 3-23 [174] (Copyright © 2008 by American Astronautical Society Publications Office, all rights reserved, reprinted with permission of the AAS).

x_0 (km)	ΔV_{LEO} (m/s)	ΔV_{MI} (m/s)	Total ΔV (m/s)	Inc (deg)	Transfer Δt (days)	Bridge Δt (days)	Manifold Δt (days)	τ
<i>Family (12)</i>								
390299	3138.3	801.0	3939.3	26.9	27.6	5.0	22.5	0.607
395448	3134.5	787.5	3922.0	27.0	25.1	4.8	20.4	0.429
400189	3130.9	769.1	3900.0	25.6	23.7	4.6	19.1	0.302
405365	3128.0	744.0	3872.0	22.9	22.3	4.4	17.9	0.200
410586	3126.4	715.0	3841.4	19.9	21.3	4.4	16.9	0.126
415399	3125.9	685.8	3811.8	17.7	20.5	4.4	16.1	0.070
<i>Family (1)</i>								
394170	3132.7	818.8	3951.5	31.4	38.7	4.6	34.1	0.961
395343	3131.6	814.3	3945.9	35.1	38.2	4.6	33.6	0.873
395820	3130.3	812.9	3943.3	34.7	37.5	4.6	33.0	0.821
396907	3129.3	808.0	3937.4	31.4	35.7	4.5	31.2	0.737
<i>Family (11)</i>								
396738	3122.9	721.1	3844.0	14.9	30.2	4.1	26.1	0.240
402272	3119.7	717.4	3837.1	11.4	27.8	3.9	23.9	0.070
407548	3117.3	712.2	3829.5	8.4	25.8	3.8	22.0	0.973
413568	3116.3	695.0	3811.4	6.4	23.2	3.8	19.4	0.873
419902	3121.3	651.3	3772.6	10.0	21.0	4.2	16.7	0.808
425400	3126.1	600.1	3726.1	8.2	19.9	4.7	15.2	0.736
430618	3131.1	510.9	3642.0	0.2	19.2	5.2	14.0	0.648
<i>Family (5, 6)</i>								
401972	3121.6	782.7	3904.4	24.7	33.3	4.1	29.2	0.587
406699	3130.4	803.3	3933.7	22.0	28.3	4.6	23.7	0.440
411226	3130.0	793.3	3923.2	21.2	26.6	4.6	22.0	0.350
415688	3128.7	772.4	3901.0	19.3	25.3	4.5	20.8	0.281
420324	3127.5	742.3	3869.8	16.7	24.3	4.5	19.8	0.225
425204	3126.7	705.0	3831.7	13.0	23.5	4.5	19.0	0.177
429490	3126.4	668.3	3794.7	6.7	23.0	4.6	18.4	0.144
<i>Family (8, 10)</i>								
399413	3114.9	687.4	3802.3	15.7	41.4	3.7	37.7	0.145
403744	3112.9	679.1	3792.0	16.7	38.7	3.6	35.0	0.053
408970	3112.5	654.2	3766.7	15.7	35.1	3.5	31.5	0.999
413531	3112.7	626.8	3739.5	13.3	33.4	3.6	29.8	0.936
418227	3112.5	607.8	3720.3	10.7	31.9	3.5	28.4	0.887

Table 3-16 Continued.

x_0 (km)	ΔV_{LEO} (m/s)	ΔV_{MI} (m/s)	Total ΔV (m/s)	Inc (deg)	Transfer Δt (days)	Bridge Δt (days)	Manifold Δt (days)	τ
<i>Family (8, 10) (cont'd)</i>								
422292	3112.0	608.8	3720.7	8.5	31.3	3.5	27.8	0.853
425682	3111.4	640.5	3751.9	6.1	31.5	3.5	28.0	0.837
427668	3110.3	690.6	3801.0	4.2	32.4	3.5	28.9	0.830
<i>Family (9)</i>								
416120	3112.2	603.2	3715.5	10.4	43.7	3.5	40.2	0.950
418419	3111.7	600.1	3711.8	10.1	42.9	3.5	39.4	0.898
420564	3111.4	599.0	3710.4	9.2	42.4	3.5	38.9	0.873
423526	3110.8	605.7	3716.5	7.6	42.3	3.5	38.8	0.849
425847	3110.2	619.5	3729.7	6.0	43.0	3.5	39.5	0.836
<i>Nearby (7)</i>								
417319	3111.8	617.5	3729.3	13.0	43.4	3.5	39.9	0.194
420771	3110.7	586.4	3697.1	13.0	42.4	3.4	39.0	0.086
422285	3110.5	569.7	3680.1	12.4	42.2	3.4	38.8	0.055
425306	3110.8	536.4	3647.2	9.0	40.7	3.5	37.3	0.004
426565	3110.6	529.4	3640.0	7.5	40.5	3.5	37.0	0.981

3.3.6 Reducing the ΔV Cost

One notices that the transfers that require the least ΔV presented in the previous sections involve missions that perform the majority of the energy-changing maneuvers deep within either the Earth's or the Moon's gravity wells where the spacecraft is moving the fastest. The most convincing example of this is the trajectory labeled (7) in Fig. 3-23: the Earth-departure maneuver is large enough to send the spacecraft out to the radius of the Moon, and the manifold-insertion maneuver is performed quite close to the Moon.

The trajectories designed here do not purposefully place the manifold-insertion maneuver near the Moon, and in fact, may not converge well if the maneuver occurs nearby. However, the total transfer ΔV may be reduced if the manifold-insertion maneuver were indeed performed near the Moon, and recent research supports this [172].

Performing a maneuver near the Moon may have energy benefits, but it does increase the operational complexity of the mission. The manifold-insertion maneuver becomes very time-critical when performed close to the Moon, and any execution errors tend to exponentially increase afterward. Other operational considerations are discussed in Chapter 6.

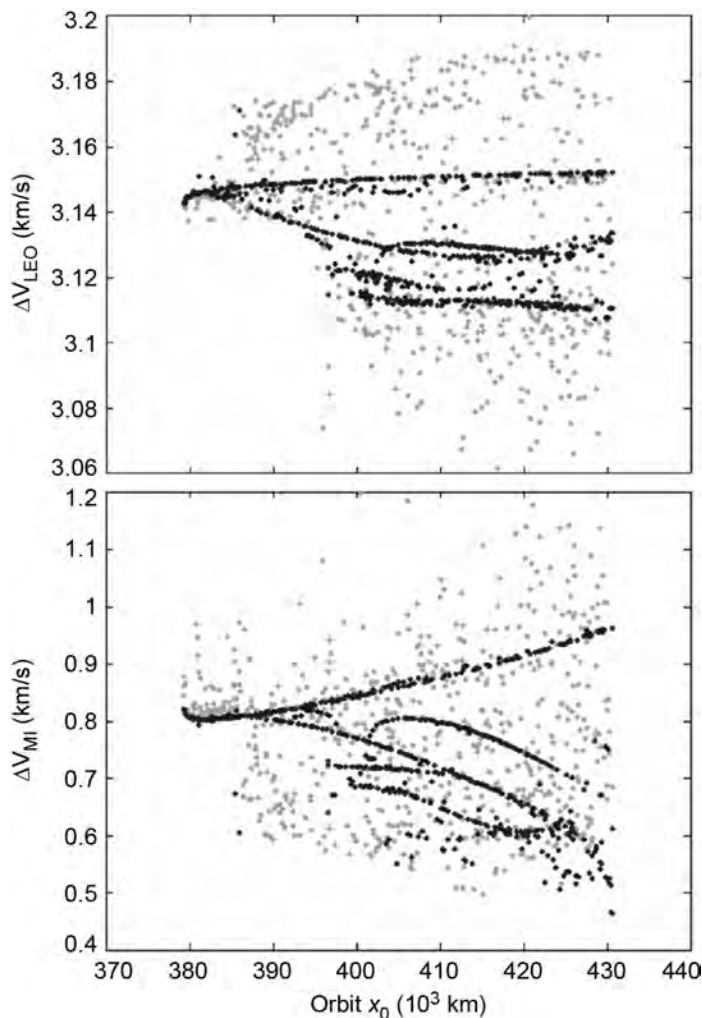


Figure 3-24 The two transfer maneuver magnitudes that combine to produce the total ΔV cost of the transfers shown in Figs. 3-22 and 3-23. Dark points correspond to locally optimal trajectories; faint points represent additional nonoptimal solutions. Top: The magnitudes of the trans-lunar injection maneuvers (ΔV_{LEO}) in each transfer; bottom: The magnitudes of the manifold-insertion maneuvers (ΔV_{MI}) in each transfer.

3.3.7 Conclusions

This section has explored direct transfers to lunar halo orbits. It has been found that short-duration transfers exist to both lunar L_1 and L_2 halo orbits, requiring approximately 5 days of transfer time. Such short-duration transfers require between

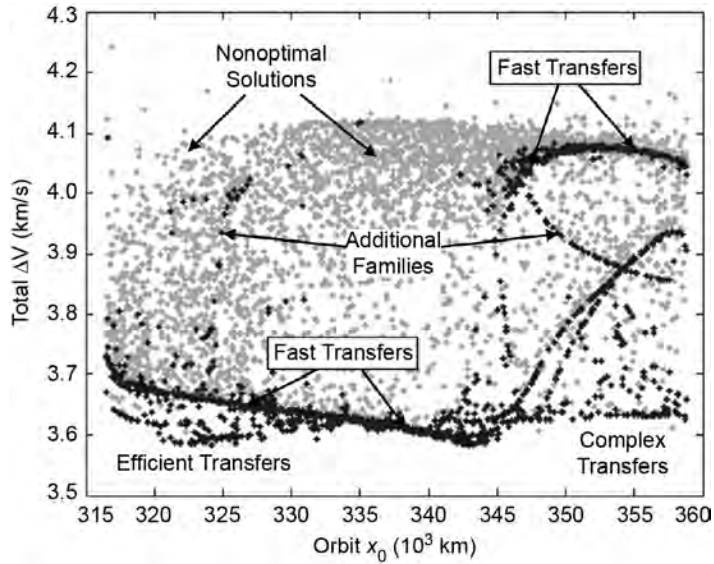


Figure 3-25 The total ΔV cost of many transfers to lunar L_1 halo orbits using either interior or exterior transfers.

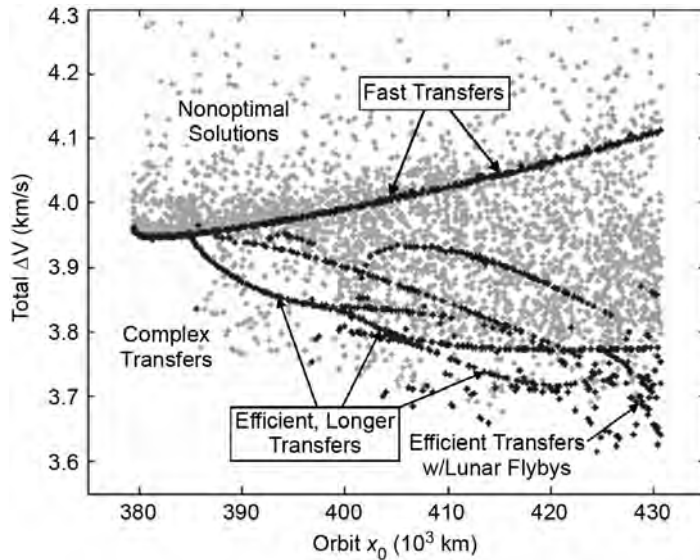


Figure 3-26 The total ΔV cost of many transfers to lunar L_2 halo orbits using either interior or exterior transfers.

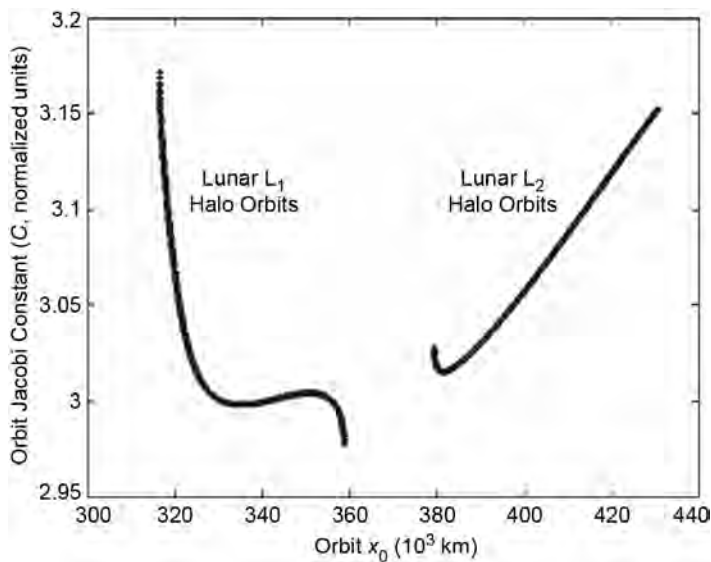


Figure 3-27 The Jacobi constant, C , of the lunar halo orbits surveyed in this work as a function of the halo orbits' x_0 -values.

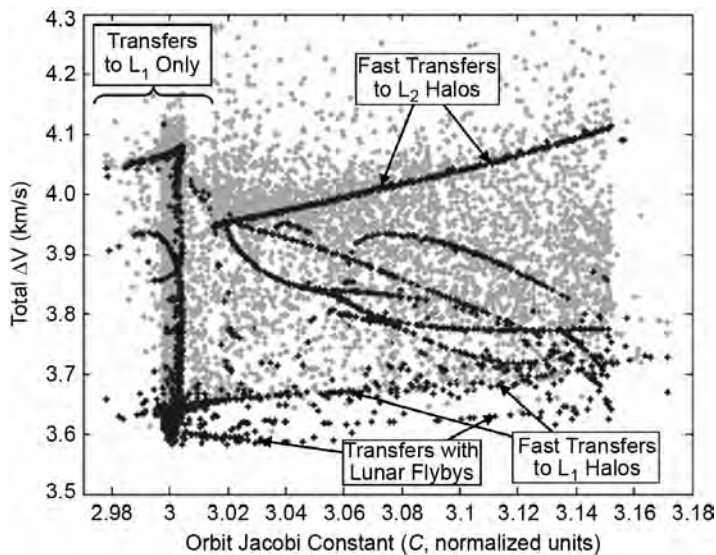


Figure 3-28 The total ΔV cost of direct lunar halo orbit transfers as a function of the halo orbits' Jacobi constant values.

3.6 and 4.1 km/s, depending on the halo orbit, when launched from a 185-km circular parking orbit. It has also been found that transfers exist between LEO and every halo orbit surveyed here that require as little as 3.59–3.65 km/s, although many of these transfers require 3 weeks or more of transfer time. Figure 3-29 summarizes the results, showing the least amount of total ΔV required to reach any halo orbit using the fastest optimized transfers, that is, transfers with a duration of approximately 5 days, as well as an envelope of longer low- ΔV transfers that require at most 2 months of transfer time. The curve representing the longer transfers is very approximate—it was produced by tracing out points that were produced successfully and interpolating between those points. Some of these transfers may be difficult to construct; other lower-cost transfers may also exist. Figure 3-30 summarizes the same results as a function of the halo orbits' C -values rather than their x_0 -values.

3.4 LOW-ENERGY TRANSFERS BETWEEN EARTH AND LUNAR LIBRATION ORBITS

Transfers between the Earth and lunar libration orbits may be constructed that require less fuel than direct transfers by taking advantage of the gravity of the Sun. The scenario involves propelling a spacecraft beyond the orbit of the Moon, about 1–2 million kilometers away from the Earth, and letting the Sun's gravity raise the spacecraft's energy. When the spacecraft returns toward its perigee after 2–4 months, it encounters the Moon. The spacecraft encounters the Moon at a much lower relative velocity than that of a direct transfer. The trajectory is crafted such that the spacecraft approaches the Moon on the stable manifold of the target lunar libration orbit.

This section illustrates low-energy transfers that arrive at a variety of lunar libration orbits, such that they require no orbit insertion maneuver whatsoever. The performance of many low-energy transfers is surveyed. First, Section 3.4.1 demonstrates how to model a low-energy transfer using dynamical systems theory. Then Section 3.4.2 provides an energy analysis of an example transfer, which illuminates how energy shifts and how one may use both two-body and three-body tools to design and analyze a low-energy transfer. Sections 3.4.3 and 3.4.4 describe the process of constructing desirable low-energy transfers in the patched three-body and DE421 ephemeris models, respectively. The dynamical systems methods used to construct low-energy transfers may be extended to construct entire families of transfers. Section 3.4.5 surveys many families of transfers that have different geometries and performance characteristics. Section 3.4.6 discusses how these transfers vary from one month to the next. Finally, Section 3.4.7 presents several additional example analyses to design low-energy transfers to different three-body orbits, including an LL_1 halo orbit and a distant prograde orbit.

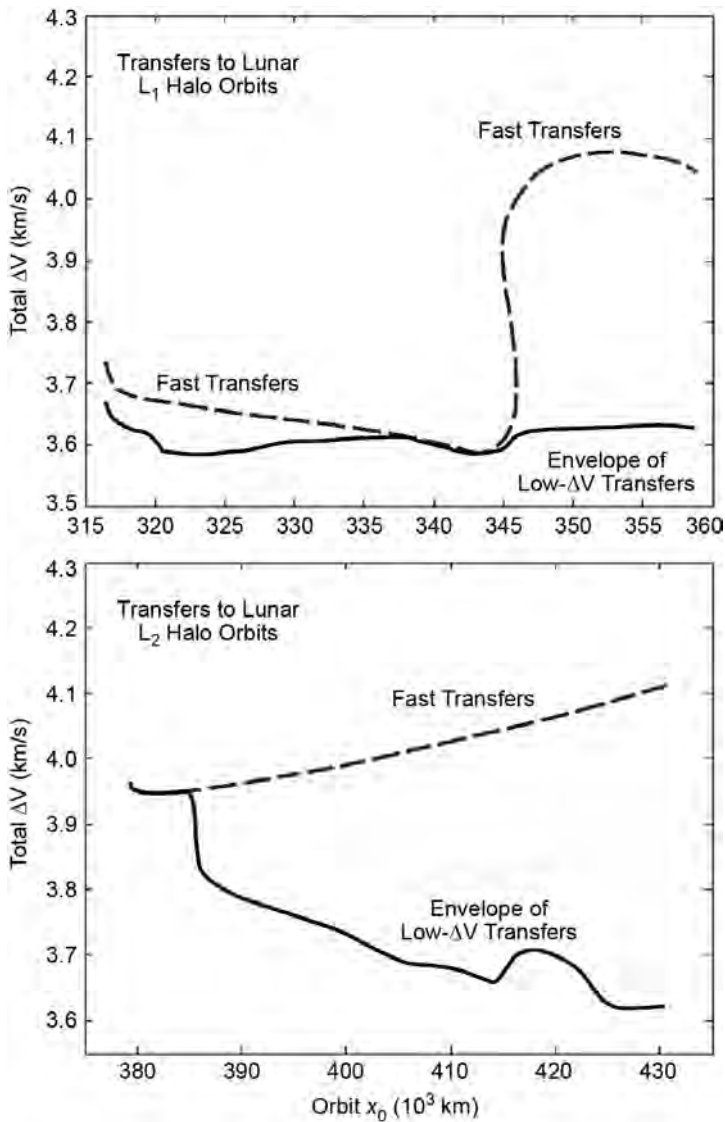


Figure 3-29 A summary of the minimum amount of total ΔV required to reach any lunar L_1 halo orbit (top) and any lunar L_2 halo orbit (bottom) surveyed here using the fastest optimized transfers (approximately 5 days) as well as an envelope of longer low- ΔV transfers (1–2 months).

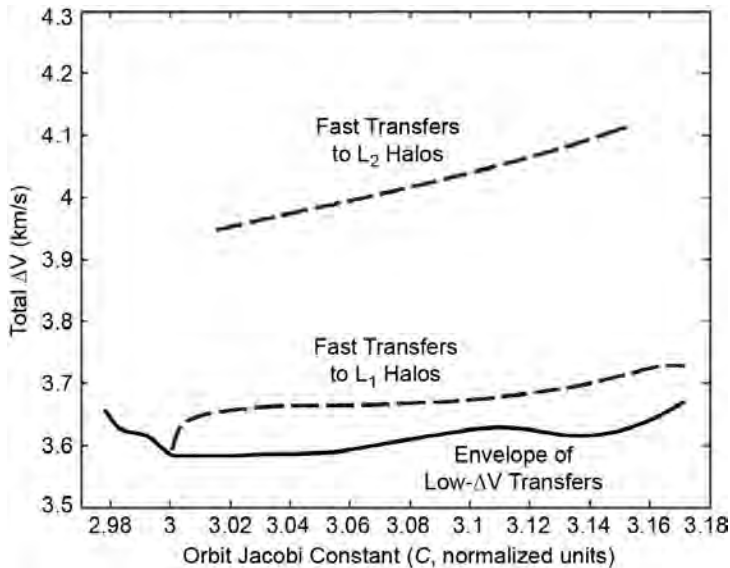


Figure 3-30 A summary of the minimum amount of total ΔV required to reach halo orbits with a given Jacobi constant.

3.4.1 Modeling a Low-Energy Transfer using Dynamical Systems Theory

Many types of low-energy transfers exist in any given month, and their characteristics tend to repeat from one month to the next. The most complex low-energy transfers typically do not appear in many consecutive months due to the asymmetries in the real Solar System; however, simple low-energy transfers reappear in a predictable fashion from one month to the next.

This section studies how to model low-energy transfers using dynamical systems theory and the Patched Three-Body Model (introduced in Section 2.5.2). It turns out that simple low-energy transfers are represented well in this simplified model of the Solar System, and that one may use the modeled trajectory as a guide to construct a realistic transfer in a more accurate model of the solar system. Because low-energy transfers may be represented in the Patched Three-Body Model, one may take advantage of tools within dynamical systems theory to analyze these transfers. The goal is to be able to build a useful low-energy transfer quickly to meet a mission's needs; dynamical systems tools provides an avenue to do this.

A low-energy ballistic transfer may be modeled as a series of heteroclinic transfers between unstable three-body orbits in the Sun–Earth system and the Earth–Moon system [39, 40, 45, 46]. Figure 3-31 illustrates these orbit transfers in the Patched Three-Body Model. One can see that a spacecraft departs the Earth on a trajectory that shadows the stable invariant manifold of an unstable three-body orbit in the

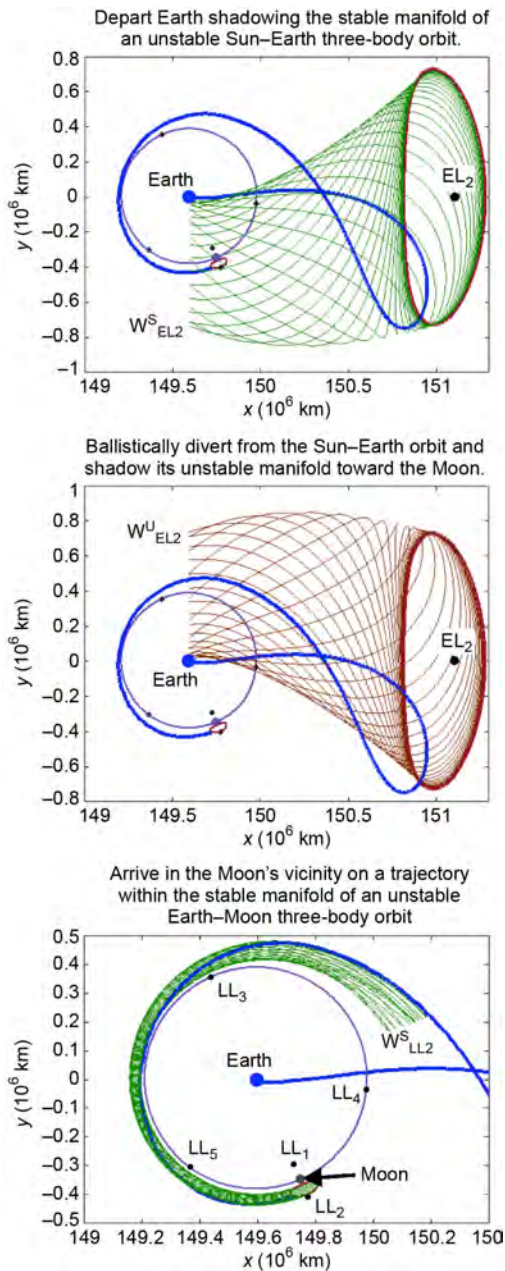


Figure 3-31 Modeling a ballistic lunar transfer as a series of heteroclinic transfers between unstable three-body orbits in the Patched Three-Body Model [97] (first published in Ref. [97]; reproduced with kind permission from Springer Science+Business Media B.V.). (*See insert for color representation of this figure.*)

Sun–Earth/Moon three-body system. The spacecraft does not arrive on that orbit, however, before it ballistically diverts and then shadows the unstable manifold of that orbit. The trajectory is designed to arrive in the stable manifold of a target three-body orbit in the Earth–Moon three-body system, for example, an LL_2 halo orbit. This process will be described in detail in this section.

A low-energy, ballistic lunar transfer may be modeled as a series of transfers from one three-body orbit to another. After the spacecraft launches from its LEO parking orbit, the spacecraft transfers to the vicinity of a three-body orbit in the Sun–Earth system, referred to in this section as the *Earth staging orbit*. The spacecraft’s LEO departure trajectory follows the flow of the Earth staging orbit’s stable manifold. Once in the vicinity of the Earth staging orbit, the spacecraft falls away from the staging orbit, following the flow of that orbit’s unstable manifold. The trajectory is chosen so that it encounters the stable manifold of a three-body orbit in the Earth–Moon system, referred to in this section as the *lunar staging orbit*. The spacecraft may use the lunar staging orbit as a final destination or as a transitory orbit, as discussed later in Section 3.5. To generalize the modeling process even further, a ballistic lunar transfer may be modeled as a transfer from Earth to one or more Earth staging orbits to one or more lunar staging orbits and then to some final destination.

Earth Staging Orbits. Many types of three-body orbits may be used as Earth staging orbits in the process of modeling or constructing a low-energy transfer. A proper staging orbit must meet the following requirements:

1. The orbit must be unstable;
2. If the orbit is the first Earth staging orbit, then the orbit’s stable manifold must intersect LEO or the launch asymptote; otherwise, the orbit’s stable manifold must intersect the preceding staging orbit’s unstable manifold;
3. The orbit’s unstable manifold must intersect the following staging orbit’s stable manifold, be it another Earth staging orbit or a lunar staging orbit.

A quasiperiodic Lissajous orbit has been selected to build the example transfer shown in this section, because it meets each of these requirements. Unfortunately, quasiperiodic orbits and their invariant manifolds are difficult to visualize since they never retrace their paths. This section illustrates the validity of a Lissajous orbit by showing that halo orbits are viable candidates to be used as Earth staging orbits.

Figure 3-32 shows four perspectives of the family of northern halo orbits centered about the Sun–Earth L_2 point. Lissajous orbits span a very similar region of space, but often do not extend as far in the z -axis.

Most libration orbits in the Sun–Earth system are unstable and hence meet Requirement 1 given above. This discussion will assume that a halo orbit from the family shown in Fig. 3-32 will be used as the only Earth staging orbit en route to a lunar staging orbit. Figure 3-33 shows two plots of an example halo orbit about the Sun–Earth L_2 point and the interior half of its stable manifold. One can see that this stable manifold intersects the Earth. Thus, a spacecraft may make a single maneuver to transfer from a LEO parking orbit to a trajectory on this halo orbit’s stable

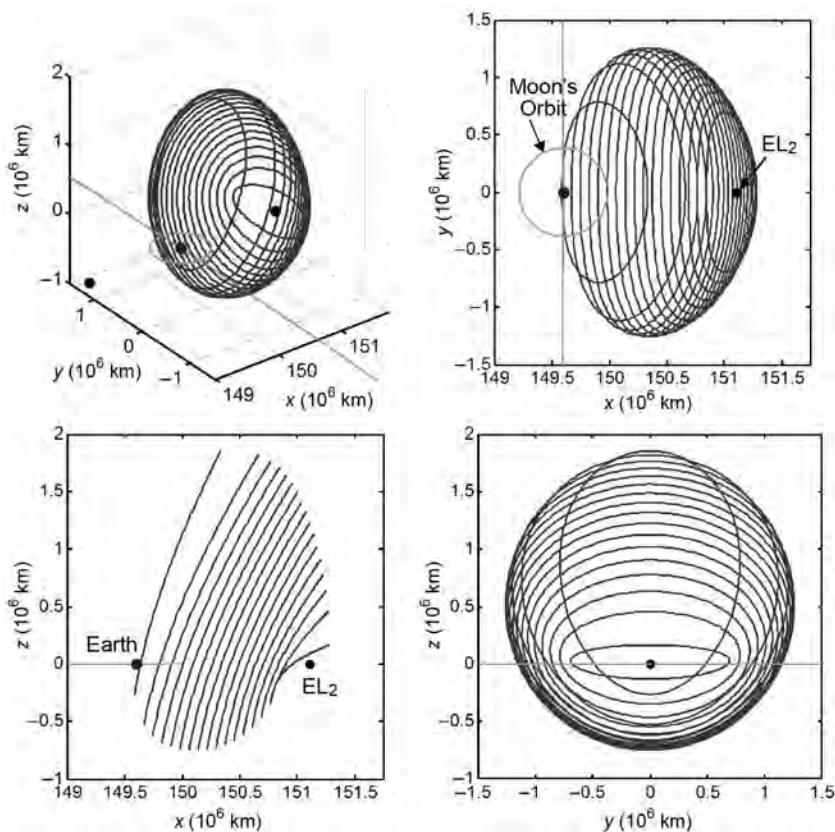


Figure 3-32 Four perspectives of the family of northern halo orbits about the Sun–Earth L₂ point.

manifold; this satisfies Requirement 2 for this itinerary. Similarly, Fig. 3-34 shows two plots of the same halo orbit's unstable manifold, showing that trajectories exist that intersect the Moon's orbit about the Earth. Thus, a spacecraft on, or sufficiently near, the halo orbit may use the orbit's unstable manifold to guide it to intersect the Moon (satisfying Requirement 3). The invariant manifolds of Lissajous orbits with similar Jacobi constants also demonstrate the same properties, making them viable candidates for low-energy staging orbits.

Lunar Staging Orbits. Many different Earth–Moon three-body orbits may be used as lunar staging orbits; the example low-energy transfer modeled in this section uses a halo orbit about the Earth–Moon L₂ point as its lunar staging orbit because it meets all of the requirements.

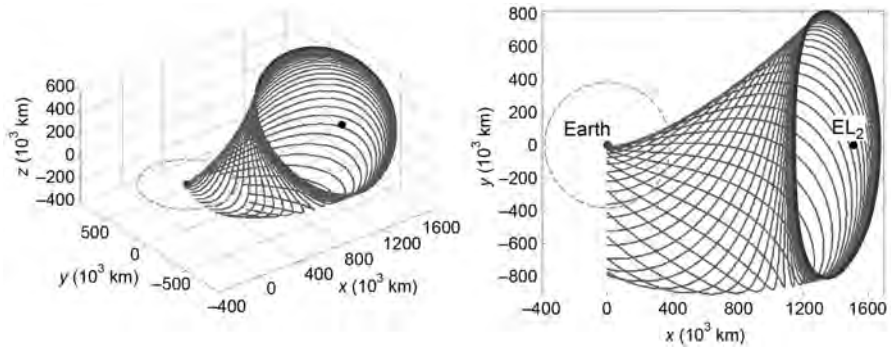


Figure 3-33 Two perspectives of an example Northern halo orbit about the Sun–Earth L_2 point, shown with the interior half of its stable manifold. One can see that the stable manifold intersects the Earth.

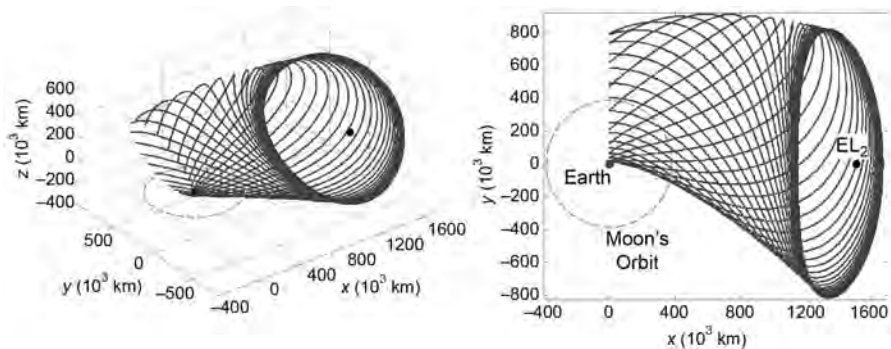


Figure 3-34 Two perspectives of the same northern EL_2 halo orbit shown in Fig. 3-33, this time shown with the interior half of its unstable manifold. One can see that the unstable manifold intersects the Moon's orbit.

The requirements for a lunar staging orbit typically come from the requirements of the mission itself. The following list summarizes the additional requirements imposed on the lunar staging orbit:

1. The orbit must be unstable;
2. The orbit's stable manifold must intersect the unstable manifold of the preceding staging orbit, be it the previous lunar or the previous Earth staging orbit;

3. If the orbit is the final lunar staging orbit, then it must meet any requirements derived from the mission; otherwise, the orbit's unstable manifold must intersect the following lunar staging orbit's stable manifold.

There are many families of Earth–Moon three-body orbits that satisfy Requirement 1, including the family of lunar L_2 halo orbits. The family of halo orbits about the Earth–Moon L_2 point closely resembles the family of halo orbits about the Sun–Earth L_2 point shown in Fig. 3-32 and won't be shown here for brevity.

Figure 3-35 shows two perspectives of an example LL_2 halo orbit along with its exterior stable manifold, propagated in the Patched Three-Body Model. If a spacecraft were to target a trajectory on this manifold it would asymptotically approach and eventually arrive onto the staging orbit. Thus, if a spacecraft were able to transfer from the Earth staging orbit's unstable manifold onto this LL_2 halo orbit's stable manifold, then the spacecraft would have achieved a ballistic transfer to this lunar orbit from LEO.

An Example Modeled Ballistic Lunar Transfer. An example ballistic lunar transfer has been modeled using dynamical systems theory and is presented here. It is a fairly simple example of a transfer: it consists of a single Earth staging orbit and a single lunar staging orbit. A Lissajous orbit about the Sun–Earth L_2 point has been selected to be the Earth staging orbit, although it is visualized here by a halo orbit with the same Jacobi constant. A lunar L_2 halo orbit has been selected to be the only lunar staging orbit. The transfer has been produced in the Patched Three-Body Model (see Section 2.5.2).

Figure 3-36 shows the first portion of the three-dimensional transfer in two perspectives. The spacecraft is launched from a 185-km low Earth orbit, travels outward toward the Sun–Earth L_2 point along a trajectory that shadows the stable manifold of an EL_2 libration orbit, skims the periodic orbit, and then travels toward the Moon. Figure 3-36 shows the representative halo orbit and its stable manifold, $W_{EL_2}^S$; the stable manifold of the actual Lissajous staging orbit does an even better job of mapping out the flow of the spacecraft's motion in space.

Figure 3-37 shows two perspectives of the same transfer trajectory, but this time plotted with the Earth staging orbit's unstable manifold, $W_{EL_2}^U$. One can see that as the spacecraft departs the vicinity of the Earth staging orbit and approaches the Moon, its trajectory shadows the unstable manifold of the Earth staging orbit.

Figure 3-38 shows the same two perspectives of the three-dimensional low-energy transfer plotted alongside the lunar staging orbit's stable manifold, $W_{LL_2}^S$. One can see that the low-energy transfer intersects the manifold in full phase space, indicating that the spacecraft has injected into the LL_2 halo orbit. Once in the final Earth–Moon halo orbit, the spacecraft has all of the options presented in Section 3.5 available to it.

Figure 3-39 shows a top-down perspective of the entire three-dimensional low-energy transfer with all three manifolds displayed.

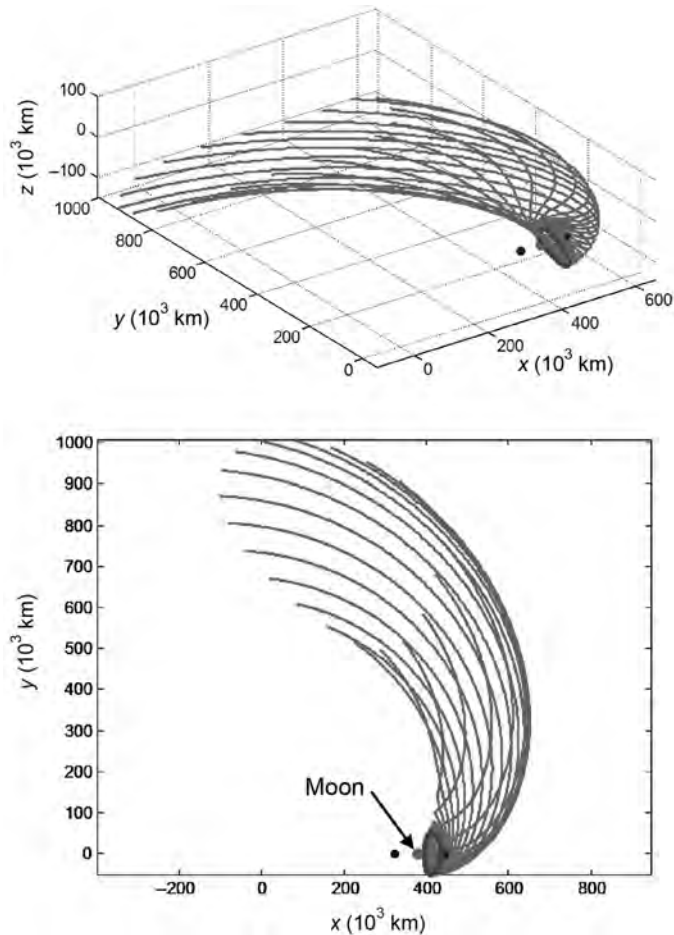


Figure 3-35 Two perspectives of an example southern halo orbit about the Earth–Moon L_2 point, shown with the exterior half of its stable manifold. One can see that the stable manifold quickly departs the Moon’s vicinity and may then intersect the unstable manifold of the Earth staging orbit.

3.4.2 Energy Analysis of a Low-Energy Transfer

Low-energy lunar transfers harness the Sun’s gravity to reduce the ΔV requirements of a lunar transfer. It is useful to observe how the two-body energy of the spacecraft with respect to each of the massive bodies changes throughout the transfer. It is also useful to observe how the Moon affects the spacecraft’s Sun–Earth Jacobi constant and especially how the Sun affects the spacecraft’s Earth–Moon Jacobi constant. These energy changes are explored in this section, applied to the example transfer

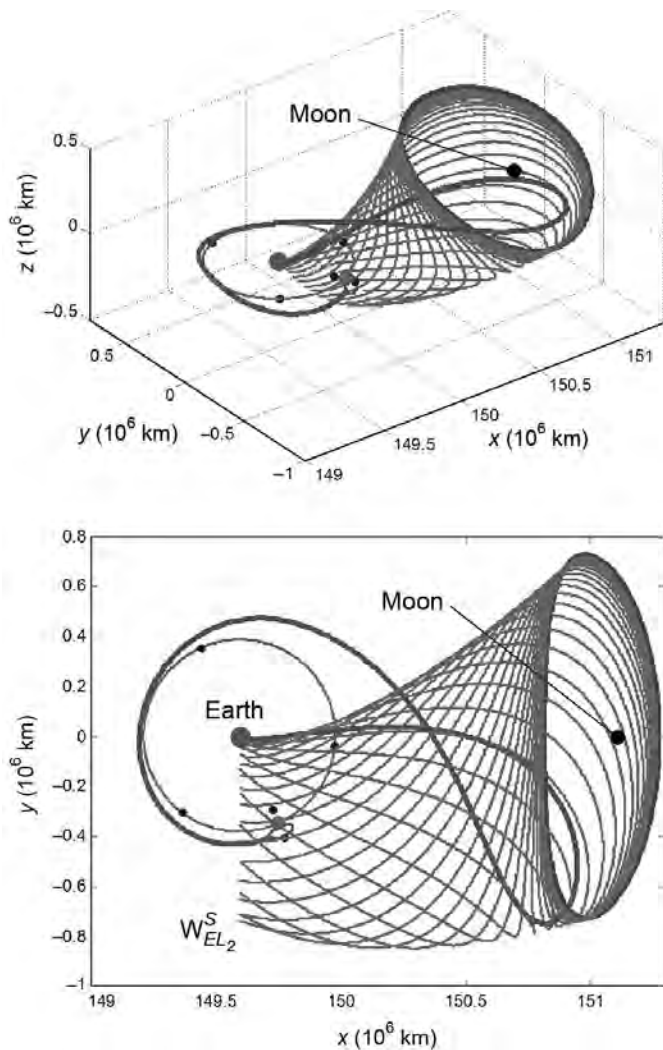


Figure 3-36 Two perspectives of the first portion of the example low-energy transfer, modeled using the stable manifold of a halo orbit about the Sun–Earth L_2 point. One can see that the spacecraft’s outbound motion shadows the halo orbit’s stable manifold.

produced in the previous section. Other low-energy transfers have been found to behave in a very similar fashion.

To begin this analysis, Fig. 3-40 shows plots of the distance between the spacecraft and both the Earth and Moon as the spacecraft traverses the low-energy ballistic lunar transfer. This is a useful illustration since both the spacecraft’s two-body energy and its Jacobi constant vary as functions of distance to these bodies. By observing

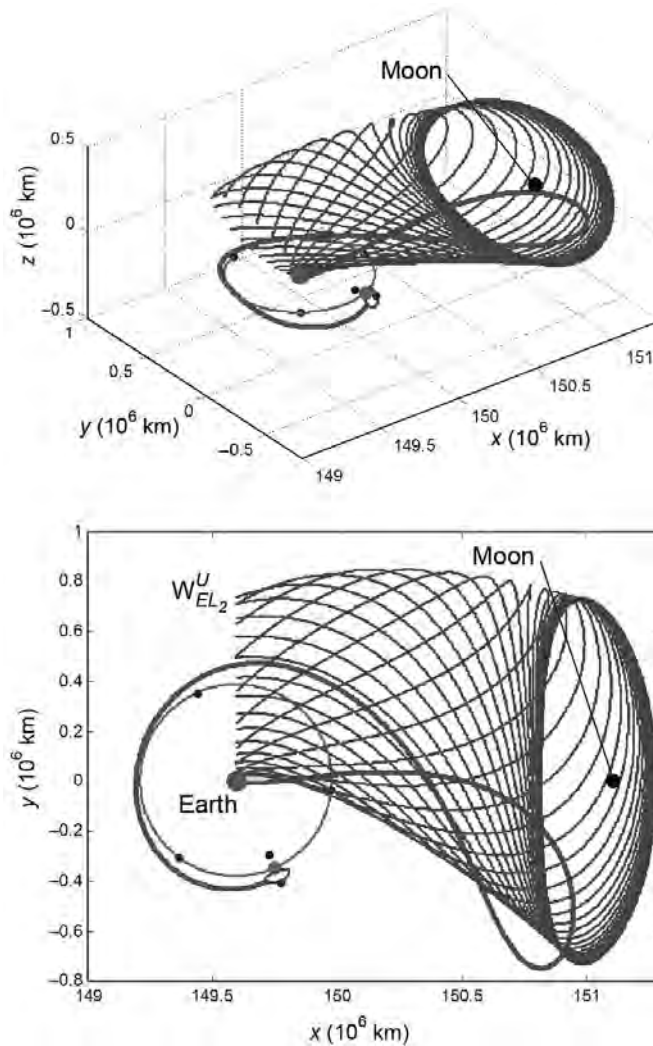


Figure 3-37 Two perspectives of the second portion of the example low-energy transfer, modeled using the unstable manifold of a halo orbit about the Sun–Earth L_2 point. One can see that as the spacecraft departs the vicinity of the Earth staging orbit and approaches the Moon, its trajectory shadows the unstable manifold of the Earth staging orbit.

Fig. 3-40, one can determine the time at which the spacecraft arrives at its lunar halo orbit destination.

It is expected that the two-body energy of a spacecraft with respect to the Earth increases over time due to the Sun’s gravity, since the spacecraft’s perigee radius gradually rises throughout the transfer. Figure 3-41 shows the two-body specific

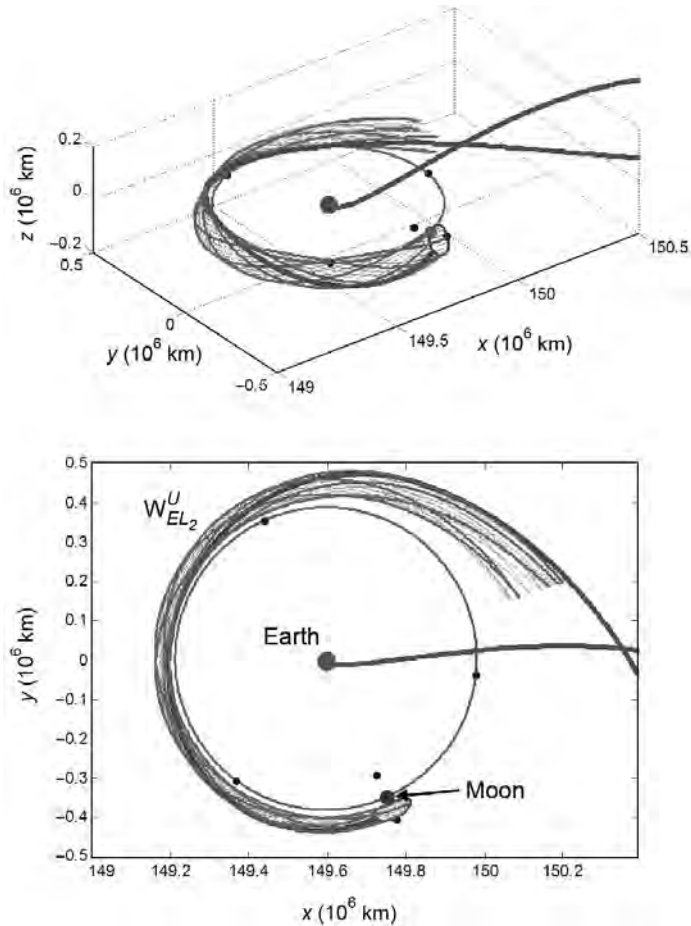


Figure 3-38 Two perspectives of the third portion of the example low-energy transfer, modeled using the stable manifold of a halo orbit about the Earth–Moon L_2 point. Every fourth trajectory has been darkened for visualization purposes. One can see that the transfer intersects the manifold in full phase space, indicating that the spacecraft has injected into the LL_2 halo orbit.

energy of the spacecraft with respect to the Earth throughout the transfer. One can see that the spacecraft's energy does indeed rise while it is in the vicinity of the Earth staging orbit. The energy then begins to vary wildly once it enters the lunar halo orbit, which makes sense because the halo orbit only exists in the presence of both the Earth and the Moon, balancing the gravity of both bodies. Figure 3-42 shows four other two-body orbital elements of the spacecraft with respect to the Earth as the spacecraft traverses the ballistic transfer, including the spacecraft's semi-major axis, perigee radius, eccentricity, and ecliptic inclination. One can see that

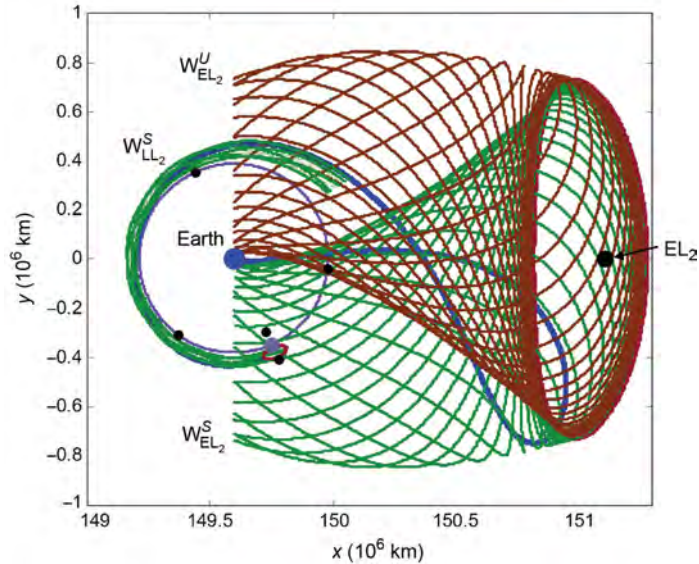


Figure 3-39 A top-down perspective of the example low-energy transfer, shown with all three manifolds that were used to model it (blue = the low-energy transfer, green = stable manifold of a three-body orbit, brown = unstable manifold of a three-body orbit). (See color insert.)

the Sun's gravity increases the spacecraft's semi-major axis and perigee radius as the spacecraft traverses the Earth staging orbit. The Sun's gravity reduces the spacecraft's eccentricity and inclination with respect to the Earth. The spacecraft enters the lunar halo orbit at approximately 110 days after launch, beyond which the Moon's gravity is the dominant source causing each of the spacecraft's orbital elements to vary over time.

It is interesting to notice that the spacecraft's inclination changes dramatically during the first half of the transfer, while the perigee radius remains near zero; then during the second half of the transfer the perigee radius rises dramatically while the spacecraft's inclination settles down. These effects may be correlated with the location of the spacecraft relative to the four quadrants of the Sun–Earth state space. In this particular transfer, the spacecraft spends several weeks near the boundary of the first and fourth quadrants before moving definitively into the fourth quadrant, where the spacecraft's perigee radius rises rapidly. Other low-energy transfers have varying geometries and their two-body orbital elements change in correspondingly different fashions.

It is also expected that the spacecraft's two-body energy with respect to the Moon decreases as the spacecraft approaches and ballistically inserts into the lunar halo orbit. Figure 3-43 shows the two-body specific energy of the spacecraft with respect to the Moon throughout the low-energy lunar transfer. One can clearly see that the

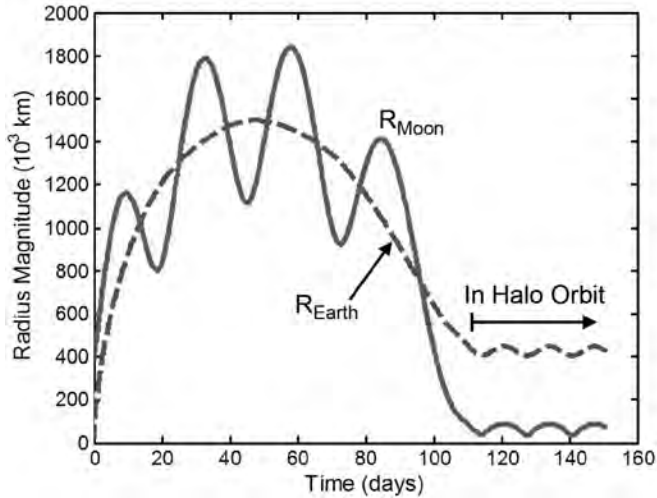


Figure 3-40 The magnitude of the radius vector of the spacecraft with respect to the Earth and the Moon as the spacecraft traverses the example low-energy lunar transfer.

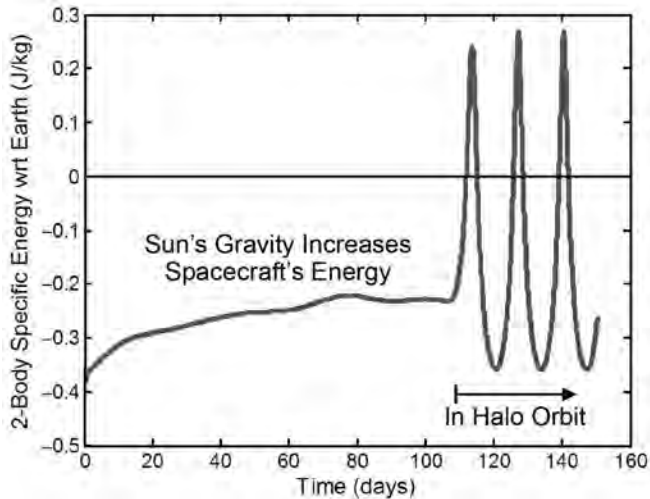


Figure 3-41 The two-body specific energy of a spacecraft with respect to the Earth over time as it traverses an example low-energy lunar transfer.

spacecraft's specific energy drops as it approaches the lunar halo orbit. Furthermore, its energy drops below zero, satisfying some authors' requirements to be temporarily captured by the Moon [29, 46, 182].

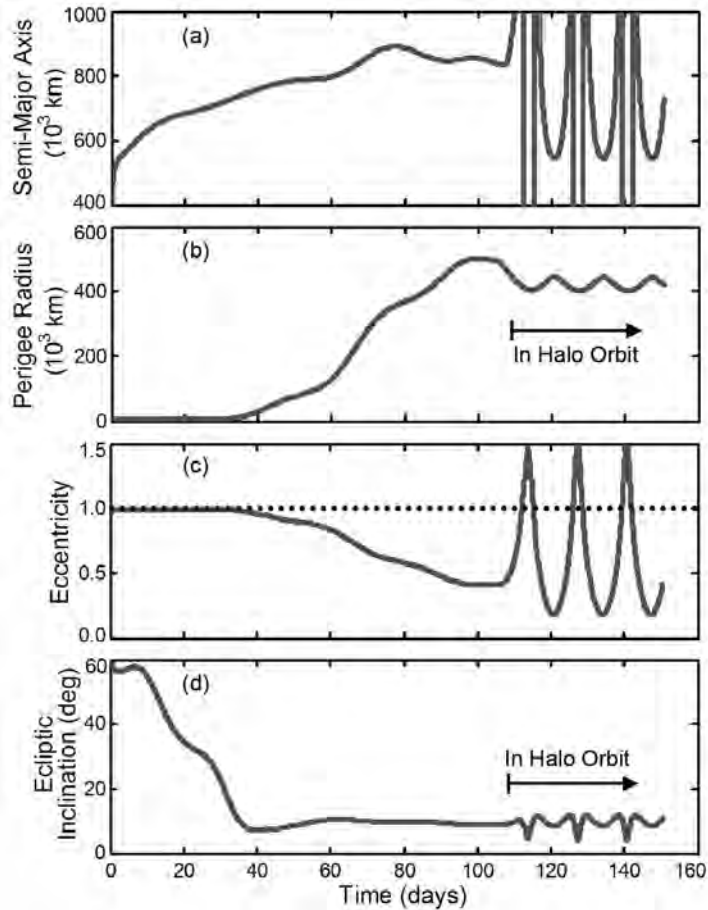


Figure 3-42 Four two-body orbital elements of the spacecraft with respect to the Earth as the spacecraft traverses the example lunar transfer: (a) the spacecraft's semi-major axis, (b) perigee radius, (c) eccentricity, and (d) ecliptic inclination.

Figures 3-44 and 3-45 show the evolution of the spacecraft's Jacobi constant with respect to the Sun–Earth and Earth–Moon three-body systems, respectively, as the spacecraft traverses the example lunar transfer. The spacecraft's trajectory has been constructed in the Patched Three-Body Model; hence, the spacecraft's Jacobi constant will be constant in one or the other three-body system at any given time, depending on which three-body system is responsible for the given segment of the spacecraft's trajectory. The spacecraft's motion has been modeled by the Sun–Earth three-body system during the first 105 days of the transfer. After the spacecraft has crossed the Earth–Moon three-body sphere of influence (3BSOI), its motion is then modeled by the Earth–Moon three-body system.

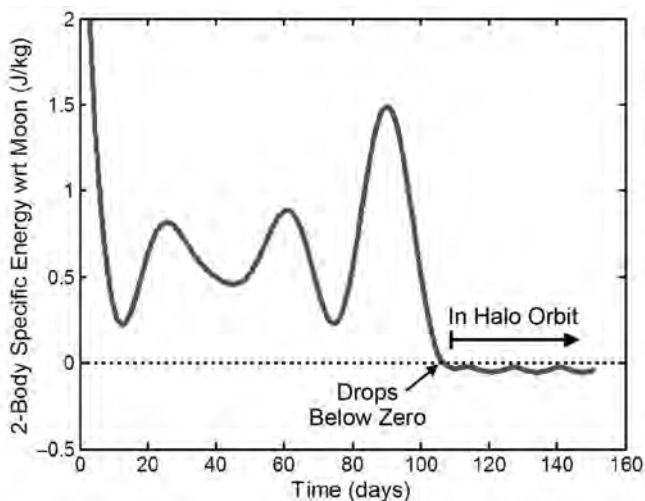


Figure 3-43 The two-body specific energy of a spacecraft with respect to the Moon over time as it traverses an example low-energy lunar transfer.

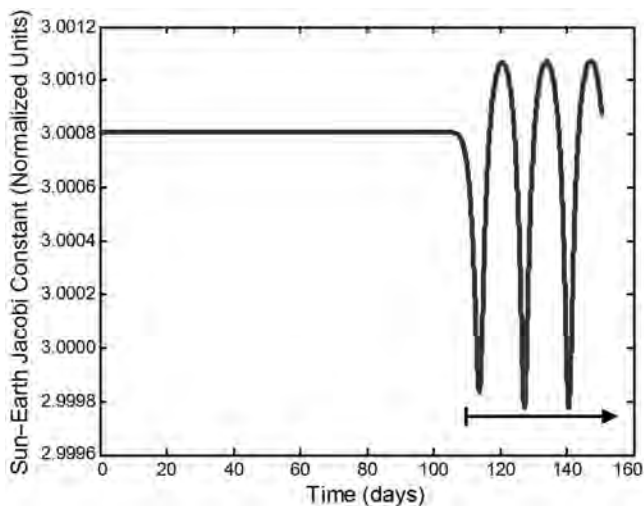


Figure 3-44 The evolution of the spacecraft's Jacobi constant with respect to the Sun–Earth three-body system as the spacecraft traverses the example lunar transfer.

Figure 3-45 presents a compelling case that it is possible to build low-energy transfers to lunar halo orbits, or other unstable Earth–Moon three-body orbits, with a wide variety of different Jacobi constants. If the spacecraft traversing the example transfer had arrived at the Moon slightly earlier or slightly later, it could have transferred to a

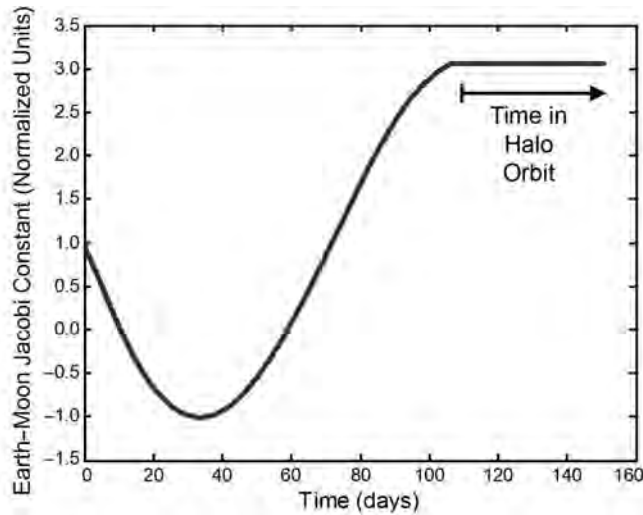


Figure 3-45 The evolution of the spacecraft's Jacobi constant with respect to the Earth–Moon three-body system as the spacecraft traverses the example lunar transfer.

lunar halo orbit with a different Jacobi constant. Furthermore, it may be possible for a spacecraft to depart one lunar halo orbit, traverse through the Sun–Earth environment for some time, and return to the Moon on the stable manifold of a different lunar halo orbit. Section 3.4.5 demonstrates that it is indeed possible to build low-energy transfers to lunar halo orbits within a wide range of Jacobi constants [46], but more work needs to be accomplished to determine how to take advantage of the time series shown in Fig. 3-45 to target a lunar halo orbit with a specified Jacobi constant.

3.4.3 Constructing a Low-Energy Transfer in the Patched Three-Body Model

Modeling a low-energy transfer using dynamical systems theory involves the use of several staging orbits and their corresponding invariant manifolds in the Earth–Moon and Sun–Earth systems. If a mission designer wishes to construct a transfer that intentionally visits certain staging orbits, then the transfer may be constructed in the same manner that it is modeled. More often, a mission designer only wishes for the spacecraft to reach the final lunar orbit, no matter its route through the Sun–Earth system. In that case, the methods used to construct a low-energy transfer may be simplified.

Ballistic lunar transfers are constructed here by propagating the stable manifold of the final lunar halo orbit backward in time for a set amount of time. After each trajectory has been propagated, the perigee point of the trajectory is identified. A proper transfer may be identified as one whose perigee point corresponds to some

desired value, for example, an altitude of 185 km. In this manner, a practical transfer may be constructed between the Earth and the lunar three-body orbit without identifying any required staging orbit.

3.4.3.1 Parameters The dynamical systems method of constructing ballistic lunar transfers provides a natural set of six parameters that may be used to define each transfer. In the Patched Three-Body Model, this set may be described by the parameters: $[F, C, \theta, \tau, p, \Delta t_m]$. Each of these parameters is described in this section.

Orbit Family Parameter: F . Depending on the mission requirements, one may wish to target any type of Earth–Moon three-body orbit. The parameter F is a discrete variable that describes the orbit family that contains the desired target orbit. The example transfer presented previously has had the parameter F set to describe the family of southern LL_2 halo orbits. There are certainly symbolic ways to represent each family of three-body orbits, but using text to do so provides a clear description of which family is being used.

Orbit Parameter: C . The Jacobi constant, C , of the targeted orbit is used in this work to specify which orbit is being targeted within the family. There are numerous ways to identify a particular three-body orbit within its family [108, 113]. The Jacobi constant is used here because it also provides information about the corresponding forbidden regions and allowable motion of spacecraft with that Jacobi constant [46].

Sun–Earth–Moon Angle: θ . The parameter θ is defined to be the angle between the Sun–Earth line and the Earth–Moon line. It is a required parameter needed to convert between the two three-body systems in the Patched Three-Body Model. Figure 3-46 shows an example of the geometry and the definition of θ .

Arrival Location: τ . Each point on a periodic orbit may be uniquely described by the parameter τ , a parameter analogous to a conic orbit’s true anomaly. This parameter was introduced in Section 2.6.2.3, but is described again here. The parameter τ may range from 0 to 1, representing a revolution number, or from 0 deg to 360 deg,



Figure 3-46 An illustration of θ , the Sun–Earth–Moon angle.

representing an angle like the true anomaly [46]. Figure 3-47 shows a plot of the definition of τ when applied to two halo orbits. For halo orbits, it is intuitive to use an angle and model τ off of a conic orbit's true anomaly; for other three-body orbits it is confusing using an angle. In any case, the only use of τ here is to identify each point about a three-body orbit, and either representation may be used.

Perturbation Direction: p . To construct a trajectory in the stable invariant manifold of a given unstable orbit, one takes the state of the orbit at a given τ -value and perturbs that state along the direction of the stable eigenvector [46, 147]. The perturbation may occur in two directions: an interior or an exterior direction, as illustrated in Fig. 3-4. The parameter p is a discrete variable that may be set to *interior* or *exterior*, indicating the direction of the perturbation.

Manifold Propagation Duration: Δt_m . The trajectory in the given three-body orbit's stable manifold is propagated backward in time for an amount of time equal to Δt_m . Typically when propagated backward in time, the trajectories that lead to desirable low-energy transfers depart the vicinity of the Moon, traverse their apogee, fall toward the Earth, and then intersect a desirable altitude above the surface of the Earth. However, transfers may also be constructed that pass near the Earth once or several times before intersecting the desirable altitude above the surface of the Earth. Such trajectories must be propagated long enough to allow the desirable perigee passage to occur. Thus, the parameter Δt_m is important in order to ensure that the proper perigee passage is being implemented by the low-energy transfer.

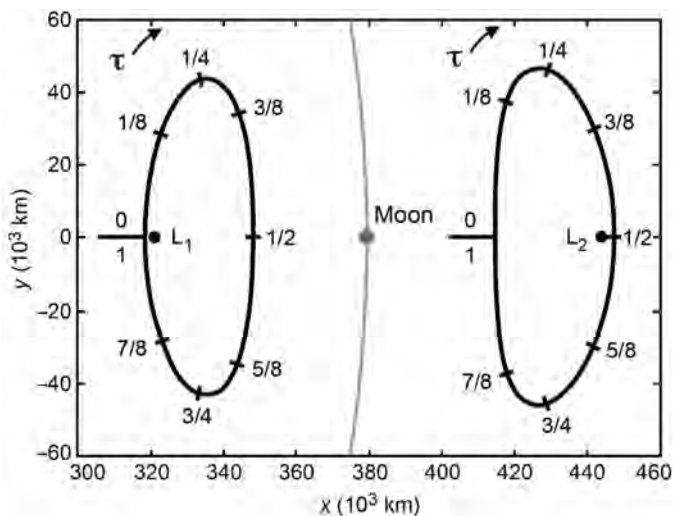


Figure 3-47 The two halo orbits shown demonstrate how the parameter τ moves from 0 to 1 about an orbit [174] (Copyright © 2008 by American Astronautical Society Publications Office, all rights reserved, reprinted with permission of the AAS).

Discussion Regarding Parameters. The set of parameters used here does not contain all continuous variables as other sets of orbital elements do, such as the Keplerian orbital element set of a two-body orbit. The present parameter set also requires knowledge about how to use it, for example, how to build the target lunar orbit given the parameters F and C . Nonetheless, this set may be used to uniquely describe any low-energy ballistic transfer between the Earth and an unstable lunar three-body orbit. Table 3-17 summarizes the parameter set.

3.4.3.2 Producing the low-energy transfer The process of producing a low-energy transfer given the parameter set $[F, C, \theta, \tau, p, \Delta t_m]$ is very simple and is described henceforth.

Step 1. First, one must build the target Earth–Moon orbit. The desired orbit must be unstable and may be identified using the parameters F and C , as defined above. The example low-energy transfer presented in this section has been produced using an orbit in the family, F , of southern halo orbits about the Earth–Moon L_2 point. The specific orbit has been identified in its family by the value of C , equal to 3.05.

Step 2. The parameter θ specifies the location of the Moon, and hence the target orbit, with respect to the Earth and Sun in the Patched Three-Body Model. The example transfer has used an initial θ -value of approximately 293.75 deg. This may be verified by inspecting the final location of the Moon in Figs. 3-36–3-39. Since the transfer is generated backward in time, the value of θ specifies the *final* position of the Moon.

Step 3. The parameter τ specifies a particular state in the unstable three-body orbit. The example transfer has implemented a τ -value of approximately 0.74, corresponding to a point roughly three quarters around the orbit from the orbit's reference point (the point where the orbit crosses the $y = 0$ plane with positive \dot{y}) [46, 108].

Step 4. The particular state in the target orbit is then perturbed in order to construct a single trajectory in the stable manifold of the orbit. The magnitude of this

Table 3-17 A summary of the six parameters used to produce low-energy transfers in the Patched Three-Body Model.

Parameter	Domain	Description
F	Discrete	Target three-body orbit family
C	Continuous	Jacobi constant of target orbit
θ	Continuous [0 deg, 360 deg]	Sun–Earth–Moon angle
τ	Continuous [0,1]	Arrival location on the target orbit
p	Discrete	Perturbation direction
Δt_m	Continuous	Propagation duration

perturbation is given by ϵ ; the direction is given by the orbit's monodromy matrix [131] and the parameter p . The orbit's monodromy matrix is used to compute the orbit's stable and unstable eigenvectors; the stable eigenvector is then mapped to the given τ -value using the orbit's state transition matrix [46, 147]. The example lunar transfer has implemented a trajectory in the halo orbit's *exterior* manifold with the value of ϵ set proportional to a 100-km perturbation.

Step 5. The resulting state is then used as the initial condition to construct a trajectory in the stable manifold of the three-body orbit. This trajectory is propagated backward in time for a duration of time equal to Δt_m . The trajectory that has produced the example transfer has been propagated for approximately 28.53 non-dimensional Earth–Moon time units (approximately 123.9 days) before encountering the desired perigee point, that is, the desired LEO injection point.

Step 6. The final step in the construction of a low-energy transfer is to connect this trajectory with a prescribed LEO parking orbit or with the surface of the Earth. It is unlikely that an arbitrary set of parameters will yield a lunar transfer that connects with its prescribed LEO starting conditions. In such a case, either the parameters should be adjusted [46], or a bridge must be constructed to connect the spacecraft's origin with the lunar transfer, as discussed in Section 3.3 [174].

3.4.3.3 Discussion The parameter set derived here is very useful if a mission designer needs to build a transfer to a specific lunar orbit that cannot exceed some maximum transfer time. In that case, the parameters F , C , and Δt_m are fixed. By setting Δt_m to the maximum transfer duration, one ensures that no transfers are constructed that require excessive transfer time, but one still permits transfers that require less transfer time. The three remaining parameters are conveniently well defined. The parameter p is binary and the parameters θ and τ are cyclic. Thus, mission designers can explore all possible low-energy transfers to a target orbit by producing two maps: one map of θ vs. τ with p set to “Exterior,” and another identical map with p set to “Interior.” Examples of these two maps that survey all possible low-energy transfers to an example halo orbit about the LL_2 point, along with several representative transfers, are illustrated in Figs. 3-48 and 3-49. The exploration of these maps will be the purpose of Section 3.4.5, and further description of these figures will appear there.

Other methods have been described in the literature that also describe parameter sets to target low-energy lunar transfers. The majority of these methods start with a spacecraft in orbit about the Earth and target a maneuver for that spacecraft to perform in order to reach the Moon's vicinity via a low-energy transfer. For instance, Belbruno and Carrico have developed a set of parameters that describe the six-dimensional state that a spacecraft would need to obtain to reach the Moon's vicinity via a low-energy transfer [27]. Five parameters are specified, including an epoch (t), the spacecraft's radial distance from Earth (r_E), its longitude (α_E), its latitude (δ_E), and its flight path azimuth (σ_E). Then, the spacecraft's speed (V_E) and flight path angle (γ_E) are varied to target a prescribed radial distance from the Earth (r_M) and a prescribed inclination (i_M), which would ultimately send the spacecraft in the general direction

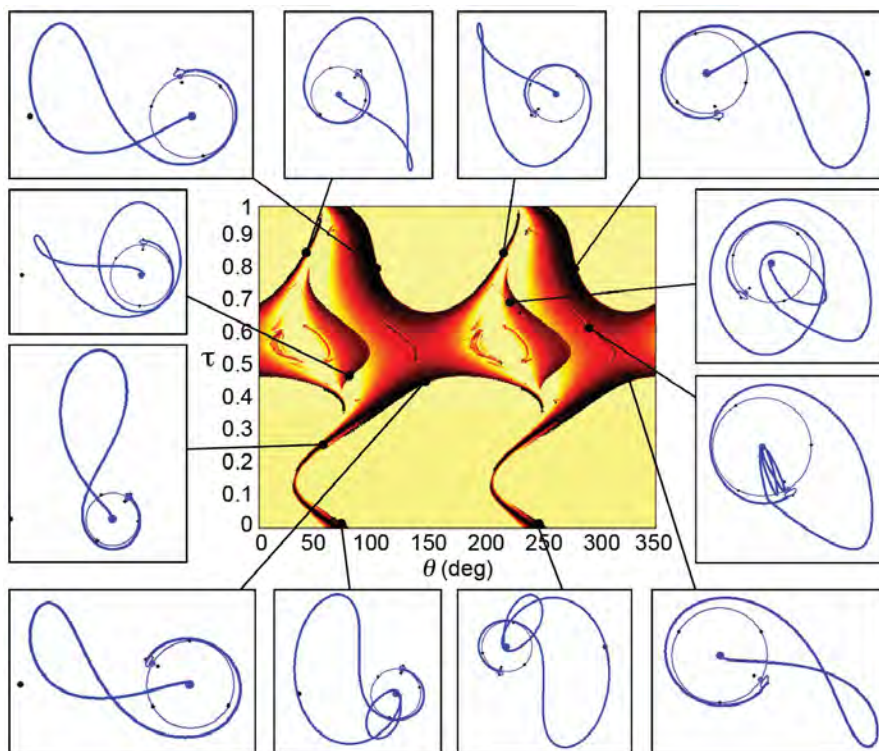


Figure 3-48 An example state space map, capturing a wide variety of low-energy transfers that exist between the Earth and an example LL_2 halo orbit. Each trajectory arrives at the halo orbit from the exterior direction, and arrives at the orbit in a geometry according to the given (θ, τ) combination. The color of the map indicates how close to the Earth the trajectory gets when propagated from the LL_2 halo orbit backward in time. All black points represent viable low-energy transfers. (See insert for color representation of this figure.)

of a low-energy transfer. The advantage of this method is that the spacecraft's initial orbit at the Earth is well-defined, which is useful when a transfer must be designed for a spacecraft that is already in orbit about the Earth. However, the technique requires a great deal of predetermined knowledge of the problem, including *a priori* estimates for the values of r_M , i_M , V_E , γ_E , and t (t is specified to obtain a proper Sun–Earth–Moon angle). The procedure is therefore constrained to build a transfer with a predefined geometry that may not be ideal.

Operationally, it is likely that a combination of these two approaches will work the best to produce practical low-energy transfers. A transfer may then be constructed that starts from a prescribed orbit, ends at a specified lunar orbit, and probably includes one or two small trajectory correction maneuvers to connect the segments.

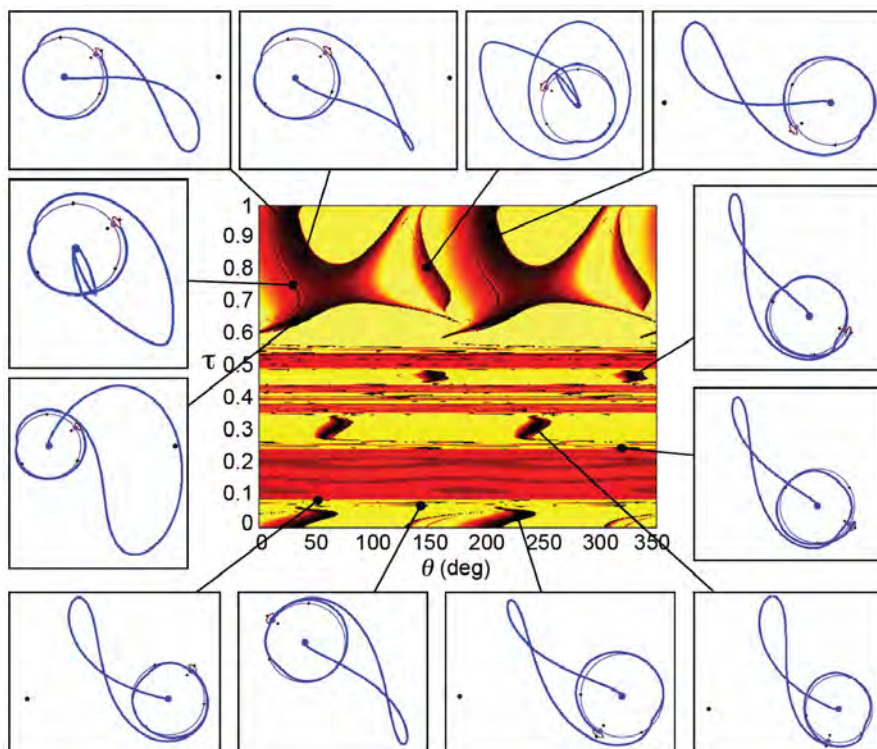


Figure 3-49 An example state space map that is identical to the map illustrated in Fig. 3-48, except that the trajectories arrive at the LL_2 halo orbit from the interior direction. (See insert for color representation of this figure.)

Chapter 6 presents such an algorithm, and the results demonstrate that it generates very successful trajectories.

3.4.4 Constructing a Low-Energy Transfer in the Ephemeris Model of the Solar System

The previous sections demonstrated how to analyze and construct a low-energy lunar transfer to a libration orbit using the Patched Three-Body Model; this section describes how to do so in the more accurate DE421 ephemeris model of the Solar System.

There are two main strategies that have been shown to work to generate a low-energy transfer in a realistic model of the Solar System, such as a model that uses the JPL Ephemerides to approximate the motion of the planets and the Moon in the

Solar System. The first strategy is to generate the transfer in a simplified model, such as the Patched Three-Body Model, and then convert the transfer into the more realistic model of the Solar System. The conversion process typically involves some combination of multiple shooting differential correction and continuation [40, 46]. The second strategy is to construct the low-energy transfer directly in the realistic model, using experience gained from the simplified models. This strategy is described in this section.

The dynamical systems methods that enabled the clear analysis and construction of low-energy ballistic lunar transfers in the Patched Three-Body Model apply to the DE421 model of the Solar System as well. The Sun, Earth, and Moon orbit their respective barycenters in orbits that are nearly circular and coplanar. Thus, many trajectories that exist in the Patched Three-Body Model are good approximations of trajectories that exist in the real Solar System.

Low-energy ballistic lunar transfers are constructed in the DE421 model of the Solar System in the same way that they have been constructed in the Patched Three-Body Model. An unstable three-body orbit is selected as a target orbit near the Moon. The orbit's stable manifold is propagated and intersected with the Earth. Those trajectories that intersect the Earth may be used as ballistic transfers from the Earth to the target orbit via the orbit's stable manifold. The most significant adjustment to this procedure involves the construction of the target three-body orbit in the DE421 model. This process is described in detail in Section 2.6.6.3.

Ballistic lunar transfers to realistic halo orbits may be uniquely specified in the DE421 model using a set of six parameters that is similar to the set used to describe transfers constructed in the Patched Three-Body Model. This set includes the parameters: $\{F, A_z, T_{\text{ref}}, p, \tau, \Delta t_m\}$, where A_z replaces the Jacobi constant and T_{ref} replaces the parameter θ from the previous set of parameters. It is very straightforward to generate a halo orbit in the DE421 model using an analytical approximation as an initial guess to the multiple shooting differential corrector (Section 2.6.5.2). The parameter A_z specifies the z -axis amplitude of the halo orbit in the analytical approximation specified by Richardson [123]. The parameter T_{ref} specifies the reference epoch that ties the initial guess of the states of the halo orbit to the DE421 model.

Table 3-18 summarizes the set of parameters that generates an example transfer in the DE421 model, shown in Fig. 3-50. The parameters F , A_z , and T_{ref} define the southern LL_2 halo orbit that is shown in Fig. 3-51. One can see that the multiple shooting differential corrector adjusted the state of the analytical approximation of the halo orbit such that the reference epoch is no longer at the $\tau = 0$ deg point, but at the $\tau \approx 3.84$ deg point. A particular trajectory in the halo orbit's stable manifold is then generated that corresponds to the parameters τ and p in Table 3-18, which propagates backward in time to a perigee with an altitude of 185 km. The distance between this trajectory and the Moon is shown in Fig. 3-52. One can see that this trajectory asymptotically arrives at the orbit from the exterior direction.

Table 3-18 The parameters used to produce the low-energy transfer shown in Fig. 3-50.

Parameter	Value
F	The family of southern Earth–Moon L_2 halo orbits
A_z	30,752 km (0.08 normalized distance units)
T_{ref}	15 January 2017 12:57:36 Ephemeris Time
τ	280.2 deg
p	Exterior
Δt_m	115.9 days

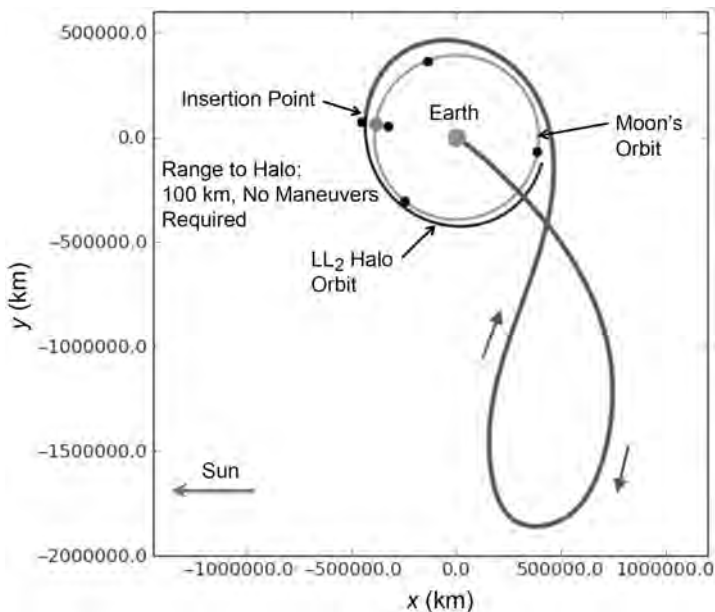


Figure 3-50 An example low-energy transfer produced in the DE421 model using the parameters specified in Table 3-18 [44] (Copyright © 2009 by American Astronautical Society Publications Office, San Diego, California (Web Site: <http://www.univelt.com>), all rights reserved; reprinted with permission of the AAS).

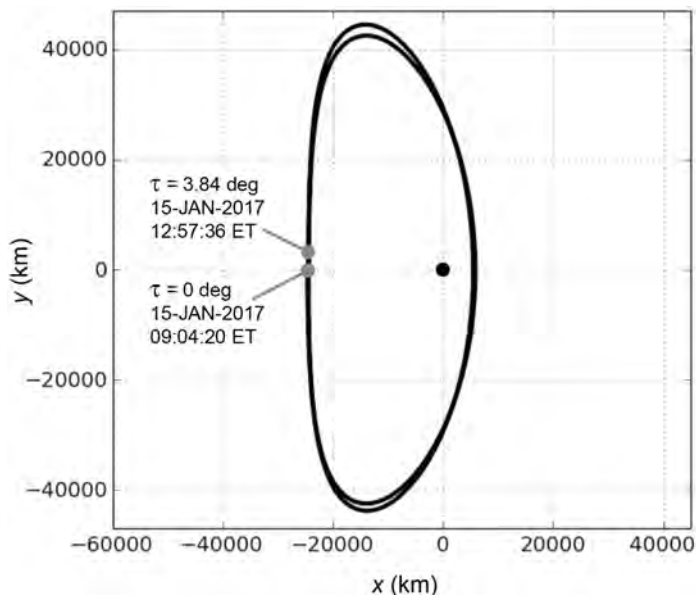


Figure 3-51 The halo orbit specified by F , A_z , and T_{ref} in Table 3-18 [44] (Copyright © 2009 by American Astronautical Society Publications Office, San Diego, California (Web Site: <http://www.univelt.com>), all rights reserved; reprinted with permission of the AAS).

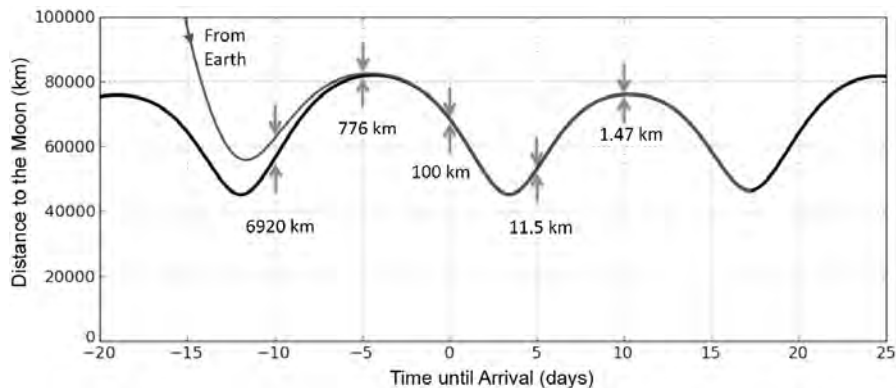


Figure 3-52 The distance between the transfer and the Moon as the trajectory approaches and arrives at the LL_2 halo orbit [44] (Copyright © 2009 by American Astronautical Society Publications Office, San Diego, California (Web Site: <http://www.univelt.com>), all rights reserved; reprinted with permission of the AAS).

3.4.5 Families of Low-Energy Transfers

A set of low-energy parameters may be used to generate the initial conditions of a trajectory that is propagated backward in time to construct a ballistic lunar transfer. If one set of parameters $\{F', A'_z, T'_{\text{ref}}, p', \tau', \Delta t'_m\}$ generates a trajectory that originates from a LEO with an altitude of 185 km, then it is typically the case that a small deviation in either T'_{ref} or τ' will generate a trajectory that originates from a LEO with a slightly different altitude. However, small deviations in both of those parameters may often be designed to generate a new trajectory that originates from a LEO with the same 185 km altitude. In that case, the two sets of parameters define two different ballistic lunar transfers that are in the same family of transfers.

Figure 3-53 illustrates how transfers may be organized into families. In this example, the lunar transfer shown in Fig. 3-50 with the parameters given in Table 3-18 is used as a reference trajectory. The transfer's parameters are all held constant, except for the parameters T_{ref} and τ , which are systematically varied through all combinations of values shown in Fig. 3-53. At each combination, a new trajectory is propagated and analyzed to determine its new perigee altitude. One can see that by reducing both T_{ref} and τ , one builds trajectories that come closer to the Earth at

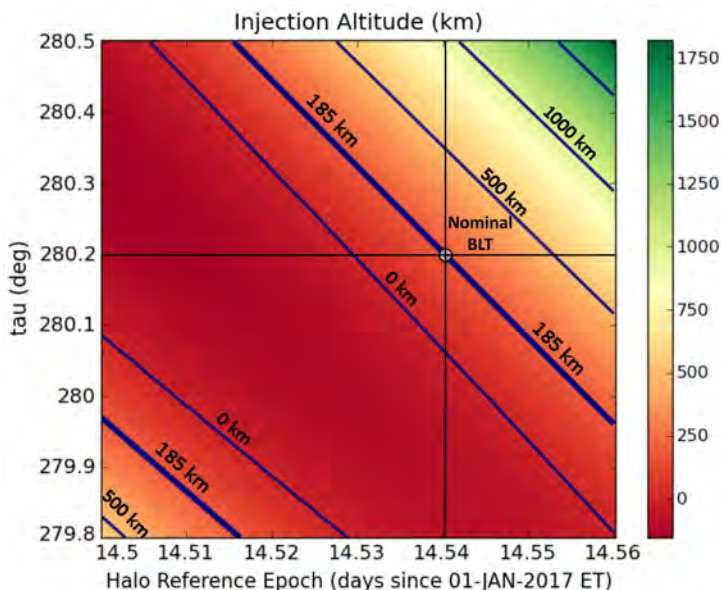


Figure 3-53 A map of the perigee altitude that each low-energy trajectory encounters as a function of T_{ref} and τ . The 185-km contour is highlighted, which includes the nominal ballistic lunar transfer presented in Table 3-18 [44] (Copyright © 2009 by American Astronautical Society Publications Office, San Diego, California (Web Site: <http://www.univelt.com>), all rights reserved; reprinted with permission of the AAS). (See insert for color representation of this figure.)

their perigee point, and vice versa. By reducing T_{ref} and increasing τ an appropriate amount, one can produce new trajectories that also have a perigee altitude of 185 km.

The exercise given above may be extended to allow T_{ref} to vary across an entire month and τ to vary across 360 deg to observe full families of low-energy lunar transfers. Figure 3-54 shows such a Ballistic Lunar Transfer (BLT) state space map given the parameter set summarized in Table 3-19. The figure shows a plot that maps the perigee altitude of each trajectory generated using each combination of T_{ref} and τ . The darkest regions contain the parameters that produce useful transfers; the white fields contain parameters that generate trajectories that do not approach the Earth. Figure 3-55 shows the same map with several trajectories plotted to illustrate the trajectories that may be generated using these parameters.

Families of transfers may be identified in the BLT state space map shown in Fig. 3-54 by tracing those combinations of T_{ref} and τ that have a perigee altitude of some desirable value, for example, 185 km. Figure 3-56 shows samples of the combinations of T_{ref} and τ that generate ballistic transfers with injection altitudes of 185 km. The points displayed in black correspond to trajectories that traverse closer to EL_2 than EL_1 and vice versa. Table 3-20 presents a summary of the characteristics of a sample of the transfers identified in Fig. 3-56. Each of these transfers is a member of a family of similar trajectories for which the characteristics vary smoothly away from those presented in the table. There are certainly many families of ballistic

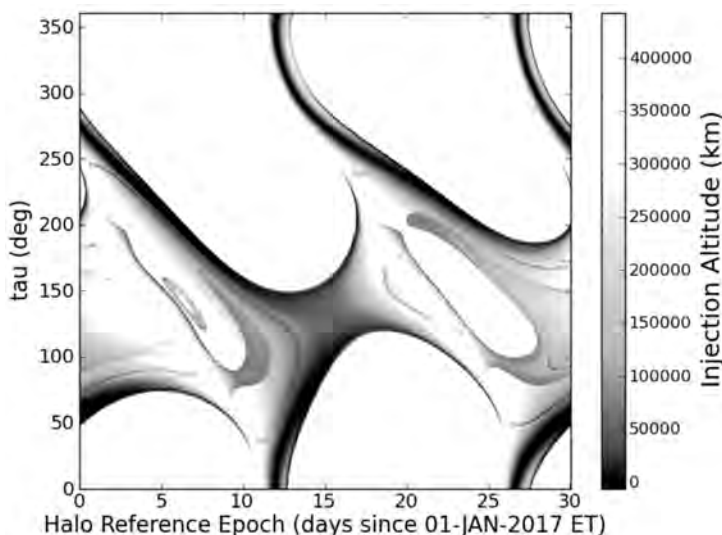


Figure 3-54 A BLT state space map that shows the perigee altitude of each generated trajectory as a function of T_{ref} and τ . The darkest regions include the combinations of T_{ref} and τ that yield transfers that begin from low Earth orbits [44] (Copyright © 2009 by American Astronautical Society Publications Office, San Diego, California (Web Site: <http://www.univelt.com>), all rights reserved; reprinted with permission of the AAS).

Table 3-19 The parameters used to produce the results shown in Figs. 3-54–3-56.

Parameter	Value
F	The family of southern Earth–Moon L_2 halo orbits
A_z	30,752 km (0.08 normalized distance units)
T_{ref}	1 Jan 2017 00:00:00 ET $\leq T_{ref} \leq$ 31 Jan 2017 00:00:00 ET
τ	0 deg $\leq \tau \leq$ 360 deg
p	Exterior
Δt_m	180 days

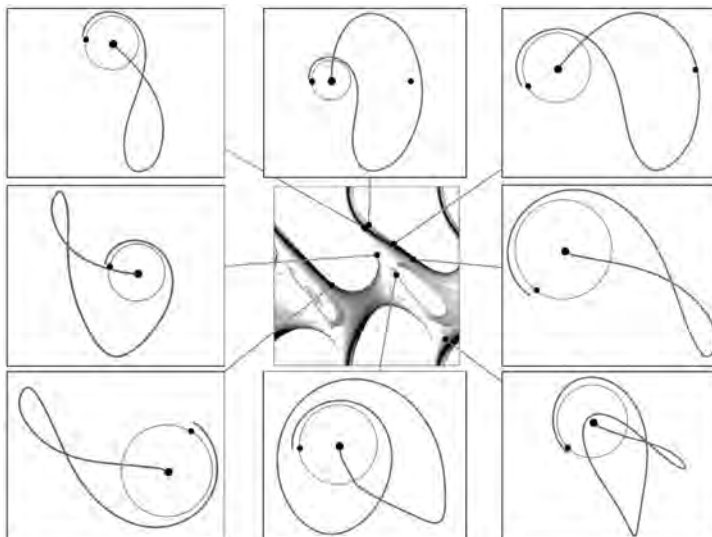


Figure 3-55 The same BLT state space map shown in Fig. 3-54 with example transfers shown around the perimeter [44] (Copyright © 2009 by American Astronautical Society Publications Office, San Diego, California (Web Site: <http://www.univelt.com>), all rights reserved; reprinted with permission of the AAS).

transfers unrepresented in the table. Figure 3-57 illustrates six example families of low-energy transfers. One can see that the general characteristics of each family varies in a smooth fashion from one transfer to the next in the family.

The quickest transfer identified in Fig. 3-56 requires fewer than 83 days between the injection and the point when the trajectory has arrived within 100 km of the lunar halo orbit. The vast majority of the transfers shown require a launch energy in the range of $-0.75 \text{ km}^2/\text{s}^2 \leq C_3 \leq -0.35 \text{ km}^2/\text{s}^2$. The transfers that include a lunar flyby often require less launch energy, particularly those that involve a lunar flyby on the outbound trajectory soon after injection. Several transfers have been identified that require a C_3 as low as $-2.1 \text{ km}^2/\text{s}^2$, implementing a lunar flyby at an altitude of approximately 2000 km. Figure 3-58 shows the relationship between the required injection C_3 and the transfer duration; Fig. 3-59 compares the required injection C_3

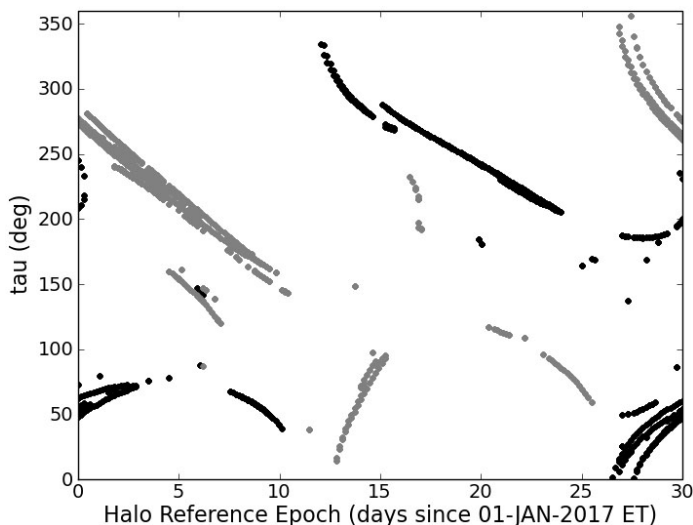


Figure 3-56 Combinations of T_{ref} and τ that generate ballistic transfers with perigee injections at an altitude of 185 km. The points displayed in black correspond to trajectories that traverse closer to EL_2 than EL_1 ; points shown in gray travel closer to EL_1 than EL_2 .

with the lowest lunar periapse altitude. One can see a clear correlation in Fig. 3-59 that the closer a trajectory gets to the Moon during the transfer, the lower the injection C_3 may be. Additional lunar flybys or Earth phasing orbits may help provide the geometry needed for a particular mission.

3.4.6 Monthly Variations in Low-Energy Transfers

The BLT state space map shown in Figs. 3-54–3-56 will repeat perfectly from one synodic month to the next in the Patched Three-Body Model, since the model is symmetric. The characteristics of the BLT state space map generated in the DE421 model of the solar system will not repeat perfectly each month, although similar features will be present in each month. Figure 3-60 shows a map of the perigee altitude of trajectories generated from the same set of parameters presented in Table 3-18. But for a wider range of T_{ref} and τ , T_{ref} is varied over 3 months, and τ is varied over two halo orbit revolutions. One can see the same features from cycle to cycle, but the details of the state space map vary. Significant variations are observed between the first halo orbit revolution ($0 \text{ deg} \leq \tau \leq 360 \text{ deg}$) and the second halo orbit ($360 \text{ deg} \leq \tau \leq 720 \text{ deg}$), mostly as a consequence of the nonzero eccentricity of the Moon's orbit about the Earth–Moon barycenter.

3.4.6.1 12-Month Survey The state space map has been further extended to 12 months to study the variations that exist throughout an entire year. It has been observed that the most prominent features continue to persist, and repeat regularly,

Table 3-20 Summary characteristics for a sample of the ballistic transfers identified in Fig. 3-56 [44] (Copyright © 2009 by American Astronautical Society Publications Office, San Diego, California (Web Site: <http://www.univelt.com>), all rights reserved; reprinted with permission of the AAS).

#	Δ Reference	τ	$EL_1 /$	C_3	Transfer	# Earth	# Lunar	Injection Inclusion (deg)	
	Epoch* (days)	(deg)	EL_2	(km^2/s^2)	Δt (days)	Flybys	Flybys	Equatorial	Ecliptic
1	12.060302	334.519	2	-0.2902	133.76	0	0	23.225	28.192
2	12.211055	333.736	2	-0.3457	132.91	0	0	131.701	151.274
3	14.170854	283.655	2	-0.3444	118.36	0	0	51.319	69.045
4	15.226131	271.069	2	-0.4944	108.76	0	1	32.329	51.431
5	15.829146	279.419	2	-0.4296	171.62	0	0	85.326	103.860
6	20.351759	238.347	2	-0.6556	130.11	0	0	115.737	137.694
7	20.351759	239.232	2	-0.5856	145.20	0	0	21.877	22.738
8	22.311558	221.171	2	-0.6904	137.51	0	1	35.973	13.527
9	23.819095	206.901	2	-0.7153	129.17	0	0	22.180	10.275
10	20.050251	180.970	2	-1.8533	171.79	0	1	97.684	92.972
11	25.025126	164.113	2	-1.9222	146.35	0	1	20.490	4.271
12	27.286432	137.373	2	-2.0307	176.72	0	2	38.302	36.809
13	28.190955	168.405	2	-2.0880	122.46	2	2	19.325	30.359
14	28.040201	185.608	2	-1.0318	145.08	0	1	34.251	11.315
15	28.040201	185.630	2	-1.6144	145.75	0	2	103.995	126.244
16	0.000000	55.325	2	-0.9032	179.35	2	1	143.590	121.792
17	0.150754	63.382	2	-0.6429	97.90	0	0	23.372	0.836
18	0.452261	54.781	2	-0.6608	132.55	0	0	145.538	168.969
19	1.507538	66.990	2	-1.1266	113.39	0	1	166.454	144.152
20	8.592965	59.539	2	-0.8393	178.32	0	1	99.214	87.676
21	8.592965	59.962	2	-0.6791	165.37	0	0	14.732	20.434
22	6.030151	144.580	2	-0.6940	170.11	0	3	23.140	17.669
23	27.889447	53.118	2	-0.9637	140.22	1	2	11.452	28.632
24	28.040201	15.470	2	-0.4261	172.37	0	1	27.743	40.712
25	28.190955	34.787	2	-0.5891	105.30	0	0	148.336	171.495
26	28.341709	43.756	2	-0.5740	96.55	0	0	20.962	3.797
27	2.110553	245.420	1	-0.5465	91.66	0	0	20.003	4.747
28	2.412060	247.372	1	-0.6290	172.42	1	0	54.249	30.825
29	2.110553	251.704	1	-0.6311	178.46	1	2	59.547	36.213
30	2.261307	255.586	1	-0.5150	154.75	0	0	65.164	44.035
31	6.934673	122.568	1	-0.7340	165.38	0	0	20.624	28.138
32	6.783920	138.709	1	-0.5098	164.58	0	2	124.809	129.384
33	11.457286	38.141	1	-1.1299	167.55	0	2	39.917	26.275
34	14.170854	65.695	1	-0.5599	143.25	0	0	19.771	14.374
35	14.170854	70.107	1	-0.6869	123.22	0	0	106.493	129.791
36	14.170854	73.417	1	-0.6246	115.20	0	0	87.048	110.261
37	16.733668	222.850	1	-0.7658	179.64	0	1	137.534	126.323
38	16.733668	223.945	1	-0.6178	171.17	0	0	11.994	14.627
39	17.035176	192.365	1	-1.5154	156.53	1	1	28.596	51.902
40	22.160804	108.406	1	-2.0107	129.17	0	1	18.754	5.377
41	23.819095	87.587	1	-0.6915	167.13	0	0	50.748	32.372
42	28.190955	313.713	1	-0.4043	177.60	0	0	140.309	130.765
43	28.492462	285.732	1	-0.4568	109.17	0	1	10.097	14.214
44	3.165829	227.614	1	-1.9572	169.47	7	2	153.358	172.197

*The reference epoch is given as a duration of time, in days, away from 1 Jan 2017 00:00:00 Ephemeris Time.

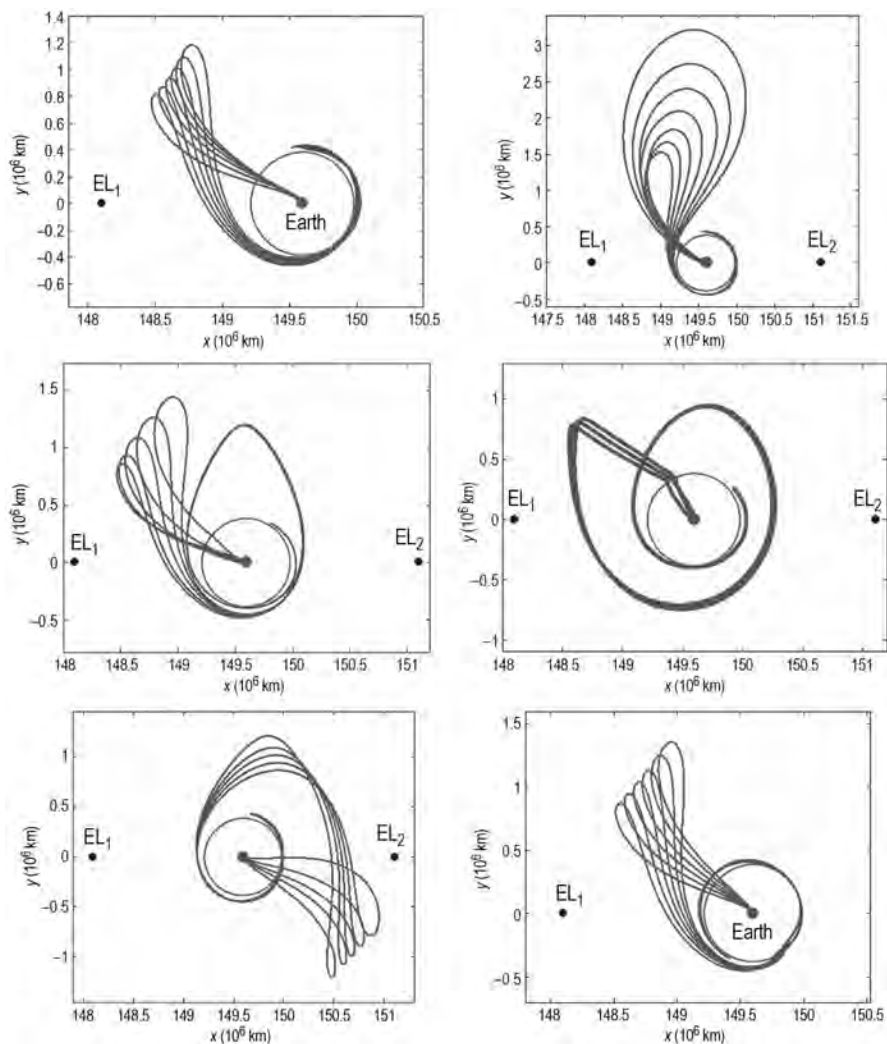


Figure 3-57 Example trajectories within six families of low-energy transfers that each may be used to transfer a spacecraft from a 185-km altitude state above the Earth to the same LL_2 halo orbit, though at different arrival times.

while subtle features appear and disappear from month to month. Figure 3-61 shows a plot of samples of the combinations of T_{ref} and τ that yield low-energy transfers between 185-km LEO parking orbits and the lunar halo orbit.

The reference epoch of each transfer shown in Fig. 3-61 may be wrapped into one synodic month to observe the changes that occur in the state space map from one synodic month to the next. Figure 3-62 shows the resulting plot, revealing the

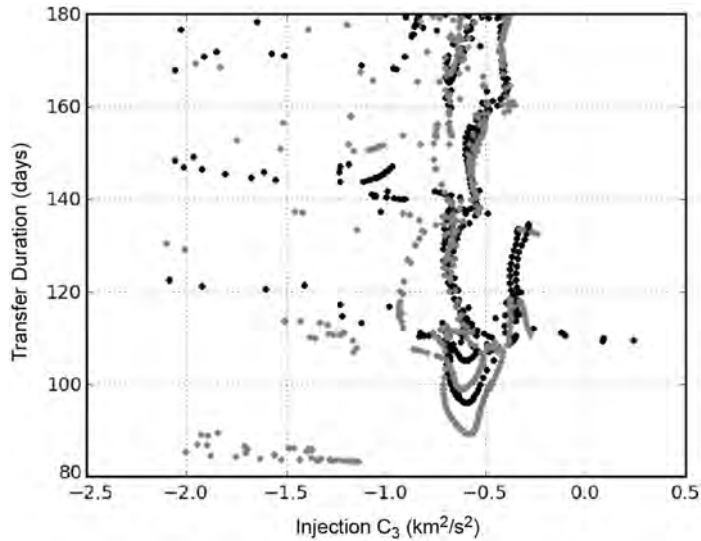


Figure 3-58 The relationship between the injection C_3 value and the duration of the transfer for each transfer identified in Fig. 3-56. The points displayed in black correspond to trajectories that traverse closer to EL_2 than EL_1 .

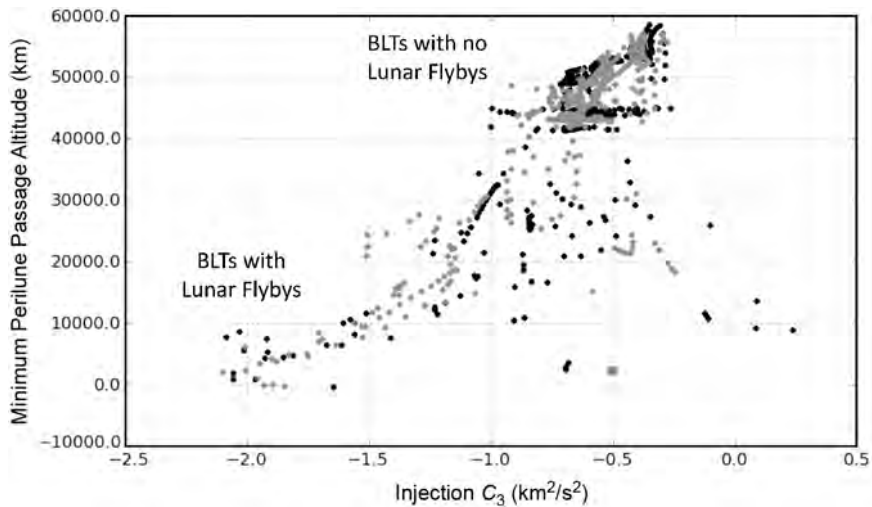


Figure 3-59 The relationship between the injection C_3 value and the lowest lunar periapse altitude during each lunar transfer identified in Fig. 3-56. The points displayed in black correspond to trajectories that travel closer to EL_2 than EL_1 .

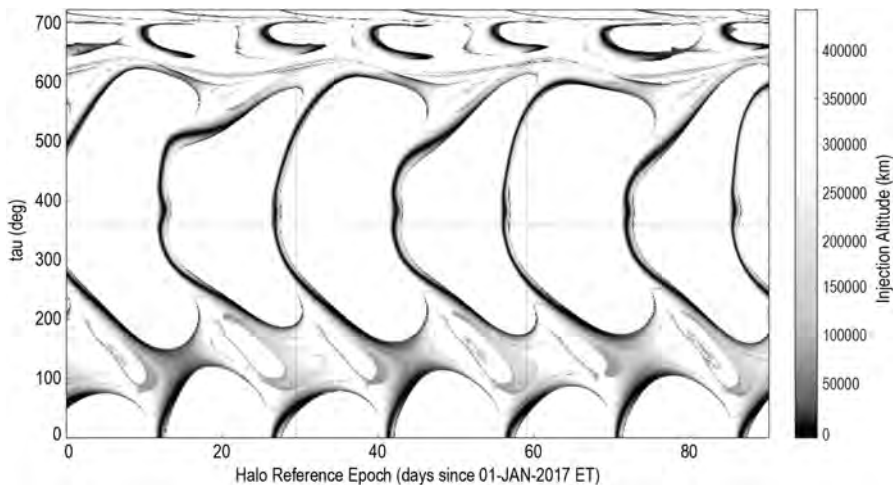


Figure 3-60 The same state space map shown in Fig. 3-54 extended to cover 90 days of reference epochs and two revolutions of the halo orbit.

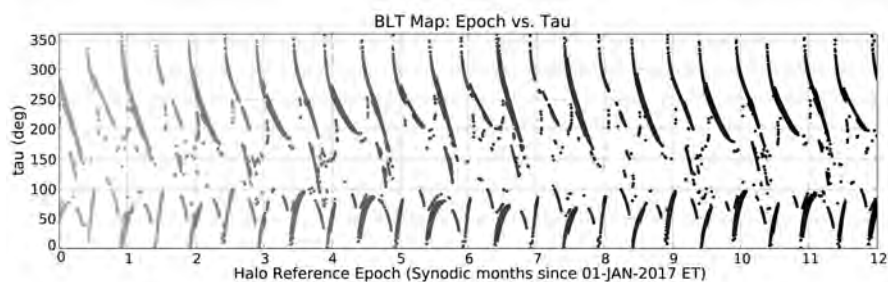


Figure 3-61 Sample combinations of T_{ref} and τ that yield low-energy transfers between 185-km LEO parking orbits and the lunar halo orbit for reference dates that span the year 2017. From lightest to darkest, the shading corresponds to reference dates from 1/1/2017 to 1/1/2018 [47] (first published by the American Astronautical Society).

variations in the locations of the curves as they shift throughout the 12 months. The transfers are shaded in Fig. 3-62 in the same manner as they are in Fig. 3-61, that is, the transfers that exist in the first month, which starts at a reference epoch of January 1, 2017, are shown in the lightest shade and the transfers in each consecutive synodic month thereafter are plotted in a darker shade. One can see that certain features repeat very closely from one synodic month to the next. Other features only appear in a subset of synodic months.

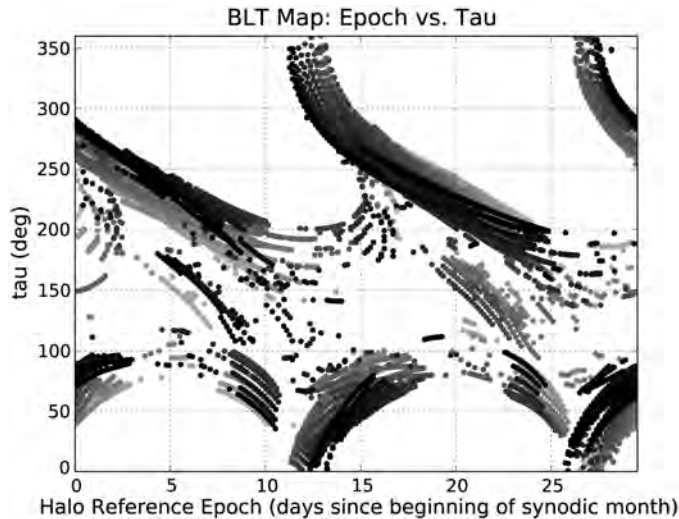


Figure 3-62 The combinations of T_{ref} and τ that yield transfers during 12 synodic months, relative to the beginning of each synodic month. The first month, which starts at a reference epoch of 1 Jan 2017 00:00:00 Ephemeris Time, is shown in the lightest shade and each consecutive synodic month thereafter is plotted in a darker shade. From lightest to darkest, the shading corresponds to reference dates from 1/1/2017 to 1/1/2018 [47] (first published by the American Astronautical Society).

Quite a few patterns exist in the families of transfers that are observed. First of all, the most pronounced curves observed in Figs. 3-61 and 3-62 correspond to transfers that do not include any lunar flybys or Earth phasing orbits. Most of them require between 90 and 110 days to transfer between the Earth and 100 km from their target orbit. Examples of these sorts of transfers may be seen in Fig. 3-55.

Several relationships exist between the launch energy of a low-energy lunar transfer and how close it gets to the Moon on its Earth-departure leg. If the transfer does not encounter the Moon, it typically requires a launch energy in the range of $-0.75 \text{ km}^2/\text{s}^2 \leq C_3 \leq -0.35 \text{ km}^2/\text{s}^2$. If a spacecraft traversing a low-energy transfer does encounter the Moon as it departs the Earth's vicinity, one finds that the Moon may either boost or reduce the spacecraft's energy, depending on how the spacecraft passes by the Moon. If it boosts the spacecraft's energy, then the lunar transfer's required launch energy drops to as low as $-2.1 \text{ km}^2/\text{s}^2$. Figure 3-63 shows a plot of the relationship between the launch energy of each low-energy transfer observed in Fig. 3-62 and how close the transfer passes by the Moon.

One can also glean a great deal of understanding about the characteristics of these transfers by observing the relationship between each transfer's injection energy and the transfer's duration. Figure 3-64 shows this relationship for each transfer in the 12-month survey. One can see that the trends in this relationship are nearly

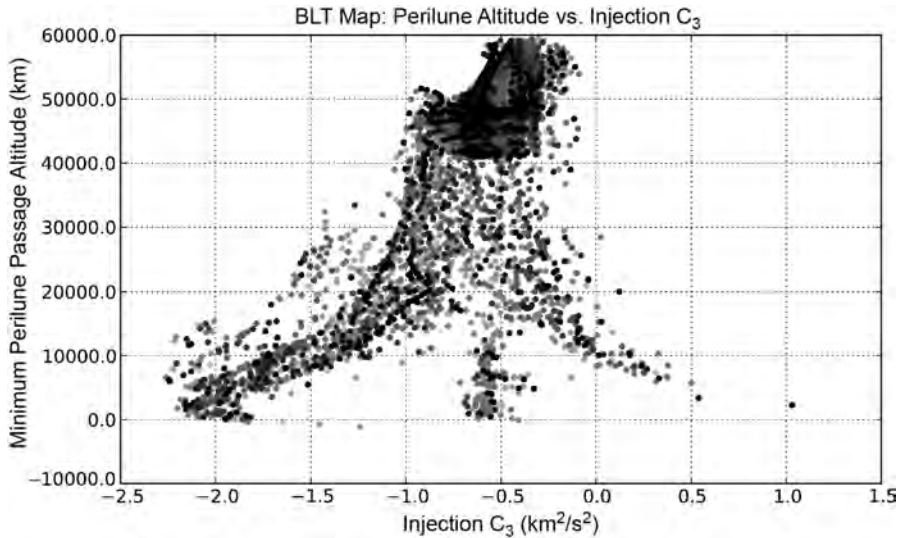


Figure 3-63 The relationship between injection C_3 and the lowest perilune altitude for each transfer in the 12-month survey. The trajectories near the top of the plot do not include any lunar flyby; trajectories toward the bottom do, where those toward the bottom-left receive an energy boost from the Moon and those toward the bottom right have energy removed by the Moon. From lightest to darkest, the shading corresponds to reference dates from 1/1/2017 to 1/1/2018 [44] (Copyright © 2009 by American Astronautical Society Publications Office, San Diego, California (Web Site: <http://www.univelt.com>), all rights reserved; reprinted with permission of the AAS).

independent of the month of the transfer. Typical mission designs prefer the transfer duration to be as short as possible. One can see that there are two types of transfers that require fewer than 100 days to perform: those that require an injection C_3 on the order of -2.1 to -1.5 km^2/s^2 and those that require an injection C_3 on the order of -0.7 to -0.5 km^2/s^2 . Clearly, those that require less injection C_3 pass near the Moon on the way out of the Earth's vicinity.

The *inertial* orientation of each low-energy transfer observed in this 12-month survey clearly depends on which month the transfer departs the Earth. However, the orientation of each similar low-energy transfer is fairly constant throughout the year when observed in the Sun–Earth rotating frame. One way to observe that is to track each transfer's departure from Earth in the Sun–Earth rotating frame. Figure 3-65 shows a plot that compares the departure state of each transfer in the 12-month survey by plotting the relationship of each transfer's right ascension of apogee vector (RAV) and declination of apogee vector (DAV) parameters of the transfer's initial apogee vector. The RAV and DAV values have been computed at the instant of the trans-lunar injection, before any perturbations change the orbit. Each transfer departs the Earth

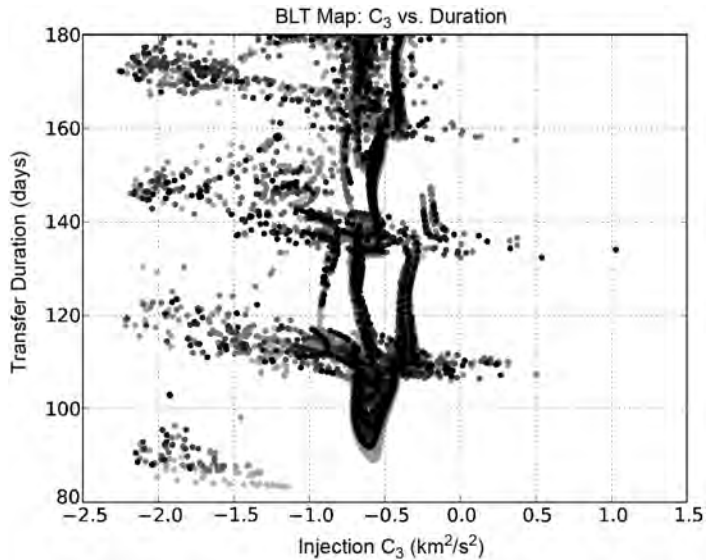


Figure 3-64 The relationship between injection C_3 and duration for each transfer in the 12-month survey. From lightest to darkest, the shading corresponds to reference dates from 1/1/2017 to 1/1/2018 [47] (first published by the American Astronautical Society).

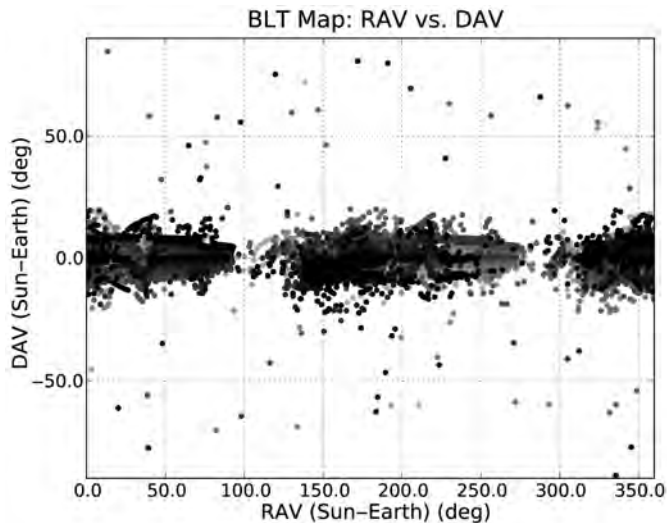


Figure 3-65 The relationship between the right ascension and declination of the apogee vector, RAV and DAV, respectively, for each transfer in the 12-month survey. From lightest to darkest, the shading corresponds to reference dates from 1/1/2017 to 1/1/2018 [47] (first published by the American Astronautical Society).

on an orbit that is highly eccentric, but still captured by the Earth. From Fig. 3-65, one can see that this initial orbit is usually oriented near the ecliptic plane and usually oriented either toward or away from the Sun. A RAV value of 0 deg corresponds to an orbit that has its apogee vector pointing away from the Sun, in the direction of positive x in the Sun–Earth rotating coordinate frame. The outlying points in the figure correspond to transfers that include some combination of Earth phasing loops and lunar flybys and typically do not reappear in the same region of this figure from one month to the next.

The largest variations observed from one synodic month to the next correspond to differences in the low-energy transfer’s injection inclination, in both equatorial and ecliptic reference frames, as illustrated in Fig. 3-66. It is apparent when studying the plots shown in Fig. 3-66 that transfers depart the Earth from orbital planes at nearly any inclination during each synodic month. It is expected that the equatorial inclination of the transfers’ injection points will vary from one synodic month to the next due to the Earth’s obliquity angle; however, significant variations also exist from month to month when observing the transfers’ injection points’ ecliptic inclination values. The variations in the geometry during the year have a more pronounced effect when the trajectories fly near the Earth or Moon.

3.4.6.2 Tracking One Family Through 12 Months The figures shown in the previous sections, as well as analyses in the literature [46] show that one can trace hundreds of different families of low-energy lunar transfers in any given reference month. The characteristics of these families often stack on top of each other in each relationship presented in Figs. 3-62–3-65, making it difficult to discern how the characteristics of one family evolve from month to month. This section studies a subset of transfers of the 12-month survey, filtered to isolate a particular set of practical low-energy transfers. It is often the case that a practical spacecraft mission benefits by shorter transfer durations; it is also usually beneficial to avoid outbound lunar flybys because they add geometrical constraints to the system that make it more difficult to establish a wide launch period. Hence, the filters that have been applied to the transfer selection include:

- Maximum duration: 105 days
- Minimum perilune altitude: 20,000 km

In addition, the set of all transfers that meets these criteria has been divided into two subsets, split such that one subset includes those transfers that travel closer to EL_1 than EL_2 and vice versa. In this way, one can compare practical EL_1 transfers and practical EL_2 transfers from one month to the next.

Figure 3-67 identifies the transfers that meet the filter criteria in the state space map. A visual comparison will confirm that these transfers exist in the most prominent features of the state space maps shown in Figs. 3-54, 3-55, 3-61, and 3-62. One can see that the location of the curves of each family on these plots varies from month to month; the variations appear to be contained within approximately 50 deg in τ and at most 5 days in the orbit’s reference date, T_{ref} .

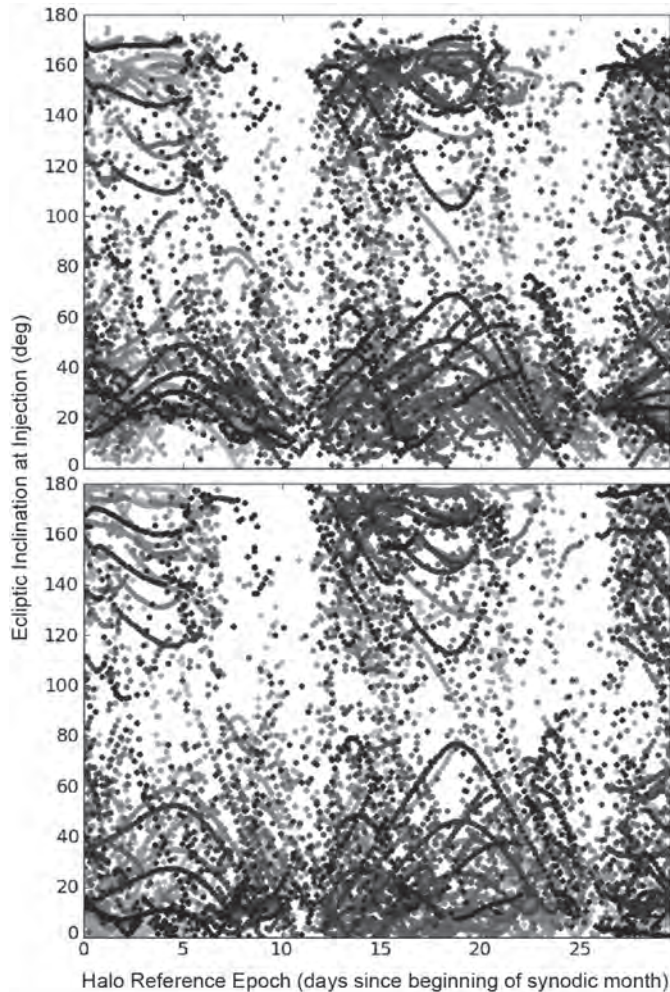


Figure 3-66 The equatorial (top) and ecliptic (bottom) inclination of the transfers' injection point for each low-energy lunar transfer identified in Fig. 3-62. The first month, which starts at a reference epoch of 1 Jan 2017 00:00:00 Ephemeris Time, is shown in the lightest shade and each consecutive synodic month thereafter is plotted in a darker shade. From lightest to darkest, the shading corresponds to reference dates from 1/1/2017 to 1/1/2018 [44] (Copyright © 2009 by American Astronautical Society Publications Office, San Diego, California (Web Site: <http://www.univelt.com>), all rights reserved; reprinted with permission of the AAS).

Figure 3-68 shows the relationship of each transfer's injection C_3 and its duration for every transfer that satisfies the filter criteria. One can clearly see that the transfers' performance parameters vary along a curve for each month, and the performance curve does not vary significantly from one month to the next. The transfer duration

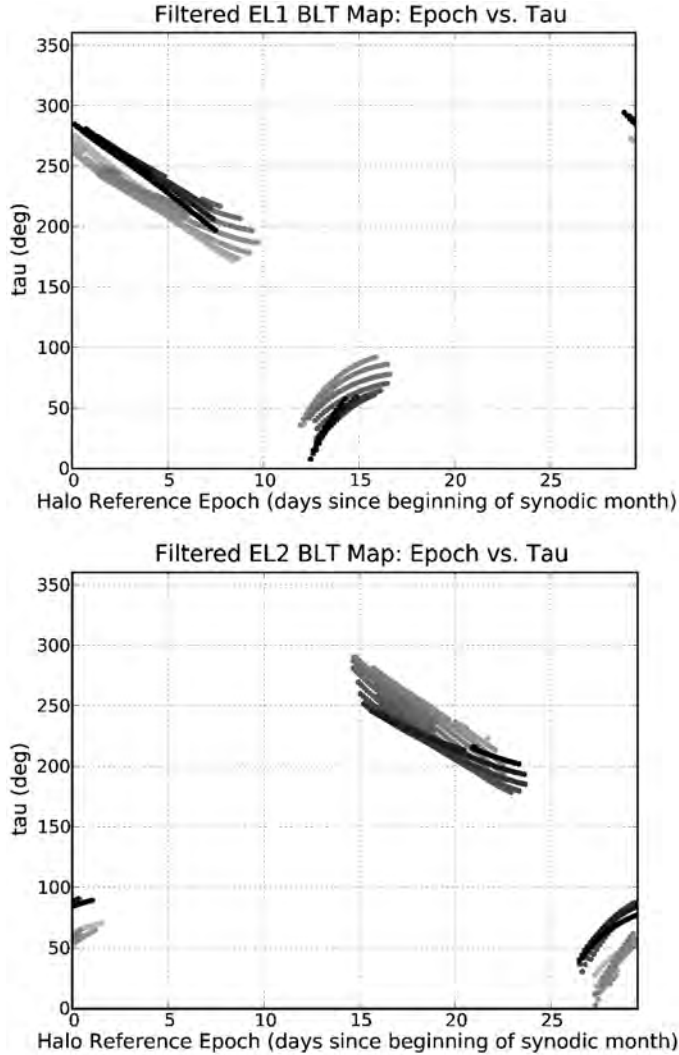


Figure 3-67 The relationship between the reference epoch and τ for each EL_1 (top) and EL_2 (bottom) transfer in the 12-month survey that satisfies the filter criteria. From lightest to darkest, the shading corresponds to reference dates from 1/1/2017 to 1/1/2018 [47] (first published by the American Astronautical Society).

may vary by several days between months, but the curves span very similar ranges of injection C_3 .

It is very interesting to plot the relationship between each transfer's injection date and its injection energy, C_3 . Figure 3-69 shows this comparison for the EL_1 and

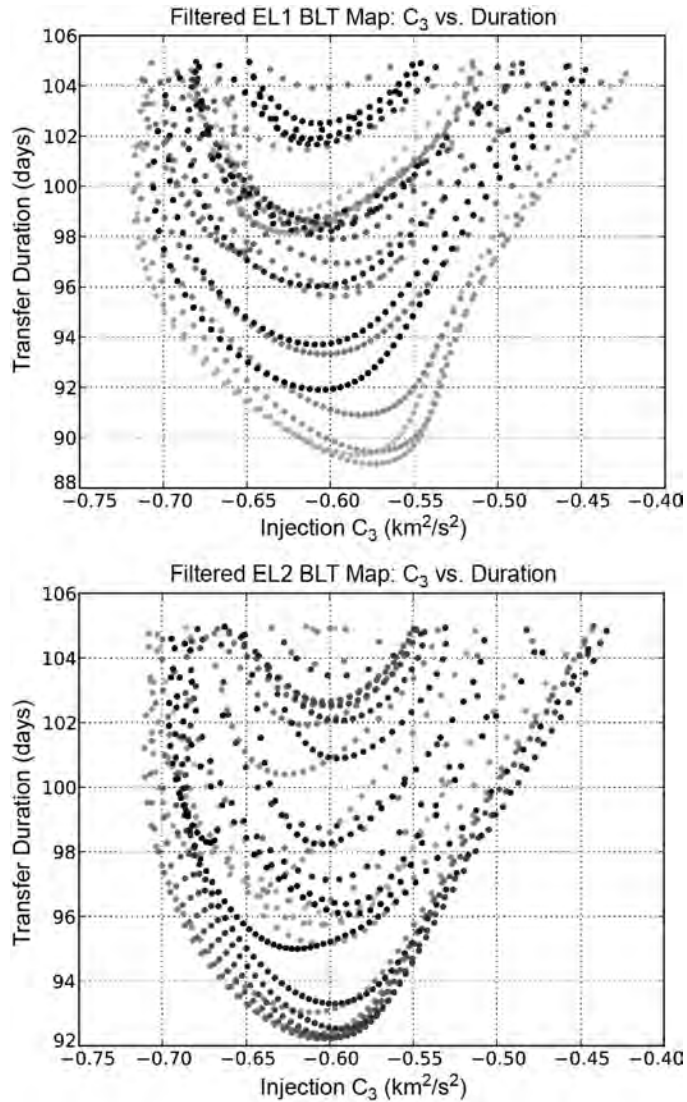


Figure 3-68 The relationship between the injection C_3 and transfer duration for each EL_1 (top) and EL_2 (bottom) transfer in the 12-month survey that satisfies the filter criteria. From lightest to darkest, the shading corresponds to reference dates from 1/1/2017 to 1/1/2018 [47] (first published by the American Astronautical Society).

EL_2 transfers. One can see that the families of transfers shift on this plot from month to month. The comparison also shows that most families of transfers span an injection date of 10 to 15 days. This suggests that there are 10 to 15 days in a launch

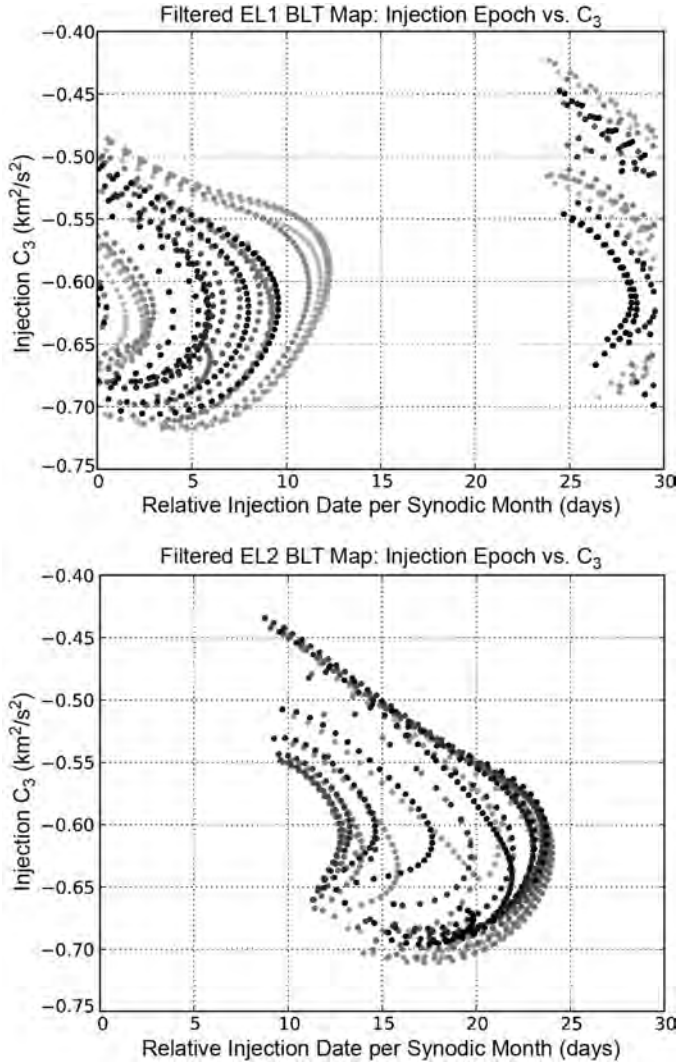


Figure 3-69 The relationship between the injection date and the injection C_3 for each EL_1 (top) and EL_2 (bottom) transfer in the 12-month survey that satisfies the filter criteria. From lightest to darkest, the shading corresponds to reference dates from 1/1/2017 to 1/1/2018 [47] (first published by the American Astronautical Society).

period to this lunar libration orbit via this type of transfer before the deep space ΔV cost increases. This relationship, however, does not take into account differences in the injection inclination throughout the family. Figure 3-69 also verifies that EL_1 transfers and EL_2 transfers depart approximately two weeks apart from each other.

The departure geometry of the filtered transfers is very consistent and predictable from month to month, given the proper analysis. Figures 3-70 and 3-71 show the RAV and DAV parameters for the EL_1 and EL_2 transfers, respectively, computed in the Sun–Earth rotating coordinate frame at the instant of trans-lunar injection. One can immediately observe that the ranges of RAV and DAV values are very limited for each set of transfers: the EL_1 transfers are confined to the approximate range of $\sim 140 \text{ deg} \leq \text{RAV} \leq \sim 170 \text{ deg}$, the EL_2 transfers are confined to the range of $\sim 320 \text{ deg} \leq \text{RAV} \leq \sim 355 \text{ deg}$, and both sets are confined in DAV to the approximate range $\sim -10 \text{ deg} \leq \text{DAV} \leq \sim 10 \text{ deg}$. The RAV values appear to cover a very similar span of values for each month, but there appears to be an annual signal in the DAV values. This systematic variation may be isolated by observing the relationship between a transfer's DAV value and the orientation of the Moon's orbital pole vector at the arrival time. The Moon's orbit has an inclination of approximately 5.1 deg relative to the ecliptic. The Moon's orbital plane is approximately fixed in inertial space, but rotates in the Sun–Earth rotating frame. Figure 3-72 shows the relationship between the transfer's injection DAV value and the right ascension of the lunar orbit pole vector in the Sun–Earth rotating coordinate frame at the time of arrival. One sees a clear annual signal in the data. A mission designer may be able to use this information to improve an initial estimate of the trans-lunar injection geometry. The injection DAV value still varies by approximately 10 deg throughout a family after accounting for the annual variation. This remaining variation may be explained by the z -axis motion of the target orbit at the time of arrival, though that relationship has not been studied sufficiently yet.

A relationship has also been observed between the injection RAV value and the injection C_3 . Figure 3-73 shows this relationship for both the EL_1 and EL_2 transfers. One can see that higher RAV values require less injection energy and there is very little monthly variation in the observed data.

Another parameter that depends closely on the relative orientation of the Moon's orbit about the Earth at the time of the transfer is the inclination of the LEO parking orbit that is used to transfer onto these low-energy transfers. The transfers are constructed by building an initial state at the Moon and propagating backward in time until they intersect a 185-km parking orbit above the Earth's surface. The inclination of that parking orbit is driven by the geometry of the transfer. A real mission launched from Cape Canaveral, Florida, would likely launch from an orbit with an equatorial inclination near 28.5 deg and perform maneuvers to target the desirable low-energy transfer [183, 184]. This is the subject of Section 6.5. That section shows that the closer the natural transfer is to having a parking orbit with a particular, desired inclination, the less ΔV is required to target that transfer from the desired parking orbit, though extended launch periods reduce the ΔV significance.

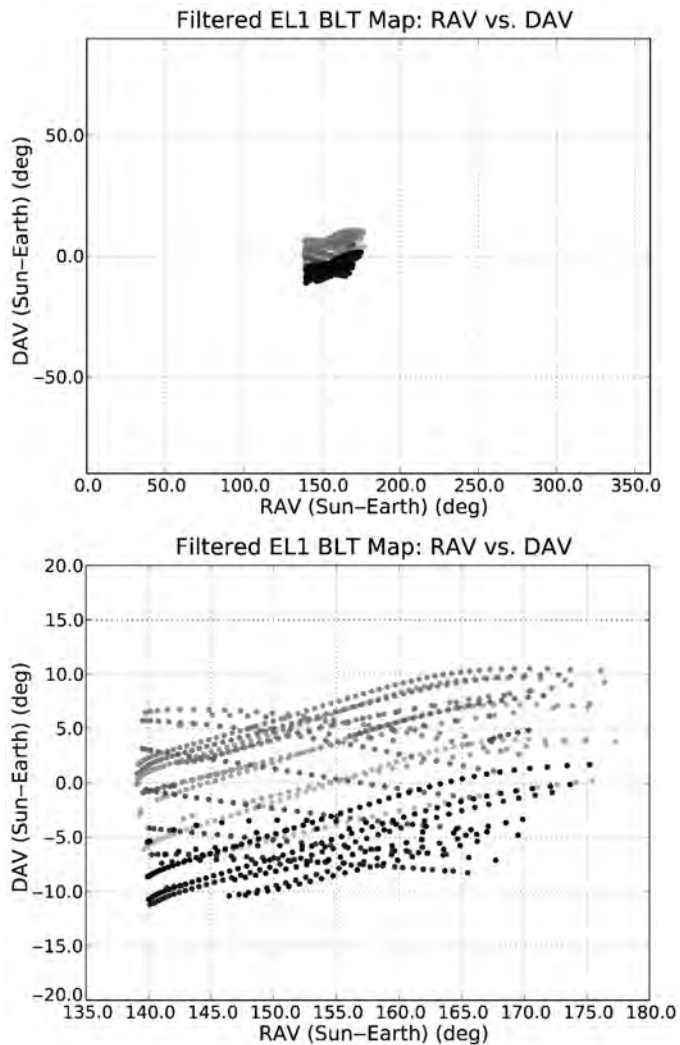


Figure 3-70 The relationship between RAV and DAV (the right ascension and declination of the apogee vector) at the time of trans-lunar injection for the filtered EL_1 transfers. From lightest to darkest, the shading corresponds to reference dates from 1/1/2017 to 1/1/2018. Top: one can see that RAV and DAV are confined in a narrow box for these transfers; bottom: a closer look at the parameter space [47] (first published by the American Astronautical Society).

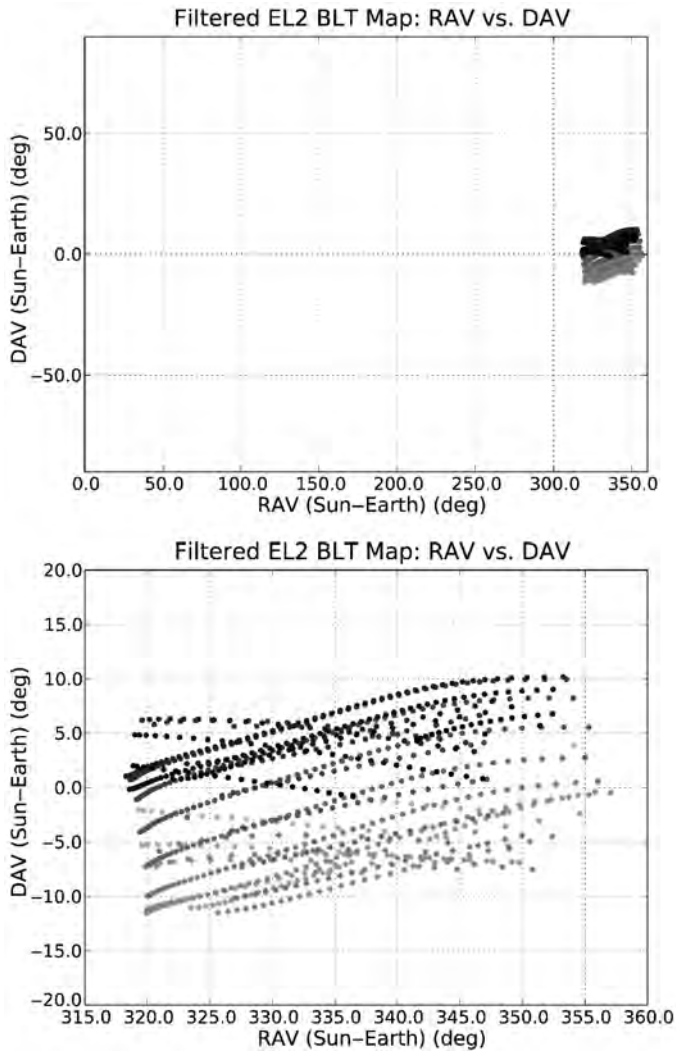


Figure 3-71 The same relationship between RAV and DAV as Fig. 3-70, but for the filtered EL_2 transfers. From lightest to darkest, the shading corresponds to reference dates from 1/1/2017 to 1/1/2018 [47] (first published by the American Astronautical Society).

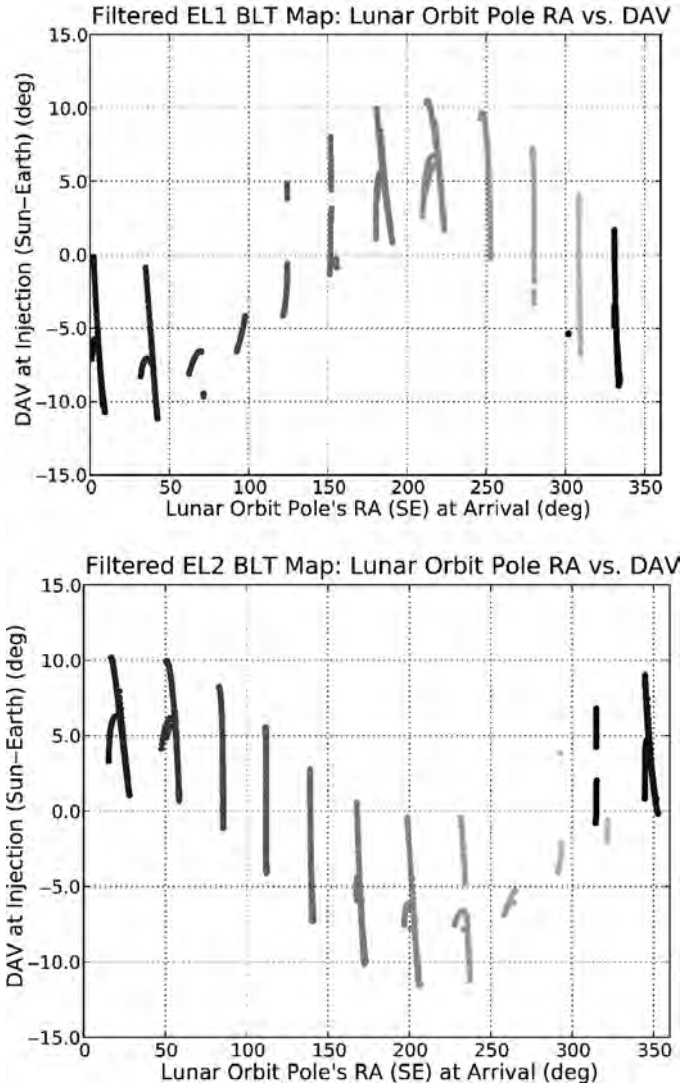


Figure 3-72 The relationship between the right ascension of the lunar orbit’s pole vector at the time of arrival and the value of DAV at the time of injection, both computed in the Sun–Earth rotating coordinate frame. From lightest to darkest, the shading corresponds to reference dates from 1/1/2017 to 1/1/2018. This relationship is shown for each EL₁ (top) and EL₂ (bottom) transfer in the 12-month survey that satisfies the filter criteria [47] (first published by the American Astronautical Society).

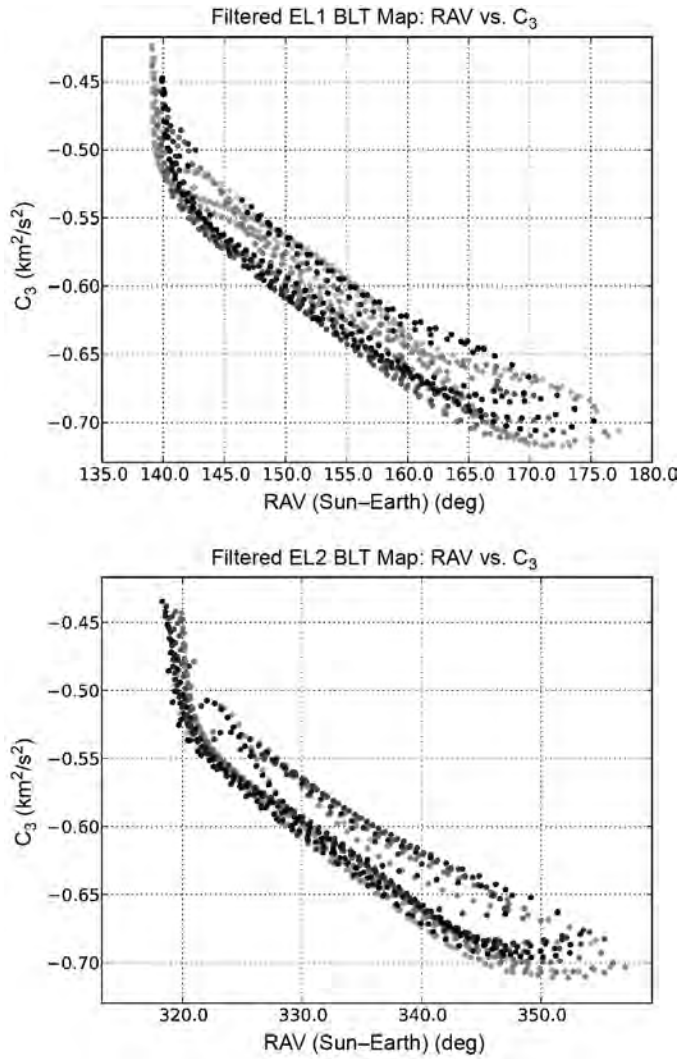


Figure 3-73 The relationship between the right ascension of the apogee vector, RAV, at the time of trans-lunar injection and the injection energy, C_3 , for each EL_1 (top) and EL_2 (bottom) transfer in the 12-month survey that satisfies the filter criteria. From lightest to darkest, the shading corresponds to reference dates from 1/1/2017 to 1/1/2018 [47] (first published by the American Astronautical Society).

Figure 3-74 shows the relationship between the reference date of the lunar halo orbit and the equatorial inclination of the natural LEO parking orbit needed to perform the transfer. One can see that the inclination varies significantly from one month to the next. Figure 3-75 shows the relationship between the right ascension of the lunar orbit pole vector and the ecliptic inclination of the LEO parking orbit. One can clearly see that there is an evolution of the inclination from one month to the next. Figure 3-76 shows the same plot, but this time presenting the relationship between the lunar orbit pole vector and the equatorial inclination of the LEO parking orbit.

3.4.6.3 Annual Variations Much of the monthly variation observed in families of low-energy lunar transfers is caused by the Moon's noncircular, inclined orbit relative to the Earth. Other variations in the Solar System change over the course of several years, evident in the analysis in Section 2.5.3. It is therefore of interest to ensure that the relationships observed here hold over the course of several years. The same analyses performed in the previous section have been performed again on a set of transfers constructed with reference dates spanning the year 2021, four years after the previous study. The results of this new examination coincide very well with the previous study. Not all of the results will be shown here for brevity.

Figure 3-77 shows the relationship between T_{ref} and τ , where the lighter shaded points are low-energy transfers that exist in 2017 and the darker points are low-energy transfers that exist in 2021. One can see that the combinations of the two parameters are very similar for both years. Figure 3-78 shows a similar comparison between the injection C_3 and duration of the transfers in both 2017 and 2021. One can see that there is very little noticeable difference between the points in 2017 and 2021.

The transfers that exist in 2021 have been filtered in the same way as the transfers presented in Section 3.4.6.2 in order to observe how the family might change during the course of four years. Figures 3-79 and 3-80 show the same relationships as shown in Figs. 3-72 and 3-75, except now for filtered transfers in 2017 and 2021. One can see that the 2021 parameters overlap the 2017 data very well, including the dramatic monthly variations observed in the data.

The evidence suggests that the yearly variations are much more subtle than the monthly variations that exist.

3.4.7 Transfers to Other Three-Body Orbits

All of the analyses performed in Sections 3.4.3 through 3.4.6 have used the family of halo orbits about the LL_2 point as the example destination, but these analyses work for any unstable three-body orbit in the Earth–Moon system.

Section 3.4.7.1 explores low-energy lunar transfers that target an example lunar L_1 halo orbit. Since this orbit is on the interior side of the Moon, the trajectories that target it must transfer from the lunar L_2 region past the Moon before encountering the target orbit.

Section 3.4.7.2 explores low-energy lunar transfers that target an example distant prograde orbit about the Moon. Orbits in this family traverse both the near and far sides of the Moon. Hence, transfers that target these orbits may demonstrate

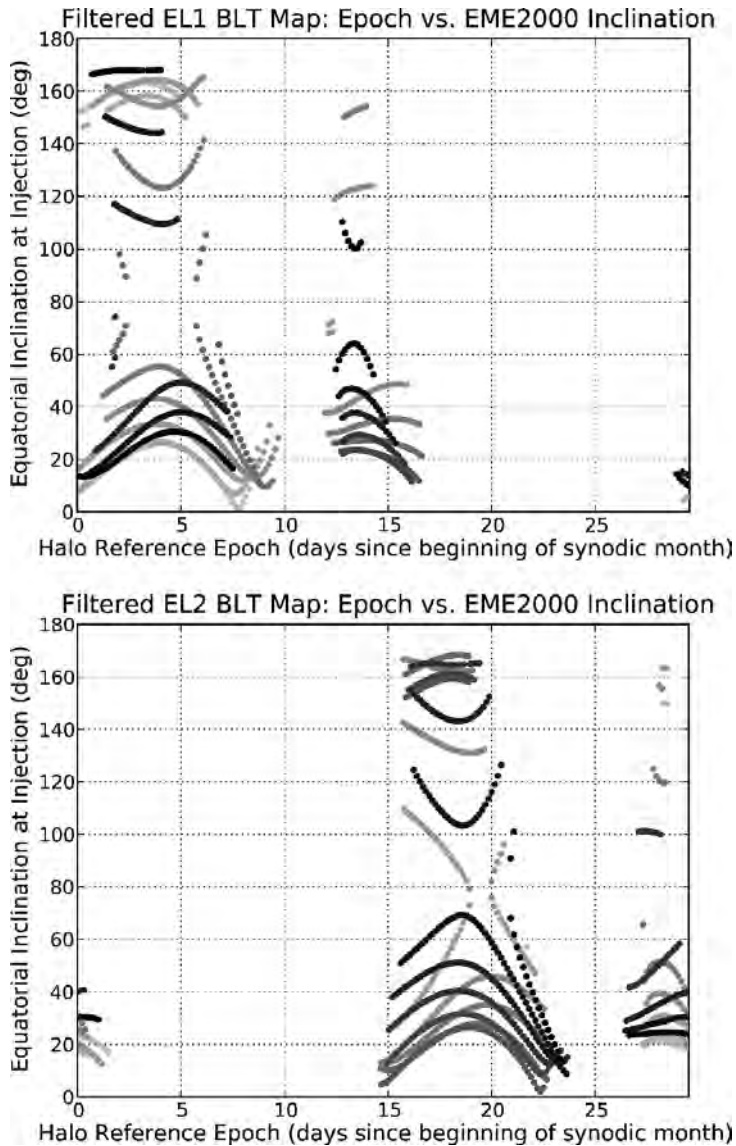


Figure 3-74 The relationship between the reference date of the lunar halo orbit and the equatorial inclination of the LEO parking orbit needed to perform the transfer. From lightest to darkest, the shading corresponds to reference dates from 1/1/2017 to 1/1/2018. This relationship is shown for each EL_1 (top) and EL_2 (bottom) transfer in the 12-month survey that satisfies the filter criteria [47] (first published by the American Astronautical Society).

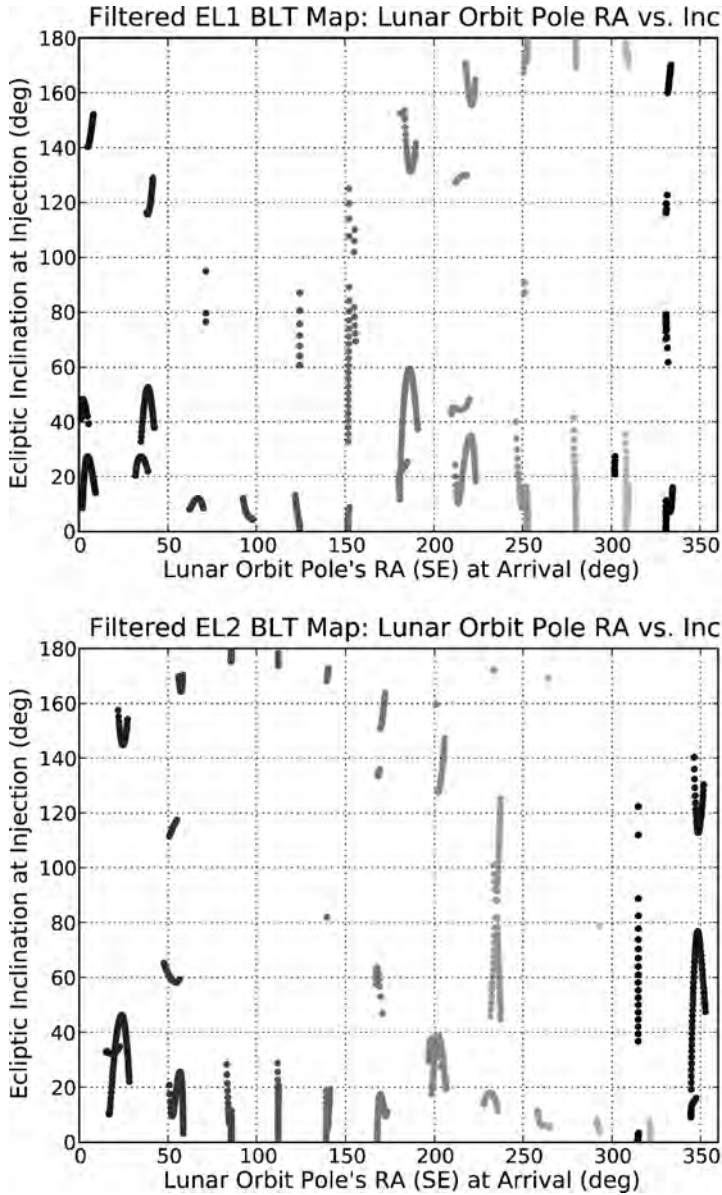


Figure 3-75 The relationship between the right ascension of the lunar orbit pole vector and the ecliptic inclination of the LEO parking orbit. From lightest to darkest, the shading corresponds to reference dates from 1/1/2017 to 1/1/2018. This relationship is shown for each EL₁ (top) and EL₂ (bottom) transfer in the 12-month survey that satisfies the filter criteria [47] (first published by the American Astronautical Society).

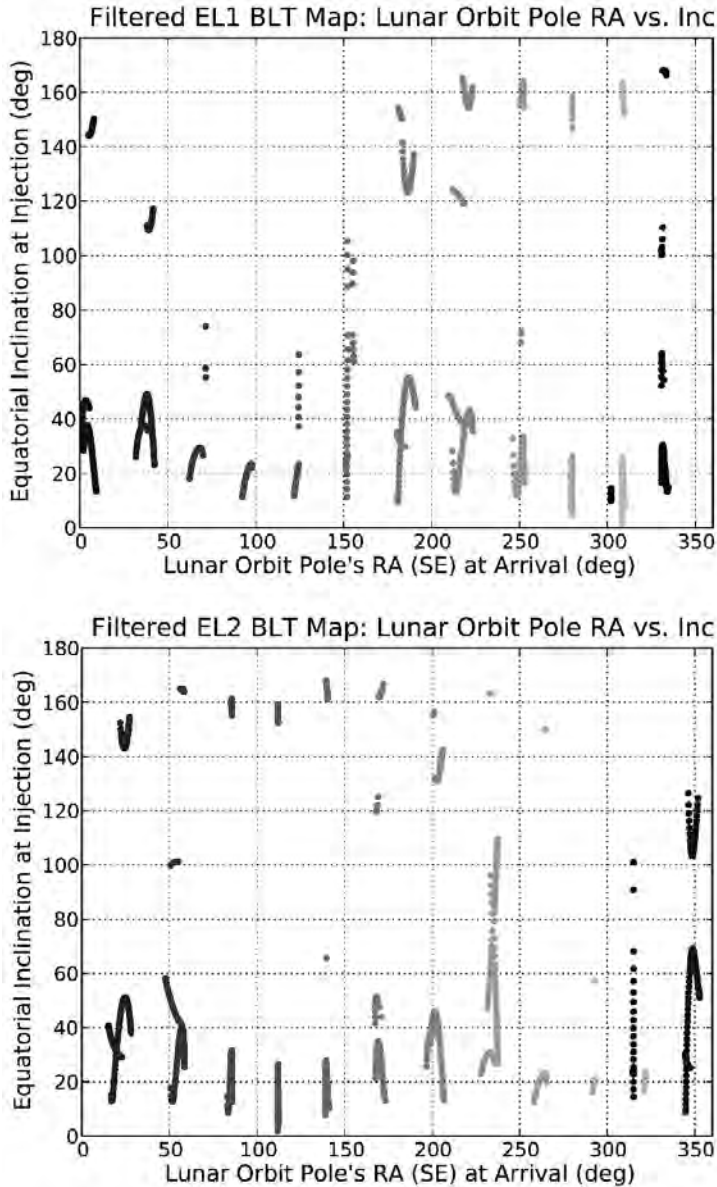


Figure 3-76 The relationship between the right ascension of the lunar orbit pole vector and the equatorial inclination of the LEO parking orbit. From lightest to darkest, the shading corresponds to reference dates from 1/1/2017 to 1/1/2018. This relationship is shown for each EL₁ (top) and EL₂ (bottom) transfer in the 12-month survey that satisfies the filter criteria [47] (first published by the American Astronautical Society).

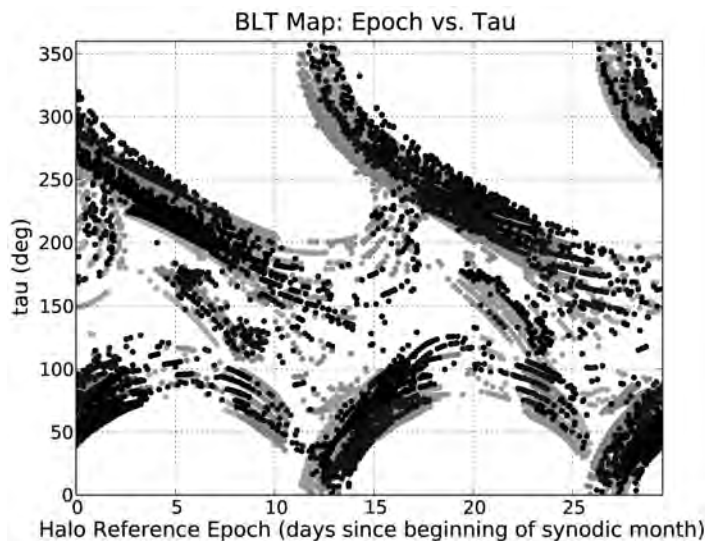


Figure 3-77 The combinations of T_{ref} and τ that yield low-energy transfers between 185-km LEO parking orbits and the target lunar libration orbit during 2017 (gray points) and 2021 (black points) [47] (first published by the American Astronautical Society).

characteristics similar to low-energy lunar transfers that target either L_1 or L_2 halo orbits.

These analyses are merely additional examples to demonstrate these analysis techniques. All analyses will likely need to be repeated given specific mission design requirements. That is, a given mission may require a spacecraft to transfer to a particular unstable three-body orbit, perhaps for communication, staging, or rendezvous reasons, and a new BLT map will need to be generated to study the trajectory options that exist.

3.4.7.1 Low-Energy Transfers to a Lunar L_1 Halo Orbit This section explores low-energy ballistic transfers to an example lunar L_1 halo orbit. For simplicity in this example analysis, the Patched Three-Body Model is used; hence, the L_1 halo orbit is perfectly periodic.

In order to reach a halo orbit about the L_1 point via a typical low-energy transfer, a spacecraft must depart the Earth and arrive in the lunar L_2 vicinity in much the same way as a spacecraft following a low-energy transfer to a lunar L_2 halo orbit. Then from the vicinity of L_2 , the spacecraft must transfer past the Moon before arriving at its target L_1 halo orbit. As usual, there are two types of transfers: transfers that implement either the exterior or the interior stable manifold of the L_1 halo orbit. Interior transfers may arrive on the L_1 halo orbit immediately after passing by the Moon since the interior stable manifold is propagated in that direction. Exterior

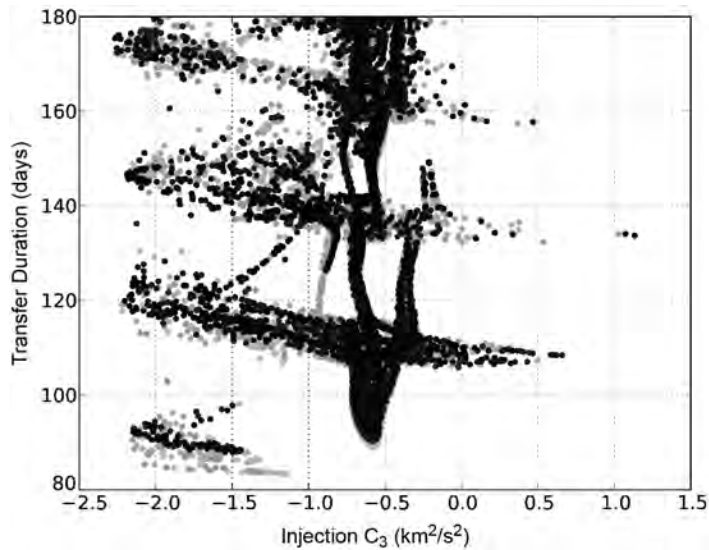


Figure 3-78 The combinations of injection C_3 and transfer duration that yield viable low-energy lunar transfers in 2017 (gray points) and 2021 (black points) [44] (Copyright © 2009 by American Astronautical Society Publications Office, San Diego, California (Web Site: <http://www.univelt.com>), all rights reserved; reprinted with permission of the AAS).

transfers to most L_1 halo orbits must first traverse some sort of Earth staging orbit prior to arriving on the L_1 halo orbit.

Figure 3-81 shows an example interior low-energy transfer to a lunar L_1 halo orbit in the Sun–Earth synodic reference frame. Figure 3-82 shows the same transfer in the Earth–Moon synodic reference frame. The characteristics of this example transfer are very similar to many of the low-energy transfers previously studied in this work that have transferred to L_2 halo orbits. The only major difference is that this example low-energy transfer passes through the L_2 region en route to the L_1 region, where it encounters its target L_1 halo orbit.

Figures 3-83 and 3-84 show an example exterior low-energy transfer to a lunar L_1 halo orbit in the Sun–Earth and Earth–Moon synodic reference frames, respectively. One can see that the transfer involves an Earth staging orbit, which permits it to encounter the L_1 halo orbit along the orbit’s exterior stable manifold. Every exterior low-energy transfer that has been constructed in this work between the Earth and this L_1 halo orbit requires the use of at least one Earth staging orbit. When propagated backward in time, the exterior lunar transfers depart the L_1 halo orbit away from the Moon; hence, they must return to the Moon via an Earth staging orbit in order to transfer out of the Earth–Moon system and into the Sun–Earth system.

Figures 3-85 and 3-86 show the interior and exterior BLT maps, respectively, for low-energy transfers to this halo orbit, making it possible to characterize many

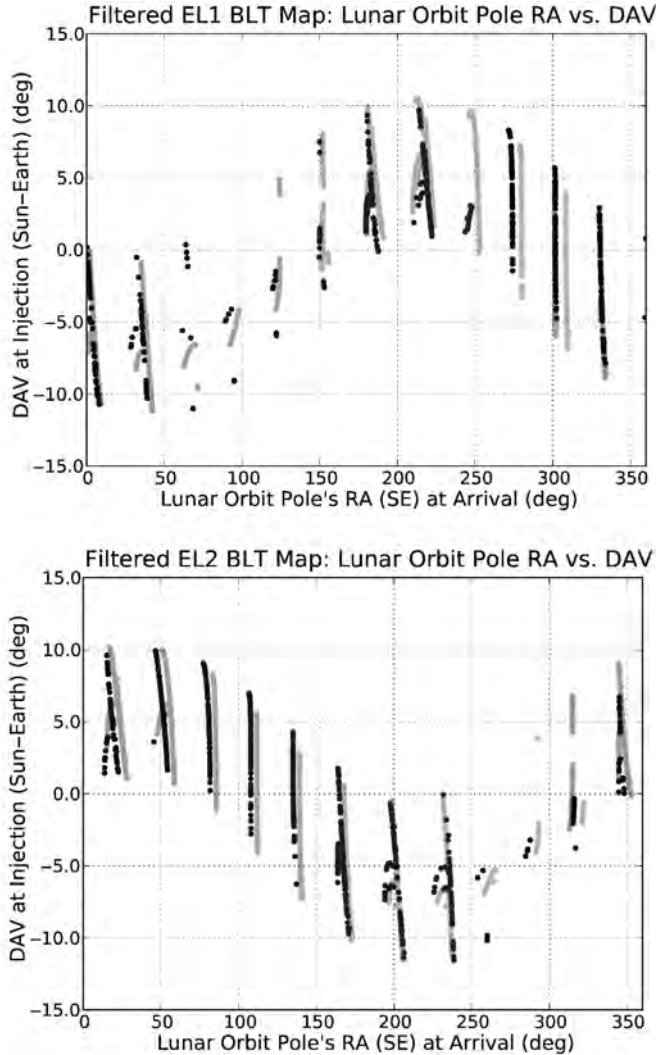


Figure 3-79 The relationship between the right ascension of the lunar orbit pole vector and the declination of the apogee vector at the time of injection. This relationship is shown for each EL_1 (top) and EL_2 (bottom) transfer in both the 2017 (light) and 2021 (dark) surveys that satisfies the filter criteria [47] (first published by the American Astronautical Society).

transfers to this orbit simultaneously. Each figure also shows eight example transfers to display some of the available transfer options that exist to this halo orbit. The BLT maps are colored according to the altitude of closest approach that each trajectory makes, given the values of θ and τ , when propagated backward in time at most

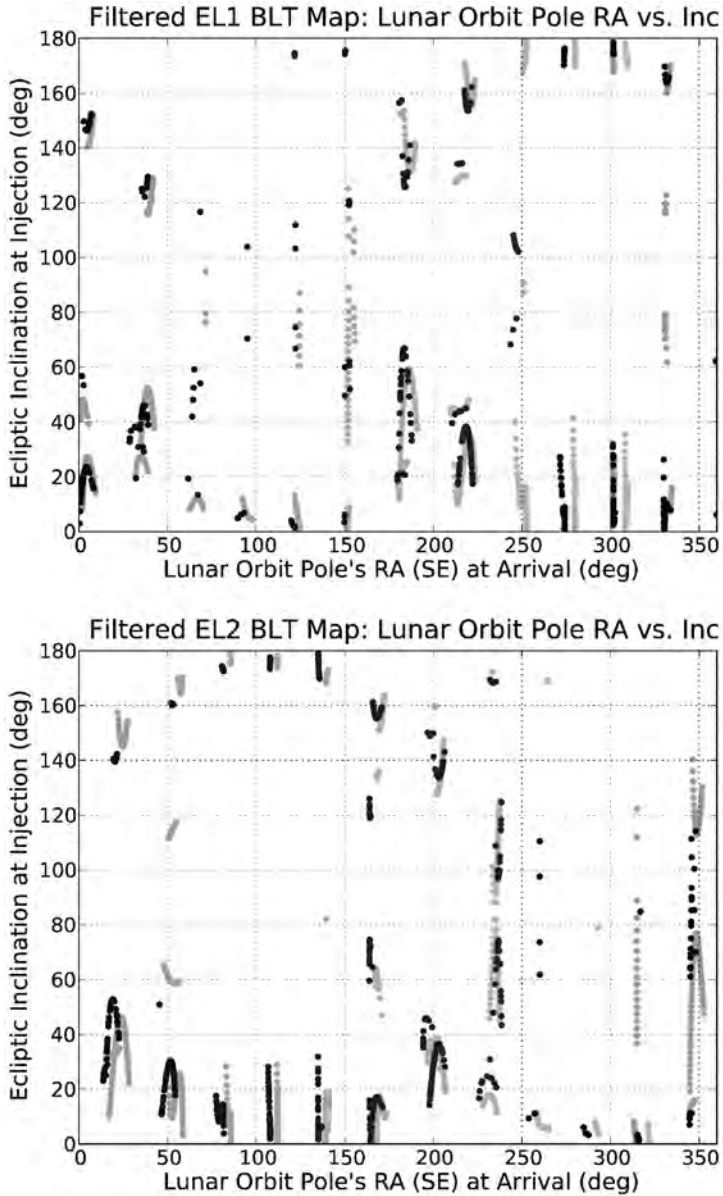


Figure 3-80 The relationship between the right ascension of the lunar orbit pole vector and the ecliptic inclination of the LEO parking orbit. This relationship is shown for each EL₁ (top) and EL₂ (bottom) transfer in both the 2017 (light) and 2021 (dark) surveys that satisfies the filter criteria [47] (first published by the American Astronautical Society).

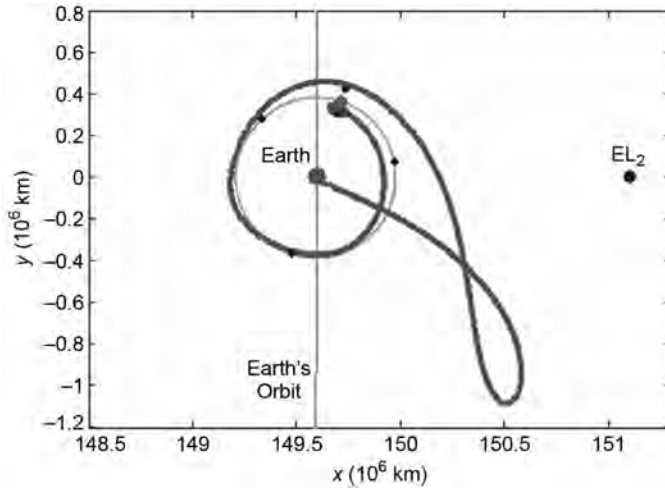


Figure 3-81 An example interior low-energy transfer to a lunar L_1 halo orbit, shown in the Sun–Earth synodic reference frame from above the ecliptic.

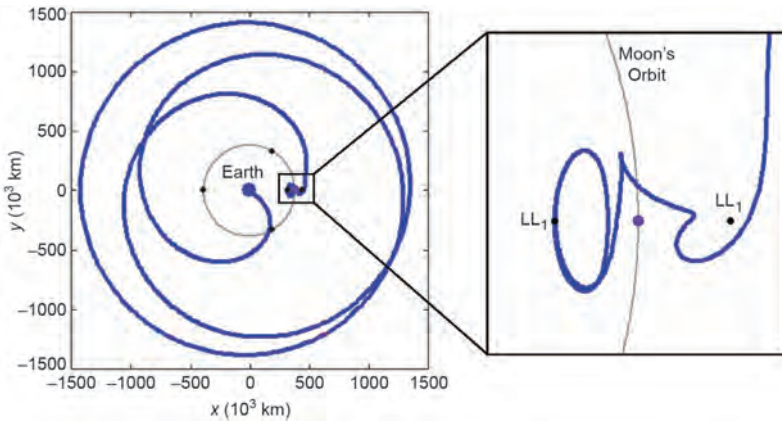


Figure 3-82 The same low-energy transfer presented in Fig. 3-81, but now shown in the Earth–Moon synodic reference frame from above the ecliptic.

195 days. Points colored black in each BLT map correspond to transfers that may be used to depart the Earth from a low-altitude orbit, or from the surface directly. The lightest colors correspond to transfers that do not approach any closer to the Earth than the L_1 orbit itself when propagated backward in time. As usual, we are only interested in the darkest regions of the BLT maps because those regions correspond with trajectories that depart from practical low Earth orbits.

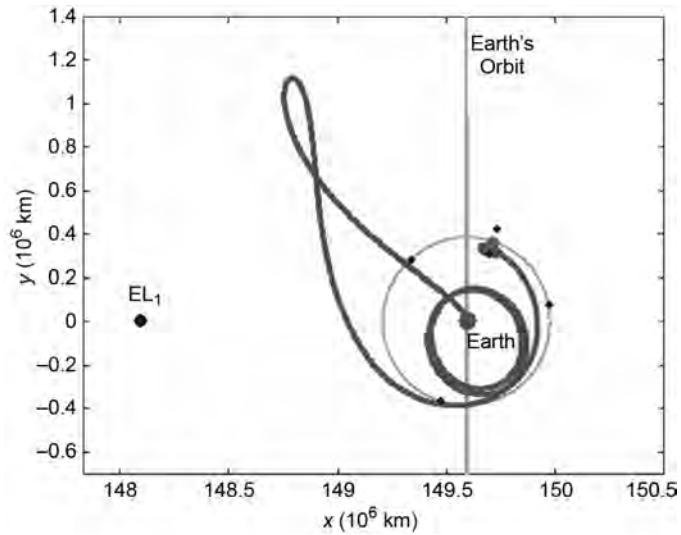


Figure 3-83 An example exterior low-energy transfer to a lunar L_1 halo orbit, shown in the Sun–Earth synodic reference frame from above the ecliptic.

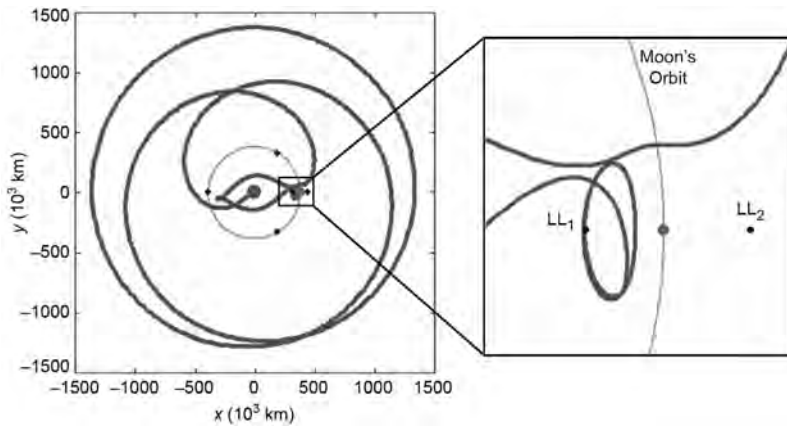


Figure 3-84 The same low-energy transfer presented in Fig. 3-83, but now shown in the Earth–Moon synodic reference frame from above the ecliptic.

One can see that the two BLT maps shown in Figs. 3-85 and 3-86 are very complex. This makes sense because the only ways to construct ballistic transfers between the Earth and this lunar L_1 halo orbit require some combination of lunar passages and Earth staging orbits.

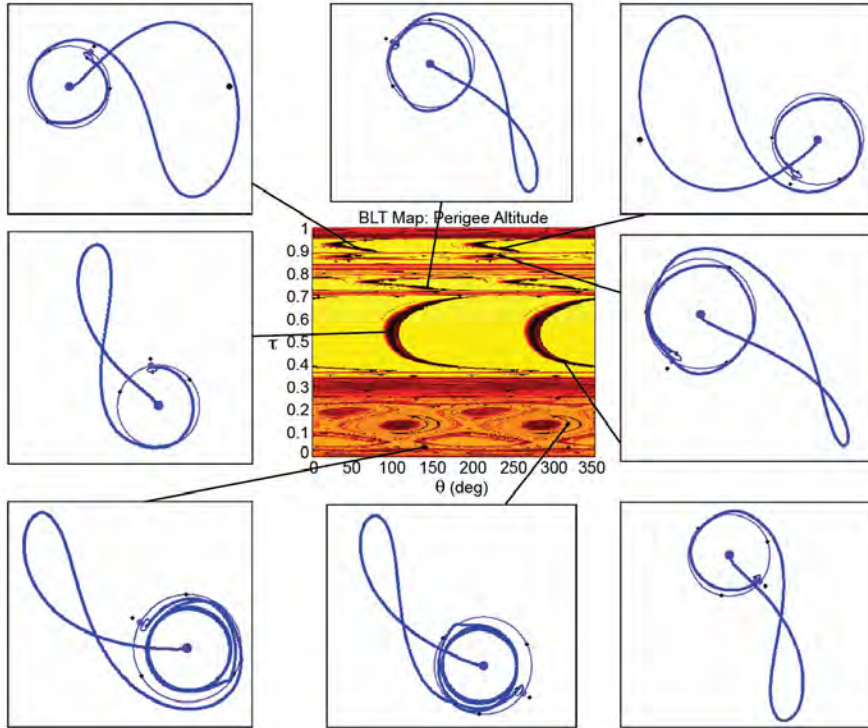


Figure 3-85 The interior BLT map for low-energy transfers to the example lunar L_1 halo orbit. Eight example low-energy transfers are shown around the BLT map to demonstrate some of the types of transfers that may be constructed between 185-km LEO orbits and this halo orbit. (See insert for color representation of this figure.)

When studying Fig. 3-85, one notices many things. First, the BLT map is rather simple in the range of τ -values between 0.4 and 0.7. This region of τ -values includes ballistic lunar transfers that make only a single lunar passage en route to the L_1 halo orbit. These transfers resemble the simplest low-energy transfers to lunar L_2 halo orbits and have very similar performance parameters. Somewhat more complex transfers are shown in the BLT map for τ -values between 0.7 and 0.96: most of these involve several close lunar passages en route to the L_1 halo orbit. Every transfer constructed with a τ -value between 0 and 0.35 involves at least one Earth staging orbit, as may be seen in the two example transfers shown on the lower-left edge of the figure.

The exterior BLT map shown in Fig. 3-86 is more complex than the interior BLT map. This is because each transfer must implement at least one Earth staging orbit in addition to whatever lunar passages are required to complete the low-energy transfer.

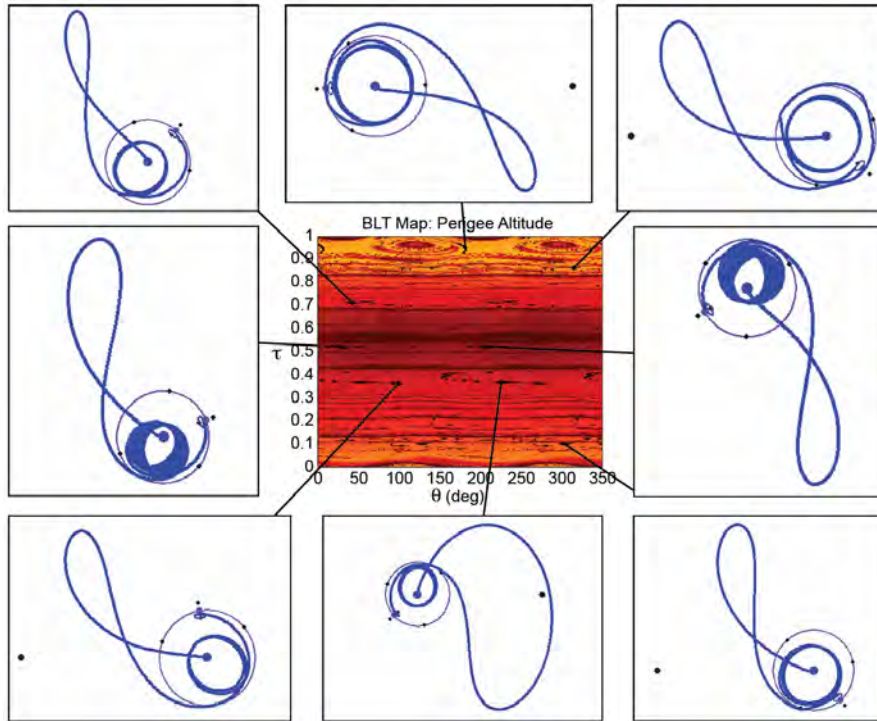


Figure 3-86 The exterior BLT map for low-energy transfers to the example lunar L_1 halo orbit. Eight example low-energy transfers are shown around the BLT map to demonstrate some of the types of transfers that may be constructed between 185-km LEO orbits and this halo orbit. (See insert for color representation of this figure.)

One may verify this by observing that every example trajectory shown around the edge of Fig. 3-86 includes at least one Earth staging orbit. Otherwise, these transfers are very similar to other lunar transfers previously studied.

3.4.7.2 Low-Energy Transfers to a Distant Prograde Orbit This section explores low-energy ballistic transfers to an example distant prograde orbit (DPO) about the Moon. Like the previous section, this analysis is performed using the Patched Three-Body Model, making the DPO perfectly periodic. Distant prograde orbits are interesting because they traverse both the near and far sides of the Moon. One might suspect that the qualitative nature of a low-energy transfer to such an orbit might take on characteristics of transfers to either L_1 or L_2 halo orbits, depending on how the specific transfer arrives at the orbit.

An example DPO has been generated here that has fairly large lobes and is easy to view in the example transfers presented here. Figure 3-87 shows an example

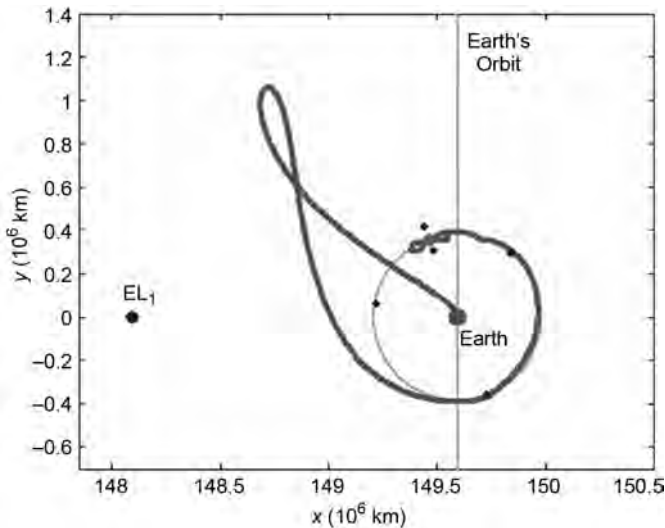


Figure 3-87 An example low-energy transfer to a distant prograde orbit, shown in the Sun–Earth synodic reference frame from above the ecliptic.

low-energy transfer to this distant prograde orbit in the Sun–Earth synodic reference frame. Figure 3-88 shows the same example transfer in the Earth–Moon synodic reference frame. One can see that this transfer does not enter any staging orbits, nor make any lunar flybys, but rather injects immediately into the distant prograde orbit. Other ballistic transfers may be produced that do use staging orbits or other complex lunar flybys en route to the orbit.

Because of the symmetry in the distant prograde orbit’s shape, the two halves of the orbit’s stable manifold are not clearly identifiable based on their immediate motion. That is, both halves of the stable manifold include both interior and exterior trajectories. However, the majority of one half of the distant prograde orbit’s stable manifold propagates toward the Earth, and the majority of the other half propagates away from the Earth. This discussion refers to the half that propagates toward the Earth as the interior stable manifold and the other half as the exterior manifold. Using this nomenclature, Figs. 3-89 and 3-90 show the exterior and interior BLT maps, respectively, for low-energy transfers to this distant prograde orbit.

Along with the exterior BLT map, Fig. 3-89 also shows eight example exterior transfers that exist to this distant prograde orbit. One can see that these transfers are very simple—they don’t require any lunar flybys or staging orbits to reach the target orbit. Because such simple transfers are prevalent in this exterior BLT map, the map is consequently not nearly as chaotic as some of the previous BLT maps studied in this chapter. The interior BLT map shown in Fig. 3-90, however, presents more complex transfers to this distant prograde orbit, including several examples of low-energy transfers that require Earth staging orbits.

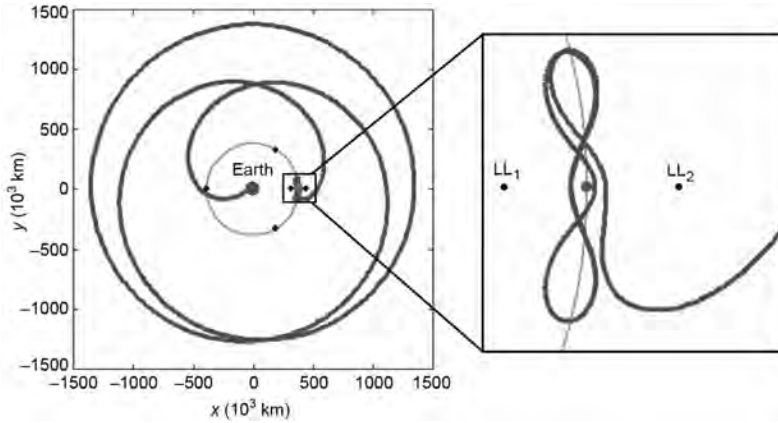


Figure 3-88 The same transfer presented in Fig. 3-87, but now shown in the Earth–Moon synodic reference frame from above the ecliptic.

The characteristics of the exterior transfers shown in Fig. 3-89 resemble the characteristics of the exterior transfers to the lunar L_2 halo orbit. The only real complexity that may be introduced into the majority of such transfers is the addition of a lunar flyby en route to the transfers' apogee passages. Conversely, the characteristics of many of the interior transfers shown in Fig. 3-90 resemble the characteristics of the exterior transfers to the lunar L_1 halo orbit shown in Fig. 3-86. This makes sense because the majority of both types of transfers involve Earth staging orbits, among other features.

3.4.7.3 Discussion This section has demonstrated that the methodology presented in this examination may be applied to many different families of unstable three-body orbits. The same techniques may be applied to quasiperiodic and aperiodic orbits as well, such as Lissajous orbits, though the parameters that generate the BLT maps will not be perfectly cyclical. The low-energy transfers and BLT maps constructed using different target orbits may appear very different. Nonetheless, families of low-energy transfers may still be identified and systematically evaluated in order to identify good candidates for practical lunar missions.

3.5 THREE-BODY ORBIT TRANSFERS

Once a spacecraft has arrived at a lunar three-body orbit, the spacecraft has several options. First, it may remain there for as long as desired, or at least until its station-keeping fuel budget is exhausted (which may be years). Lunar halo orbits may be a desirable location for communication and/or navigation satellites; they may also be a desirable location for space stations or servicing satellites.

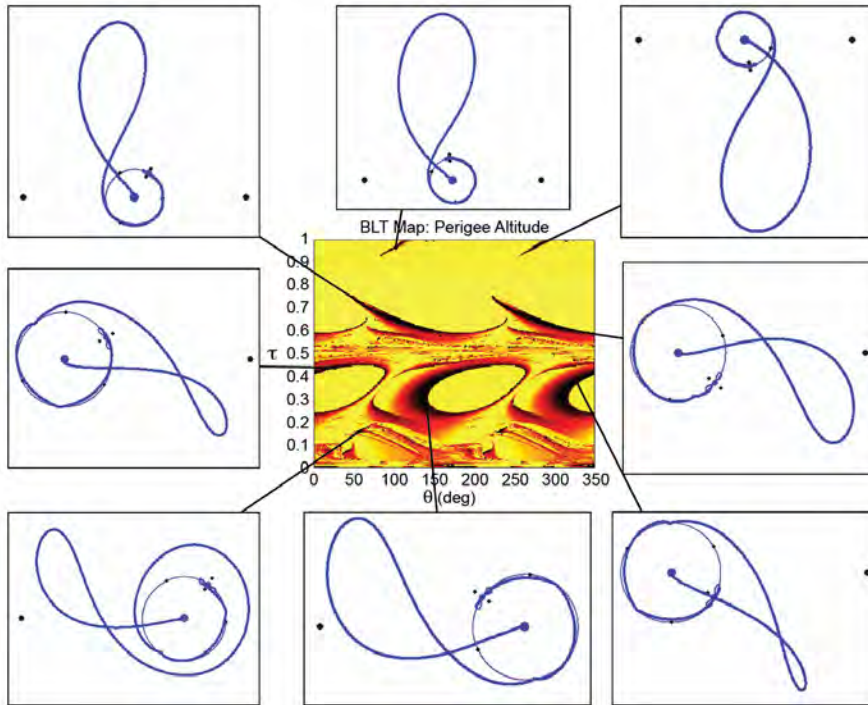


Figure 3-89 The exterior BLT map for low-energy transfers to the example distant prograde orbit about the Moon. Eight example low-energy transfers are shown around the BLT map to demonstrate some of the types of transfers that may be constructed between 185-km LEO orbits and this lunar orbit. (See insert for color representation of this figure.)

The spacecraft may transfer from the three-body orbit to a different three-body orbit in the Earth–Moon system for very little energy, provided that both orbits are unstable and have the same Jacobi constant [162, 185, 186]. For instance, the spacecraft might arrive at a lunar L_2 halo orbit and then later transfer to a lunar L_1 halo orbit. Section 2.6.11 presents several methods that one may use to identify and construct such transfers.

The spacecraft may also transfer from the nominal three-body orbit onto its unstable manifold and follow that trajectory to a desirable stable lunar orbit. It has been found that nearly any low lunar orbit is accessible in this way, and every transfer studied has required a smaller orbit-insertion maneuver than any conventional, direct transfer to the same low lunar orbit [46]. An example of such a transfer will be described in more detail below.

Similarly, the spacecraft may follow the unstable manifold of the three-body orbit down to the surface of the Moon. It has been found that any point on the surface

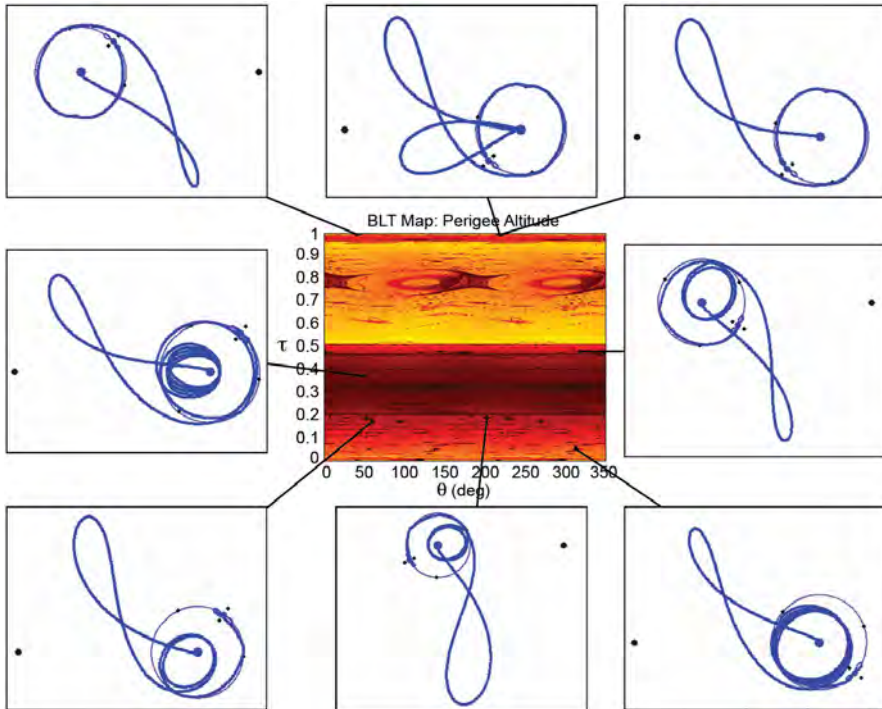


Figure 3-90 The interior BLT map for low-energy transfers to the example distant prograde orbit about the Moon. Eight example low-energy transfers are shown around the BLT map to demonstrate some of the types of transfers that may be constructed between 185-km LEO orbits and this lunar orbit. (See insert for color representation of this figure.)

of the Moon may be reached, although some points require several orbits about the Moon prior to touch-down [11, 46]. Again, the required ΔV to land from the lunar three-body orbit is smaller than the required ΔV to land following a conventional, direct transfer from the Earth.

Finally, the spacecraft has the option to return to the Earth following a low-energy Earth-return trajectory. Every low-energy lunar transfer has a symmetric Earth-return counterpart; the Earth-return trajectory does not need to be a mirror image of the trajectory used to arrive at the lunar orbit.

If the spacecraft's final destination is not the lunar three-body orbit, then the spacecraft does not need to inject into that orbit. Instead, the orbit's stable manifold may be used to guide the spacecraft to its final destination rather than to inject the spacecraft onto the three-body orbit. The stable manifold may be used as an initial guess into a trajectory optimization routine, such as a multiple-shooting differential corrector (Section 2.6.5.2).

3.5.1 Transfers from an LL_2 Halo Orbit to a Low Lunar Orbit

The discussion henceforth graphically illustrates some example options that a spacecraft has upon arriving at a lunar halo orbit. Figure 3-91 shows one such lunar halo staging orbit and its unstable manifold. A spacecraft on this halo orbit may depart along any one of these trajectories. These trajectories fly by the Moon at different radii and inclinations, indicating that many different final lunar orbits are accessible from this staging orbit. When one considers all halo orbits in the family of L_2 halo orbits, one finds that nearly any low lunar orbit may be accessed by a low-energy lunar transfer. Figure 3-92 shows the available options that have been identified for

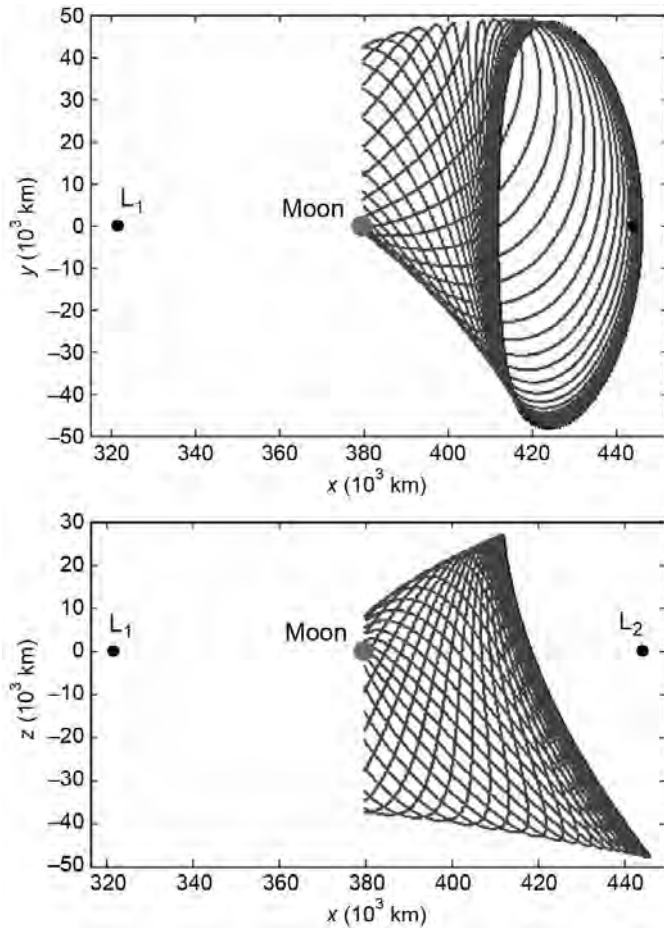


Figure 3-91 An example lunar halo staging orbit and its unstable manifold, viewed in the Earth–Moon rotating frame from above (top) and from the side (bottom). A spacecraft on this halo orbit may depart along any one of the trajectories shown.

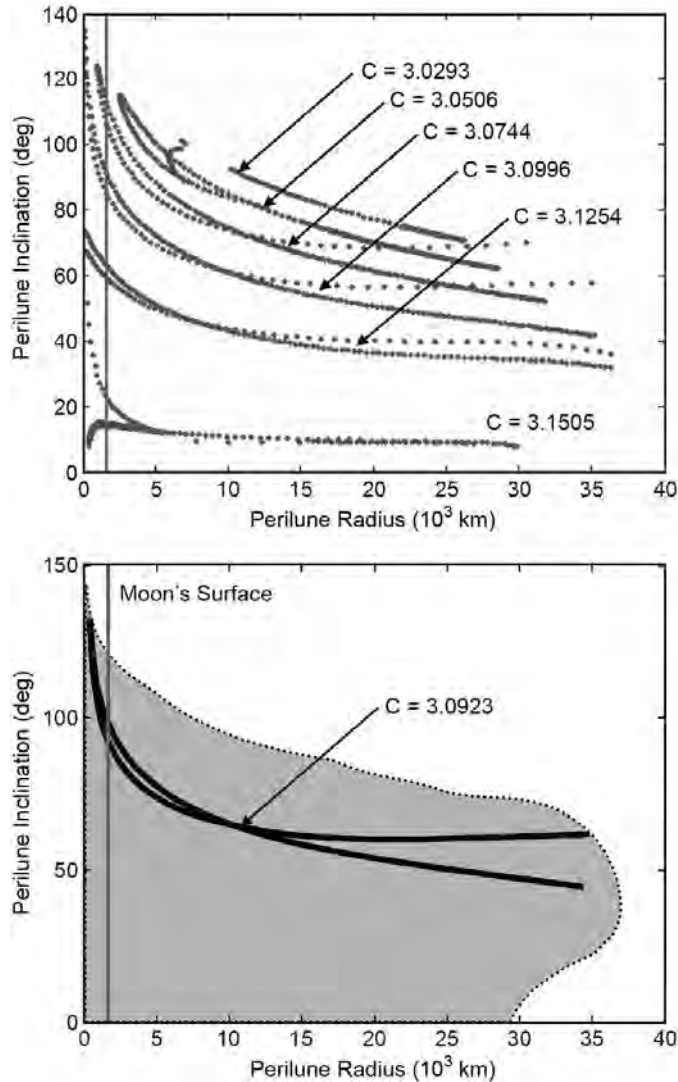


Figure 3-92 Available options identified for the radius and inclination of lunar orbits accessed by southern lunar L_2 halo orbits. Top: The radii and inclination combinations that may be obtained at perilune of the unstable manifolds of six different lunar L_2 halo orbits, where each orbit's available options are labeled with that orbit's Jacobi constant. Bottom: The radii and inclination combinations that may be obtained at perilune of the unstable manifolds of many orbits in the family of southern halo orbits. The highlighted options in the plot at right correspond to the available options for the halo orbit shown in Fig. 3-91.

the radius and inclination of lunar orbits that may be accessed by southern lunar L_2 halo orbits. The shaded field in the right plot has been constructed by sampling the unstable manifolds of hundreds of halo orbits and interpolating between the results. The highlighted points in the plot on the right are those points that are accessible from the example southern halo staging orbit shown in Fig. 3-91. Northern halo orbits can access the same set of lunar orbits except with a negative inclination. In each case, it is assumed that the orbit-insertion maneuver is performed at the perilune of the unstable manifold, but this is not required.